Tyco Laboratories, Inc.
16 Hickory Drive
Waltham, Massachusetts 02154

NiCd BATTERY ELECTRODES

Final Report

by

G. Holleck
M. Turchan
J. Hopkins

May 1972

Contract No. 953185-NAS7-100

Prepared for

California Institute of Technology
Jet Propulsion Laboratory
4800 Oak Grove Drive
Pasadena, California 91103

This work was performed for the Jet Propulsion Laboratory, California Institute of Technology sponsored by the National Aeronautics and Space Administration under Contract NAS7-100.

This report contains information prepared by Tyco Laboratories under JPL subcontract. Its content is not necessarily endorsed by the Jet Propulsion Laboratory, California Institute of Technology, or the National Aeronautics and Space Administration.

Tyco Laboratories, Inc.
16 Hickory Drive
Waltham, Massachusetts 02154

NiCd BATTERY ELECTRODES

Final Report

by

G. Holleck
M. Turchan
J. Hopkins

May 1972

Contract No. 953185-NAS7-100

Prepared for

California Institute of Technology
Jet Propulsion Laboratory
4800 Oak Grove Drive
Pasadena, California 91103

This work was performed for the Jet Propulsion Laboratory, California Institute of Technology sponsored by the National Aeronautics and Space Administration under Contract NAS7-100.

ABSTRACT

The objective of this research program was to develop and evaluate electrodes for a negative limited nickel-cadmium cell and to prove its feasibility. The program consisted of three phases: (1) the development of cadmium electrodes with high hydrogen overvoltage characteristics, (2) the testing of positive and negative plates, and (3) the fabrication and testing of complete negative limited NiCd cells.

The following electrode structures were manufactured and their physical and electrochemical characteristics were evaluated: (1) silver sinter-based Cd electrodes, (2) Teflon-bonded Cd electrodes, (3) electrodeposited Cd sponge, and (4) Cd-sinter structures. All cadmium electrode structures showed a sharp increase in potential at the end of charge, with the advent of hydrogen evolution occurring at approximately -1.3 V versus Hg/HgO. The hydrogen advent potentials on pure cadmium structures were 50 to 70 mV more cathodic than those of their silver-containing counterparts.

Silver sinter-based Cd electrodes were prepared by the chemical impregnation method from silver sinter plaques of high porosity. The developed plaques covered a wide variety of different structures with respect to both pore size and pore size distribution. The initial utilization of active material depended on the plaque type. In all cases, however, the capacity decreased with increasing cycle number. The rate of this capacity decrease was remarkably independent of plaque structure. It was considerably higher than with nickel-based Cd electrodes tested under the same conditions. Scanning electron micrographs of cycled electrodes showed the presence of needle-shaped crystals in silver sinter-based Cd electrodes which could not be detected in nickel sinter based-electrodes.

At the present state of development, Teflon-bonded cadmium electrodes showed the best overall performance as practical negative plates with high hydrogen

overvoltage characteristics.

The electrochemical behavior of Teflon-bonded electrodes was investigated systematically at various temperatures (0, 25, and 50°C) and charge rates (C, C/3, C/10). They were found to operate well at all test conditions. The advent potentials for hydrogen evolution were slightly more cathodic at the lower temperature.

The effect of charge rate on capacity was small at room temperature, larger at 0°C, and largest at 50°C. Lower charge rates resulted in higher capacities. Thinner electrodes were less rate sensitive. At C/10 charge, the average capacity at 0°C was 87% of the capacity at 25°C.

The rate of oxygen evolution at positive plates of different loading levels was measured as a function of temperature (0, 25, and 50°C) and charge rate (C, C/3, C/10, C/30). Throughout a large part of the charging process the absolute rate of O_2 evolution at a given temperature was independent of charge rate, thus making high rate charging more efficient. The rapid increase in O_2 evolution rate towards the end of charge, however, occurred earlier at the higher charge rate. Oxygen evolution increased dramatically with rising temperature. The lowest rate of oxygen evolution was observed at an intermediately loaded positive ($\sim$5 Ahr/in.^{3}).

The feasibility of a negative limited NiCd cell was demonstrated by the fabrication and testing of six experimental cells with 3 Ahr capacity. The cells contained Teflon-bonded negatives and a negative to positive ratio of approximately 1:2. To allow a detailed analysis, each cell was further equipped with a NiO_x reference electrode, a thermocouple, a pressure gauge, and a pressure release valve. The cells were operated between preset cell voltages of 0.8 to 1.7 V at various temperatures (0, 25, 35°C) and at two charge rates (C/3, C/10). The delivered capacity was nearly independent of charge rate and temperature. Since the positive plates start to evolve oxygen at a low state of charge, the cell must have some oxygen recombination capability. Thus, the oxygen pressures in the cells varied during a cycle and were dependent on the electrolyte fill level and on operating temperature. No significant temperature increase occurred at the end of charge and no nonconsumable gas (H_2) was evolved during testing.

Table of Contents

List of Illustrations

List of Illustrations (Cont.)

List of Illustrations (Cont)

List of Illustrations (Cont)

List of Tables

I. INTRODUCTION

The objective of this research program was to develop and evaluate electrodes for a non-gassing negative limited nickel-cadmium cell and to demonstrate the feasibility of the concept. The concept is based on the elimination of low hydrogen overvoltage materials from the negative plate. The onset of hydrogen evolution is then marked by a sharp increase in cell voltage, i.e., a signal that can be used to terminate the charging process.

In addition to all cadmium structures, silver appeared to be a suitable support material for high hydrogen overvoltage electrodes. We therefore proposed to investigate fabrication techniques and the electrochemical behavior of the following structures for use as negative plates:

1. Cadmium impregnated silver sinters.
2. Teflon-bonded cadmium hydroxide on silver and cadmium substrates.
3. Cadmium sinter structures on silver and cadmium substrates.
4. Electrodeposited porous cadmium on silver or cadmium substrates.

The development program consisted of three phases: (1) the development and characterization of electrode structures with high hydrogen overvoltage characteristics, (2) the electrochemical testing of positive and negative plates at various rates and temperatures, including an investigation of their gassing characteristics, and (3) the fabrication and testing of complete negative limited cells to demonstrate the feasibility of the concept.

II. THE NON-GASSING NiCd CELL, BACKGROUND AND APPRAISAL

In the following we summarize the known characteristics of the positive and negative plates in present NiCd batteries. This will allow us to define the constraints in both plate manufacture and cell operation that are relevant to the implementation of the present program.

The present design of hermetically sealed cells depends on:

1. Preventing H_2 evolution at the negative on charge by providing a large excess negative plate capacity.

2. Limiting oxygen evolution at the positive plate to a rate at which oxygen can be recombined at the negative plate.

In concept, this mode of operation is sound; in practice, the capacity of the negative plate decays, eventually leading to H_2 generation and cell failure. (There is no effective mechanism for H_2 recombination in NiCd cells.) In effect, these statements define the principal characteristics of nickel-cadmium battery plates that must be accommodated in a sealed cell design: (1) the inherent inefficiency of charge acceptance at the positive plate, and (2) the requirement to avoid H_2 evolution at the negative plate. Initially, let us examine these two problems in the context of the proposed configuration of the non-gassing cell. The gassing reactions on cell reversal in a battery and the particular problems associated with operation at temperature extremes will be considered later.

The principal design modification proposed for the non-gassing NiCd cell is that the ratio of the negative to positive capacities be such that the negative plate, rather than the positive plate, is limiting. Under these circumstances, overcharge cannot be tolerated, and it is necessary to clearly identify the fully-charged condition without an appreciable time lag. This is most easily realized in practice by eliminating low overvoltage materials from the negative plate. The onset of hydrogen

evolution is then marked by a sharp increase in cell voltage, i.e., a signal that can be used to terminate the charging process.

Again, as with the positive limited cell, the system is sound in concept. Any oxygen generated due to inefficient charge acceptance by the positive active material can still be consumed at the negative plate, thus maintaining the initial capacity ratio. This is one of the principal advantages of the negative limited cell. The delivered capacity of the cell positive plate, since overcharge is avoided, will be determined by the available capacity of the negative plate. Thus, any fade in negative capacity will be manifested only as a loss in cell capacity and will not result in catastrophic pressure buildup as occurs with the conventional positive limited cell. If negative fade is a reversible process, a series of conditioning cycles may restore the negative plate capacity; then the positive plate will still be able to match the improved negative capacity.

There are good arguments for the use of positive plates with appreciable excess capacity in negative limited batteries. For example, if excess capacity in the charged state (precharge) is built into the positive plate, the cell can tolerate limited cell reversal if it is capable of withistanding some internal pressure. Hydrogen evolution is thus precluded. Oxygen recombination is then averaged out over the whole duty cycle. More specifically, positive precharge permits oxygen accumulation in the cell without the cell becoming positive limited. This could give more flexible operation if occasional arduous duty cycles are involved.

There is also a good argument for excess positive capacity in the discharged state to such an extent that the plate can cycle below 70% of its rated capacity. Below the 70% of state of charge, charge acceptance is almost 100% efficient at normal charging rates and temperatures[1] and the self-discharge rates are lower.*

The proposed design, in which the total capacity of the positive would be twice that of the negative, does not lead to an excessive penalty in energy density when compared to conventional cells. By reducing the quantity of cadmium necessary for a particular nominal capacity, one compensates for the excess positive material required. Cell volume and configuration need not be compromised

---

*In the absence of overcharge, very little of the γ form of the charged active material will be produced.[2] The γ "NiOOH"[3] in which the nickel valence is greater than three is considered to have a much higher self-discharge rate than the tervalent-NiOOH.

since positive plates of high specific capacity (8-10 Ahr/in.^{3}) can be prepared by electrochemical impregnation methods.[4,5] The experience with Ni-Cd batteries seems to indicate that a more lightly loaded negative plate shows better utilization and longer life.

There are additional aspects of sealed cell operation that require further investigation. One of these is the fading of cadmium negative electrodes. Very little is known about the fading mechanism; however, there might be a correlation with the extent of O_2 recombination which would be much smaller than in conventional designs. This would also avoid the problem of heat generation towards the end of the charging cycle.

Another factor worthy of consideration is the effect cell operation with flooded electrolyte might have on the loss of capacity in the negative plate. It has been suggested that concentration gradients are responsible for cadmium migration.[6] In the flooded condition, the magnitude of these gradients may be different.

The negative limited cell also offers advantages in the event of limited accidental cell reversal. H_2 evolution would be avoided as long as part of the excess positive capacity is present in the charged state at the time of sealing. (It is envisioned that the positive would normally cycle between 20% and 70% state of charge.) Thus, on cell reversal, O_2 would be evolved at the negative plate yet hydrogen would not be generated until the excess positive capacity in the positive was discharged. Oxygen evolution on the negative plate could also be avoided by inclusion of an antipolar mass to ensure gas-free operation on limited cell reversal.

III. DEVELOPMENT OF NEGATIVE ELECTRODE STRUCTURES

A. Hydrogen Overvoltage Studies

Exploratory measurements of the overvoltage for hydrogen evolution on silver (in the form of wires) and cadmium (in the form of sheets and flattened beads) have been carried out. The results are shown in Fig. 1. The current densities were calculated per geometric cm^2. No attempt was made to correct for surface roughness. The Tafel plots (log I versus E) have a slope of 150 mV/decade on cadmium and 125 mV/decade on silver. There is no satisfactory explanation for the slightly high Tafel slope on cadmium. Recent results by Lee on the hydrogen overpotential on cadmium electrodes in 6 N KOH agree very well with our data. For comparison we also measured the hydrogen overvoltage on nickel and included in it Fig. 1. Here the Tafel slope is 60 mV/decade. At a hydrogen evolution current density of 1 mA/cm^2, for example, the potential on Cd is approximately 400 mV more cathodic than on Ni; silver is only about 100 mV anodic with respect to Cd. Furthermore, we observed that very small amounts of Cd in solution shift the hydrogen overpotential even closer to that of pure cadmium. Thus, silver appears to be a suitable substrate material for negative electrode structures with high hydrogen overvoltage characteristics.

B. Electrochemical Test Cell Design

The three-compartment cell for the electrochemical evaluation is schematically shown in Fig. 2. Figs. 3 and 4 show the test cell arrangement before and after assembly. The cell consisted of three plexiglas parts with viton o-ring gaskets and allowed for two symmetrically located counterelectrodes (positive plates) and a mercuric oxide reference electrode, as well as gas inlets for electrolyte gas presaturation. The transparent cell permitted visual observations of the electrode surface, and quantitative measurement of the gas evolved via a microburette. The cell was sealed to the atmosphere by polyethylene covered rubber stoppers. Temperature was controlled by immersion in a thermostated bath.

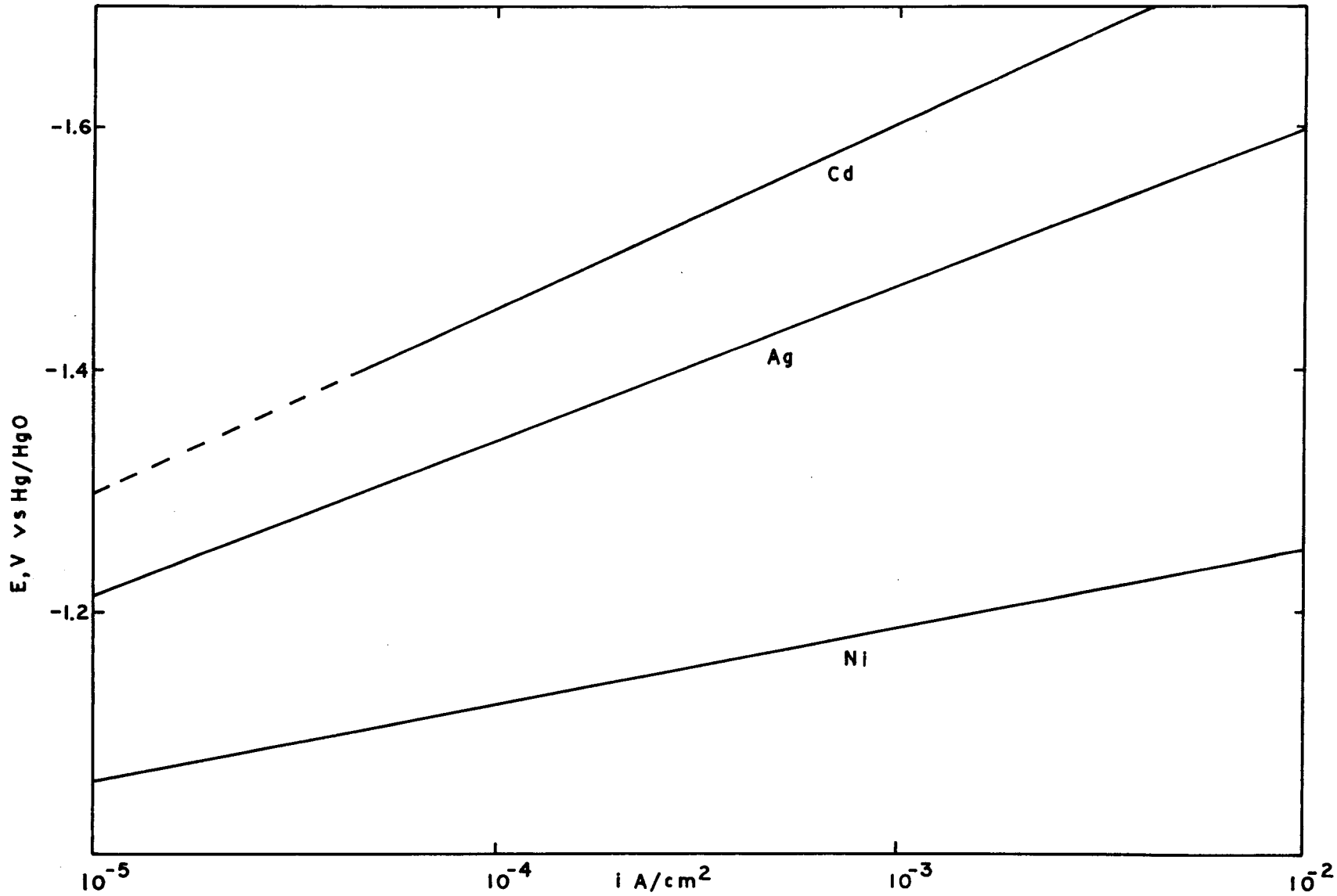

Fig. 1. Evolution of hydrogen on cadmium, silver, and nickel, 25% KOH, room temperature

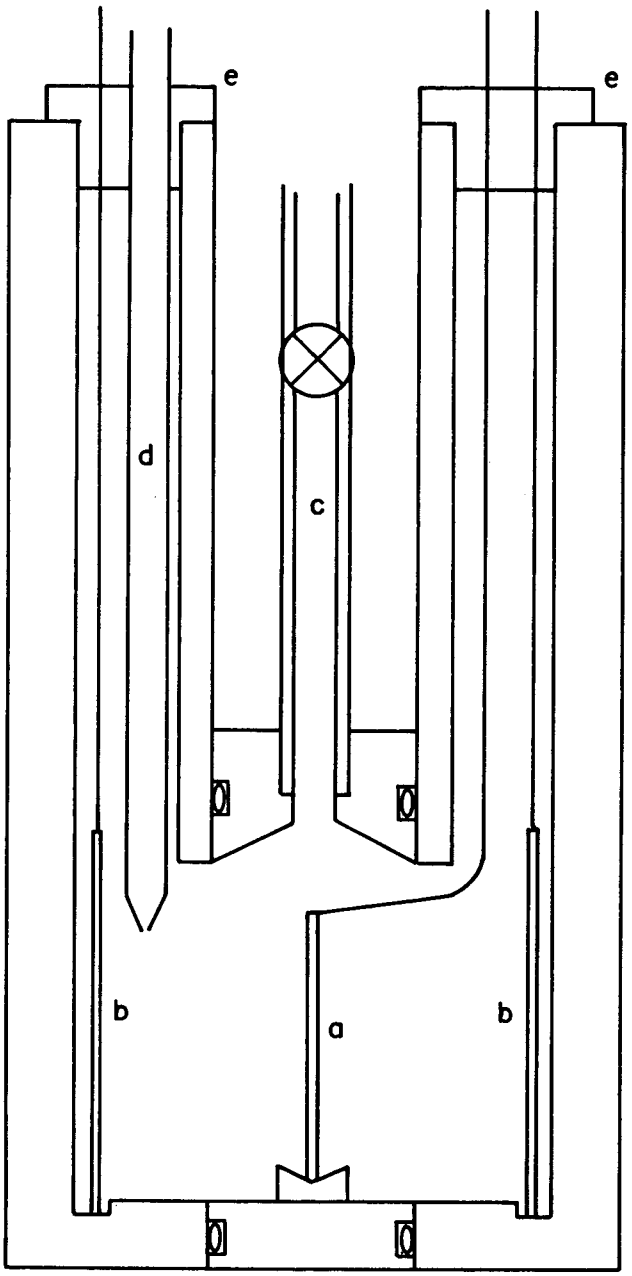

Fig. 2. Three part plexiglass cell [(a) negative plate, (b) positive plate, (c) calibrated gas burette, (d) Hg/HgO reference electrode, (e) rubber seal]

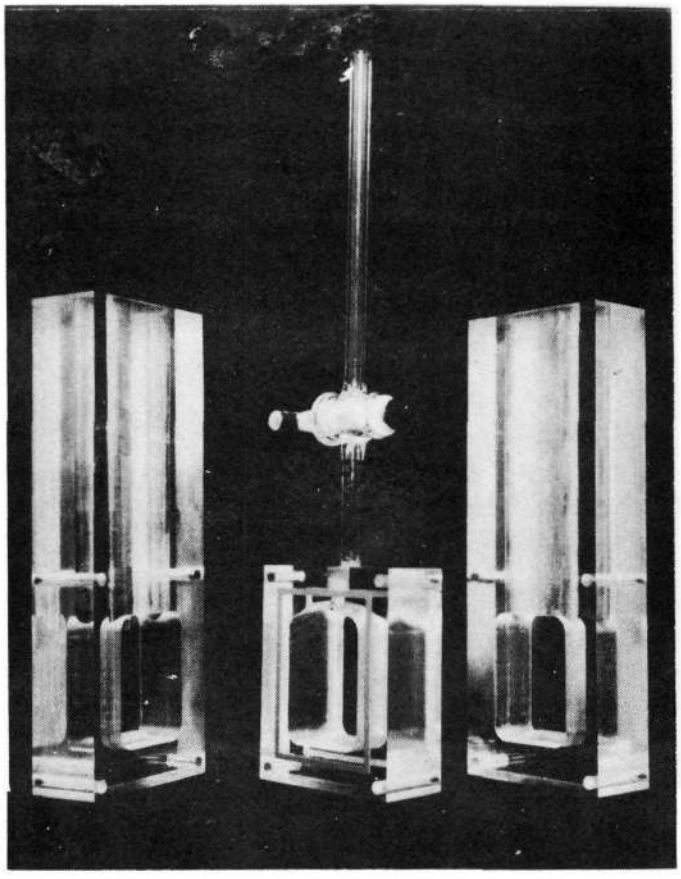

Fig. 3. Electrochemical test cell (disassembled)

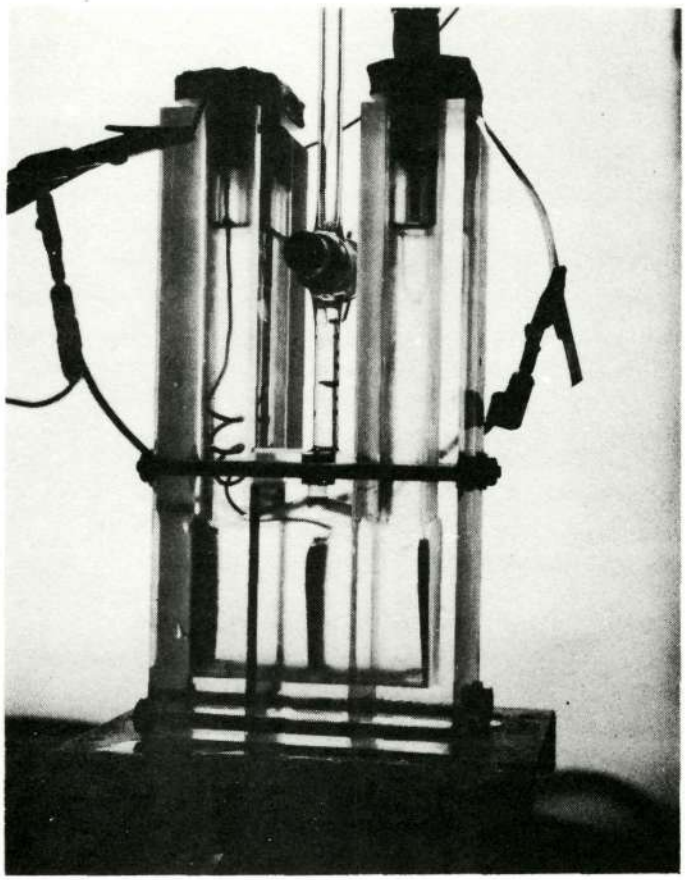

Fig. 4. Electrochemical test cell (assembled)

C. Cadmium Impregnated Silver Sinters

1. Introduction

Presently highly successful cadmium electrodes are based on the impregnation of suitable nickel plaques with cadmium hydroxide. We therefore considered an analogous approach where the nickel sinter is replaced by a silver sinter, with appropriate structure as being most promising to reach the objective of a practical negative electrode. Furthermore, silver sinters should have an excellent electrical conductivity and, at the operating potential of the cadmium electrode, a clean oxide-free surface. If silver plaques could be developed with similar structures as nickel plaques, basically the same technology for fabrication and impregnation could be used to manufacture these negative plates. Therefore, in analogy to Ni sinters, we set out to develop Ag plaques with a high porosity. Conventionally used Ag sinter plates (e.g., in Ag-Zn cells) have only low porosities characteristically between 35 and 60%. Such plates would not allow impregnation to a high specific capacity and the plates would also be quite heavy. Initial exploratory experiments[8] demonstrated the importance of structure and therefore we investigated a number of different plaque types.

2. Silver sinter structures

A large variety of different silver sinter structures with high porosities was prepared. This was achieved by utilizing various silver powders and by using different preparation techniques, such as the sintering of loose powder layups and of compacts prepared by pressing a mixture of sodium fluoride and silver powder. The latter requires, as a final step, the removal of the inert filler by a leaching process. In the following discussion, the structures, coded according to the silver powder used, were investigated more closely by means of scanning electron microscope photographs of the powder and of the sintered plaques. Cross sections were obtained by fracturing the plaques in liquid nitrogen. The macroscopic characteristics of the various Silpowders are summarized in Table I.

a. Plaque type "150"

Silpowder "150" is shown in Figs. 5 and 6. It consisted of relatively large agglomerates of individual particles. Both the agglomerates and the individual particles exhibited a wide range of differing sizes. Plaques obtained by

Table I. Silpowders

(Manufacturer - Handy & Harman, New York, N.Y.)

Type	130	150		220		300
Process	Chemical Precipitate	Galvanic Precipitate		Chemical Precipitate		Chemical Precipitate
% Ag	99.6	99.9		99.99		99.5
Screen Analysis, %						
+100	-	0.5 max		-		-
+200	-	-		-		-
+325	-	-		2.0		-
-325	100%	30.0 max		98.0		100
Batch No.	B-918	B-5692	B-5794	B-475	B-554	B-156
Average Particle Diameter Microns (Fisher Sub-Sieve Sizes)	1.2	10.4	15.2	5.2	5.2	1.1
Apparent Density, g/cc (Scott Volumeter)	(0.61 - 1.22)	(1.52 - 2.43)	2.53	(1.55)	1.54	(0.36 - 0.425)

( ) Manufacturer data

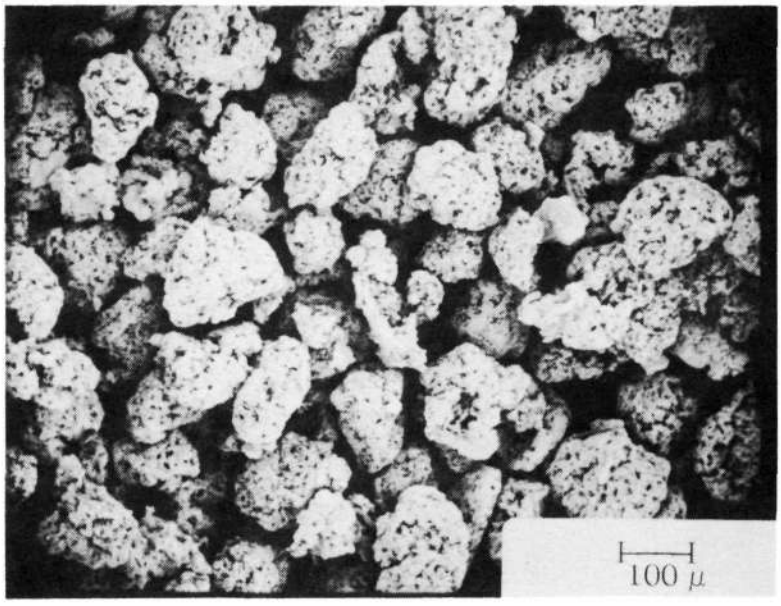

Fig. 5. Silver powder, Handy and Harman 150

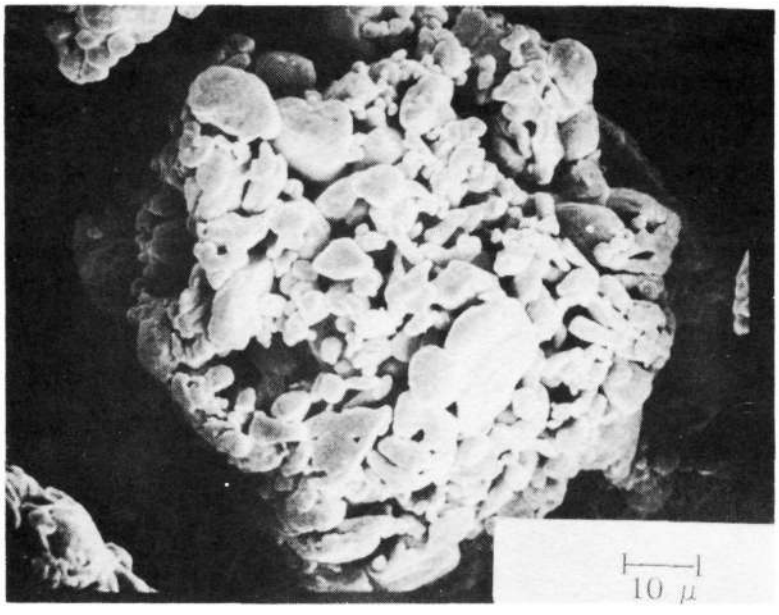

Fig. 6. Silver powder, Handy and Harman 150

sintering (30 min at 550 °C) of dry layups of this powder retained these characteristics (Figs. 7 and 8). They exhibited a very pronounced double porosity. Large pores were formed between the individual agglomerates which themselves remain porous. They showed, however, considerable necking by interdiffusion. The macroscopic porosity was approximately 75%.

b. Plaque type "130"

Silpowder "130" (Fig. 9) shows a very small average particle size and a nearly spherical shape. It too contained particles with a wide variation in size. This powder had poor flow characteristics and exhibited a tendency to agglomerate. These agglomerates had, however, no characteristic size or shape as opposed to Silpowder "150". A typical plaque obtained by sintering and leaching of a NaF compact (60 vol % NaF, 25,000 psi, 30 min at 600 °C) is shown in Figs. 10 and 11. The pore-size distribution was much more uniform than in the "150" plaque. The cross section in Fig. 10 also showed a directional orientation of the silver agglomerates introduced by the pressing of the compact.

c. Plaque type "220"

Fig. 12 shows Silpowder "220". These particles had an irregular, elongated shape and the particle-size distribution was much more uniform than the previously mentioned silver powders. The macroscopic flow characteristics of the Ag powder were quite good. The powder contained some agglomerates, although without characteristic size or shape. A fractured cross section of a sintered "220" powder layup is shown in Fig. 13. It appeared as a double structure with larger and smaller pores. The shape of the pores and the necking between the particles is illustrated in Fig. 14.

Modified "220" type plaque structures were obtained by: (1) mixing 10% silver oxide (Fisher purified Ag_2O, lot no. 742450) with the Ag powder before making the dry layup, and (2) by vacuum impregnating a "220" plaque with a saturated $AgNO_3$ solution followed by decomposition to Ag at 450 °C. The reasoning behind these modifications was to increase the internal surface area of these structures. The results of both methods were quite similar. Fig. 15 shows an Ag_2O modified structure. It was very similar to the regular "220" plaque except for the presence of small dimples on the internal surface.

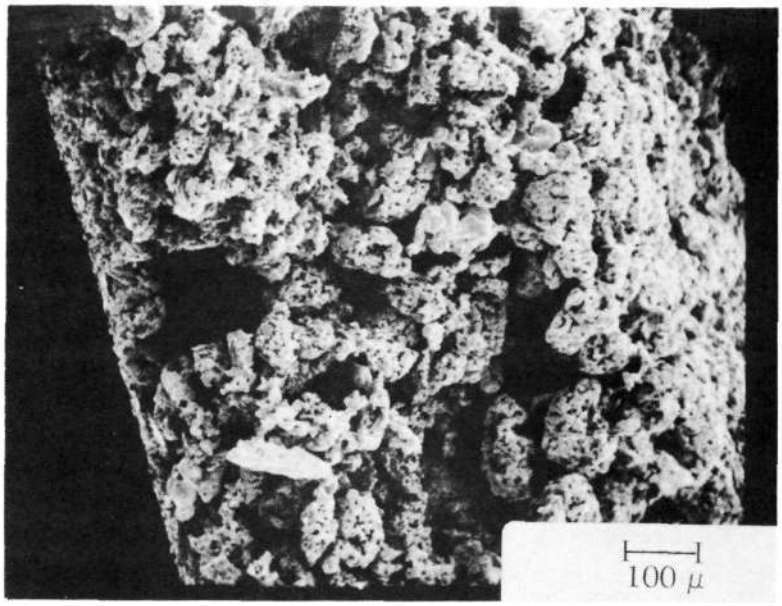

Fig. 7. Silver sinter plaque 150

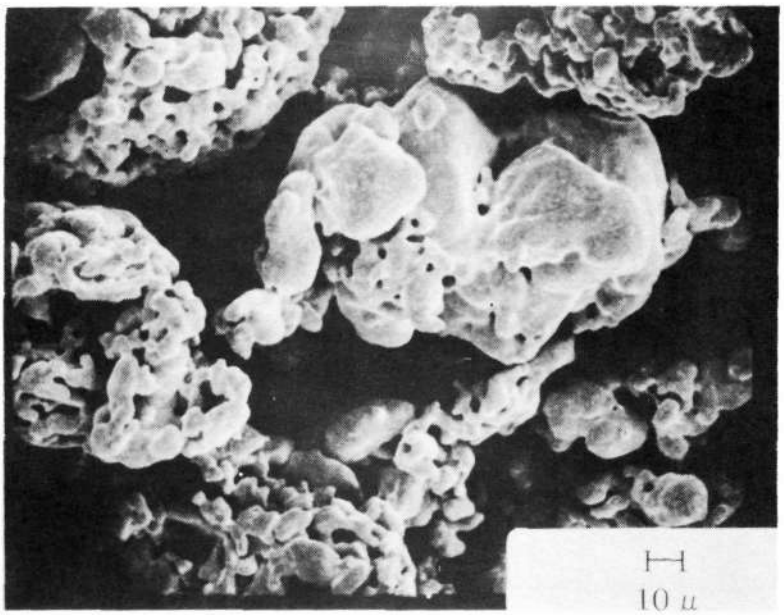

Fig. 8. Silver sinter plaque 150

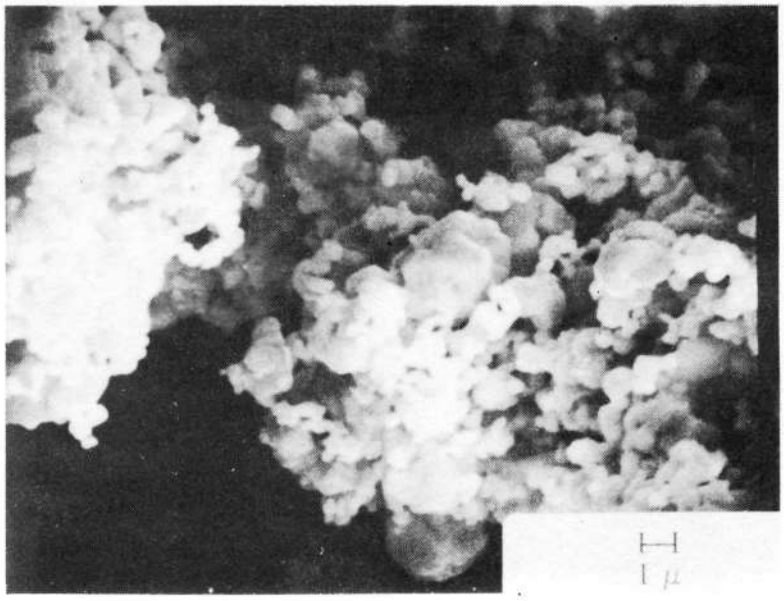

Fig. 9. Silver powder, Handy and Harman 130

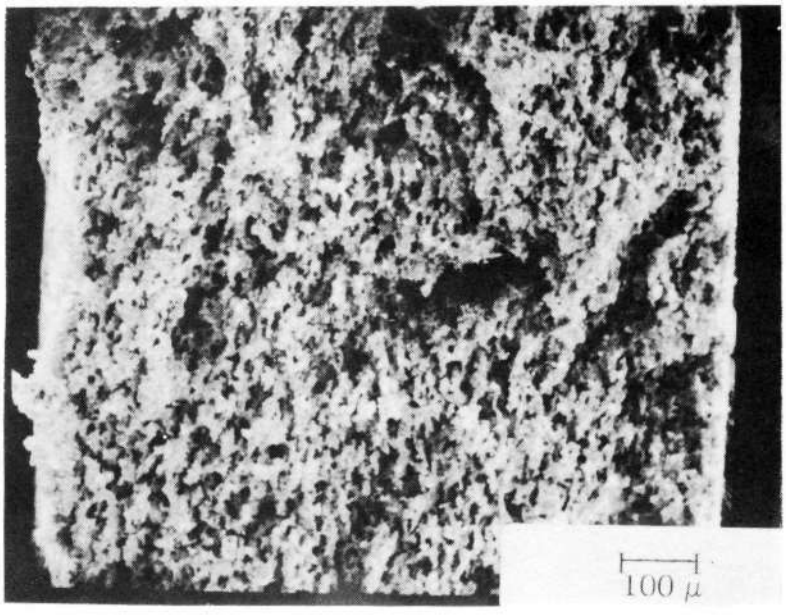

Fig. 10. Silver sinter plaque 130 (NaF compact)

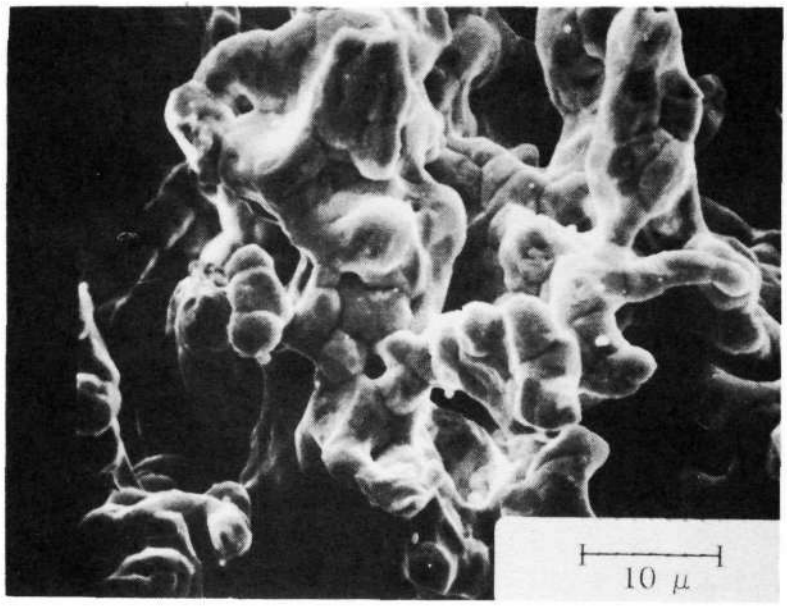

Fig. 11. Silver sinter plaque 130 (NaF Compact)

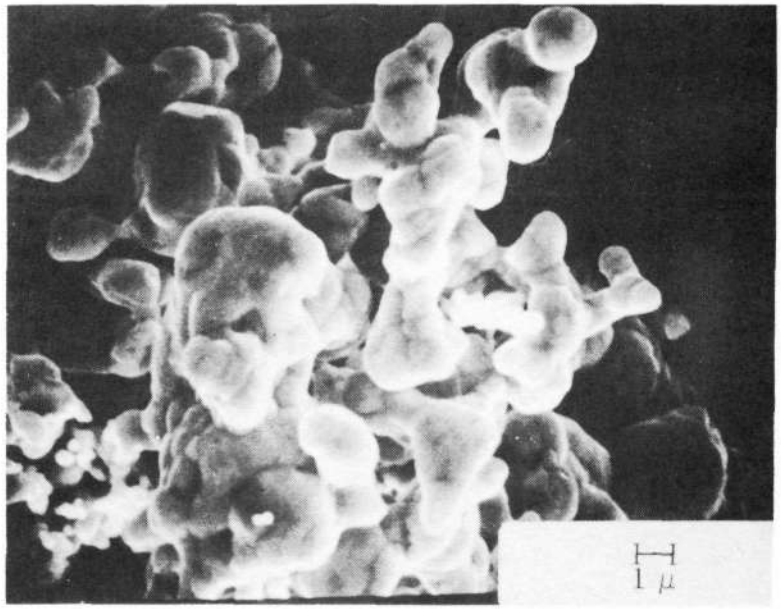

Fig. 12. Silver powder, Handy and Harman 220

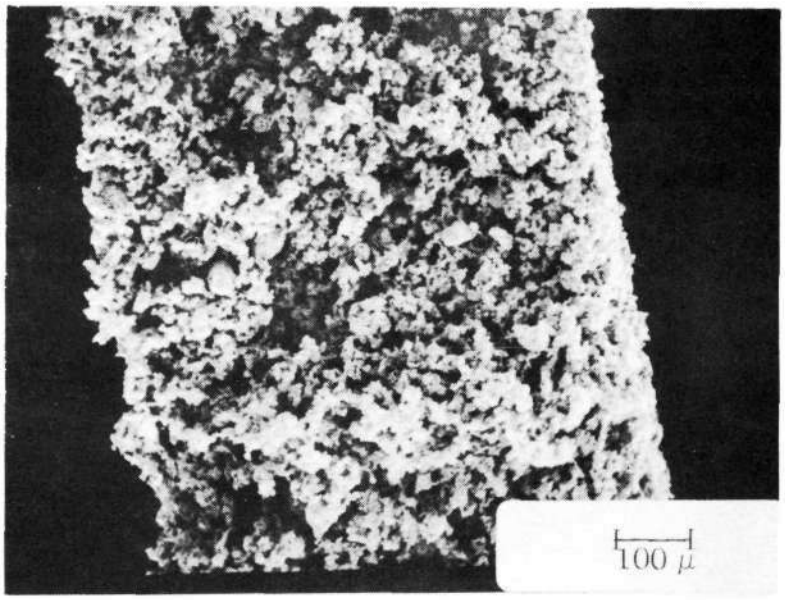

Fig. 13. Silver sinter plaque 220

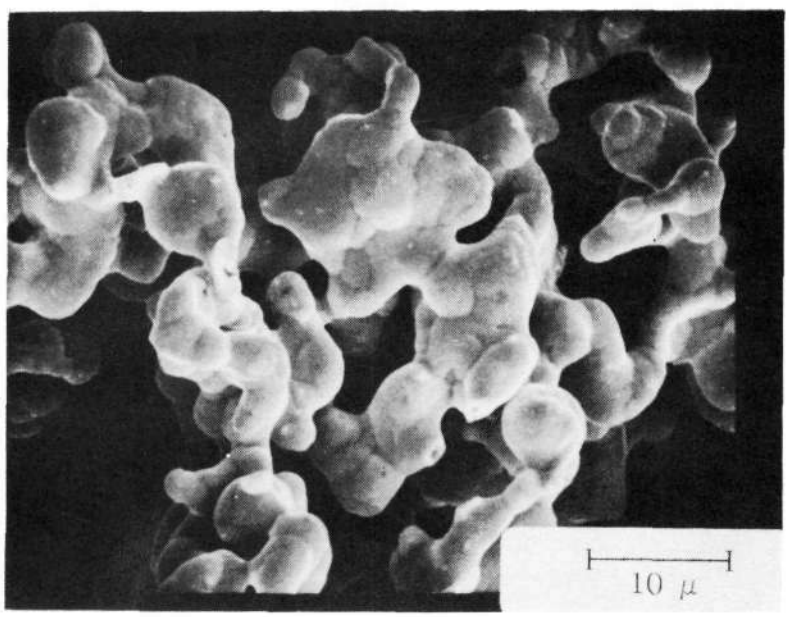

Fig. 14. Silver sinter plaque 220

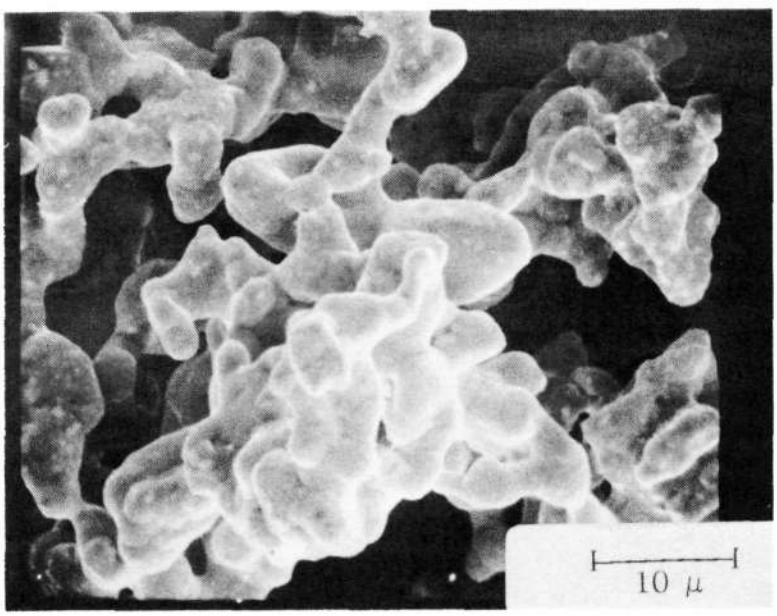

Fig. 15. Silver sinter plaque 220 (Ag_2O modified)

A different plaque structure was obtained by sintering and leaching a sodium fluoride compact. Fig. 16 clearly shows the structural orientation parallel to the surface. The surface also had a distinctly different appearance (Fig. 17). Here we see relatively large flat areas with only small pores, whereas the surface appearance of sintered dry layups is very similar to cross sections of such structures.

d. Plaque type "300"

The Silpowder "300" is shown in Figs. 18 and 19. It exhibited a double structure similar to Silpowder "150" and consisted of agglomerates of various size made up of small dendritic particles (Fig. 19). Sinters produced from this powder also showed a dual porosity range. Fig. 20 shows the sintered structure to be much finer than in the previously discussed plaques. It retained many features of the dendritic powder. The mechanical stability of the type "300" plaque was poorer compared to the other plaques. An increase of the sintering time from 30 min (at 550°C) to 60 min slightly improved the mechanical stability without noticeable changes in plaque structure.

For purposes of comparison, Fig. 21 shows the structure of a commercial nickel plaque. The pore-size distribution seemed to be somewhat more uniform than in most silver sinter plaques; however, we found a number of large pores. With regard to average pore size, the nickel sinters would have to be placed between the "300" silver plaque and the remaining types of silver sinter structures.

3. Electrochemical evaluation of silver sinter structures

The various silver sinter structures discussed above were impregnated with cadmium hydroxide by the chemical conversion method, i.e., vacuum impregnated with saturated $CdNO_3$, dried, then chemically converted in KOH at 80°C. The plaque characteristics and the loading of these cadmium electrodes are summarized in Table II. The charge and discharge voltage profiles of the various silver sinter-based Cd electrodes were very similar. Characteristic examples are shown in Figs. 22 to 24. The charge and discharge plateaus were quite flat, and the advent of gas evolution as characterized by the initial appearance of small individual gas bubbles at the electrode surface occurred at approximately -1.25 V versus Hg/HgO.

The capacity of the various electrodes (stated as per cent of their theoretical capacity) as a function of the number of cycles is summarized in Table III. Table III

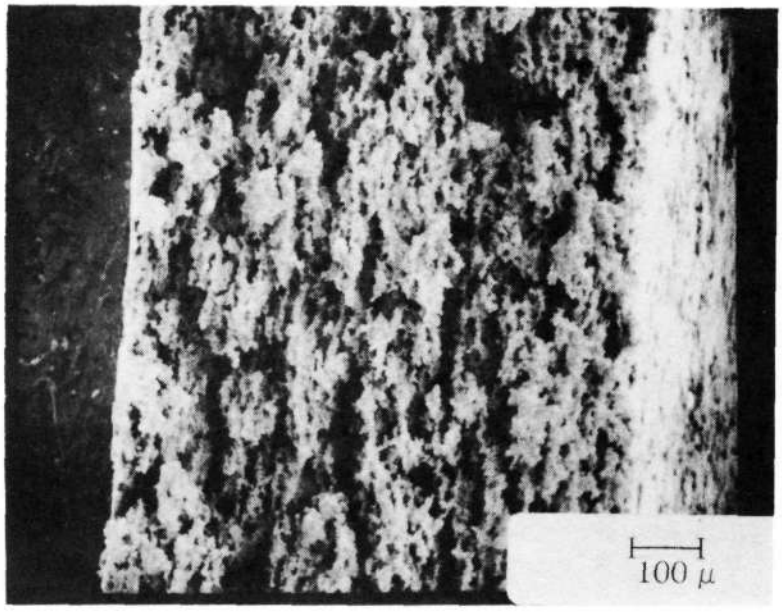

Fig. 16. Silver sinter plaque 220 (NaF compact)

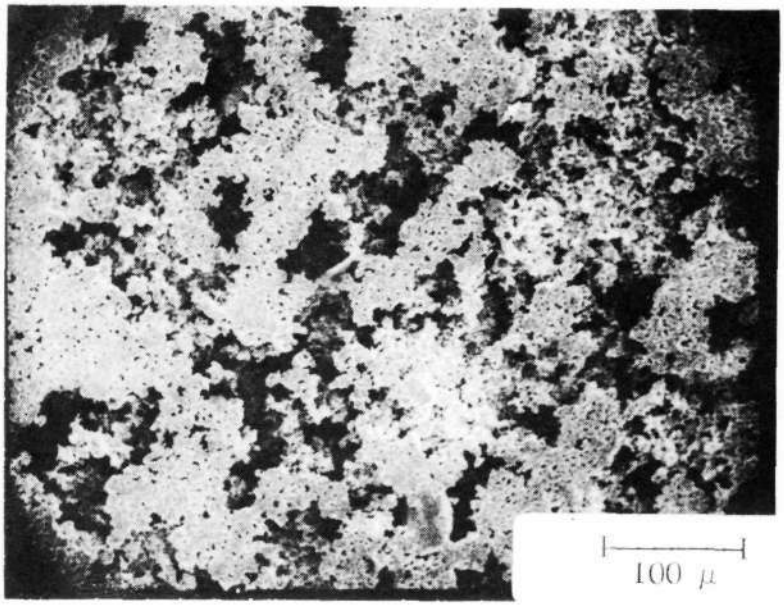

Fig. 17. Silver sinter plaque 220 surface (NaF compact)

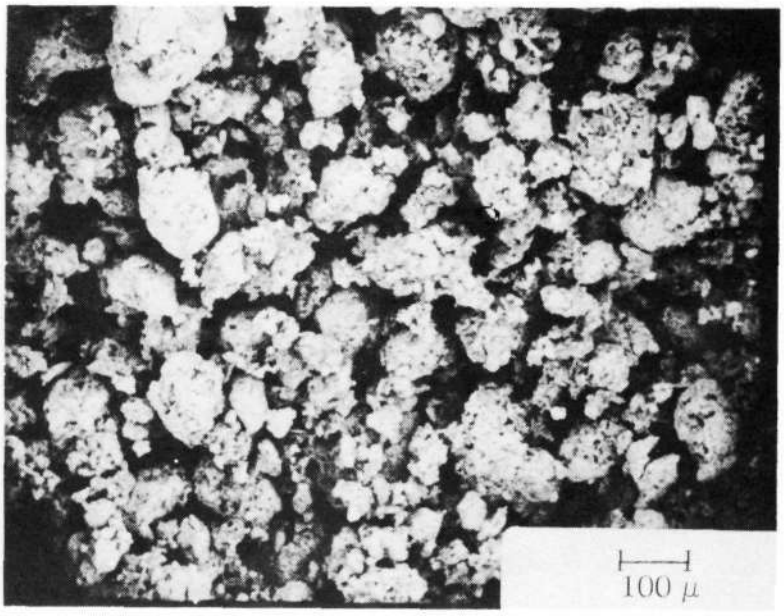

Fig. 18. Silver powder, Handy and Harman 300

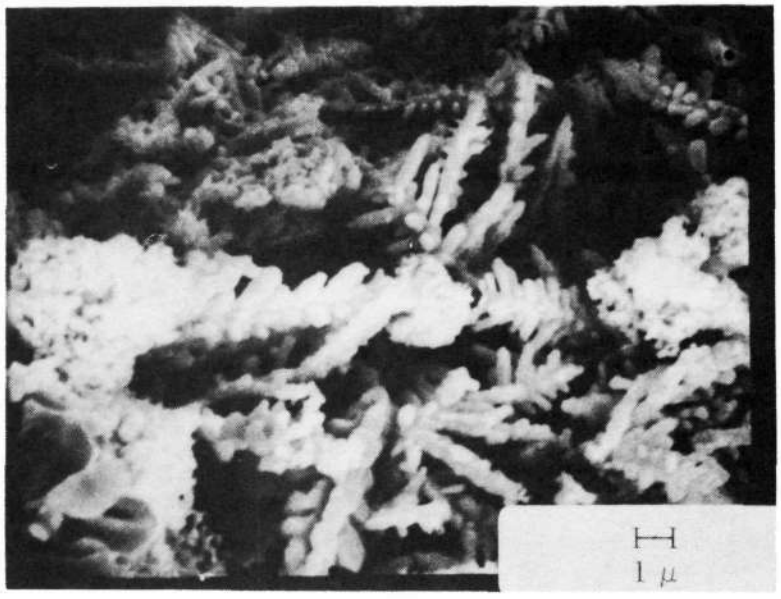

Fig. 19. Silver powder, Handy and Harman 300

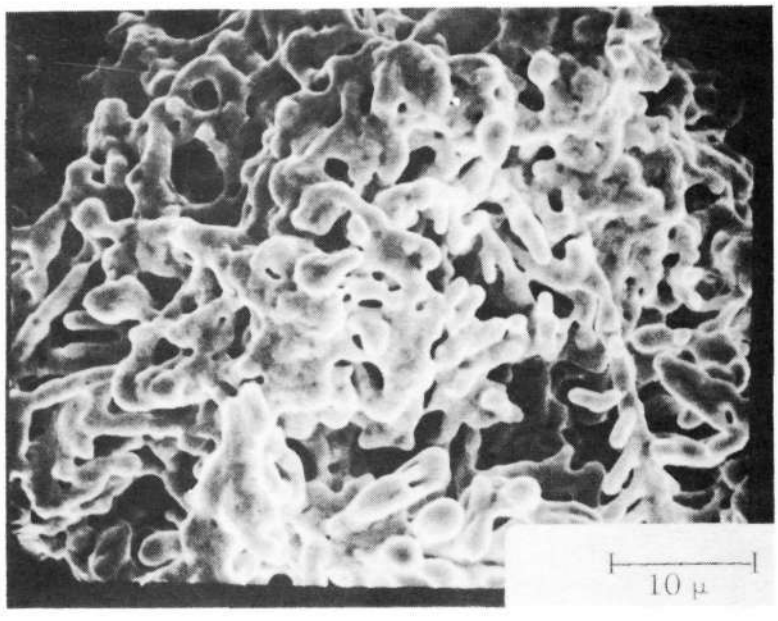

Fig. 20. Silver sinter plaque 300

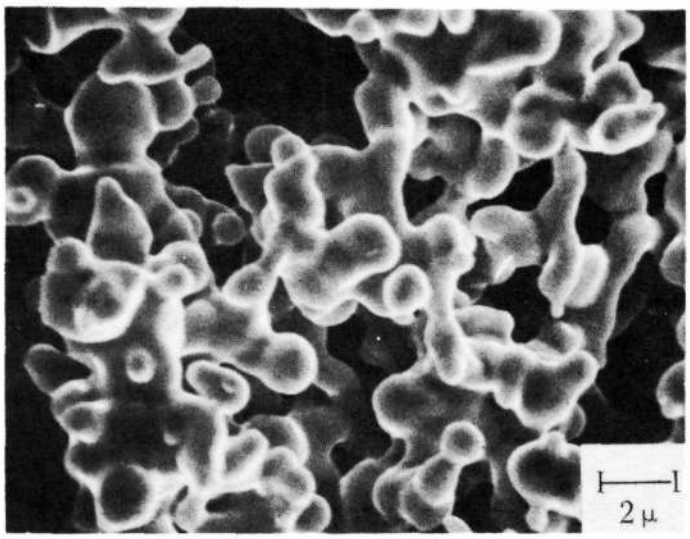

Fig. 21. Commercial nickel plaque

Table II. Characteristics of Silver Sinter-Based Cd Electrodes

Electrode	Plaque Type	Plaque Porosity, %	Plate Thickness, mil	Theoretical Capacity	
				Ahr	Ahr/in.^{3}
SS Cd-1	Ag 150 dry layup (sample)	74	30	0.364	8.1
SS Cd-2	Ag 130 NaF compact	71	39	0.248	6.3
SS Cd-3	Ag 220 dry layup	77	28	0.218	7.9
SS Cd-4	Ag 130 dry layup	76	25	0.160	6.6
SS Cd-5	Ag 150 dry layup (batch)	72	32	0.223	5.2
SS Cd-6	Ag 220 dry layup	77	24.5	0.133	3.6
SS Cd-7	Ag 220 dry layup	78	25	0.134	3.7
SS Cd-8	Ag 220 dry layup ($AgNO_3$ modified)	81	19	0.142	4.9
SS Cd-9	Ag 220 dry layup ($AgNo_3$ modified)	81	19	0.139	5.1
SS Cd-10	Ag 220 dry layup (Ag_2O modified)	78	21	0.106	4.9
SS Cd-11	Ag 300 dry layup	82	21	0.162	5.3
SS Cd-12	Ag 300 dry layup	82	21	0.124	4.8
SS Cd-13	Ag 300 dry layup	82	21	0.146	4.9
NS Cd-3	Ni 287 dry layup	76	35	0.325	12.2
NS Cd-4	Ni 287 dry layup	76	35	0.650	12.2

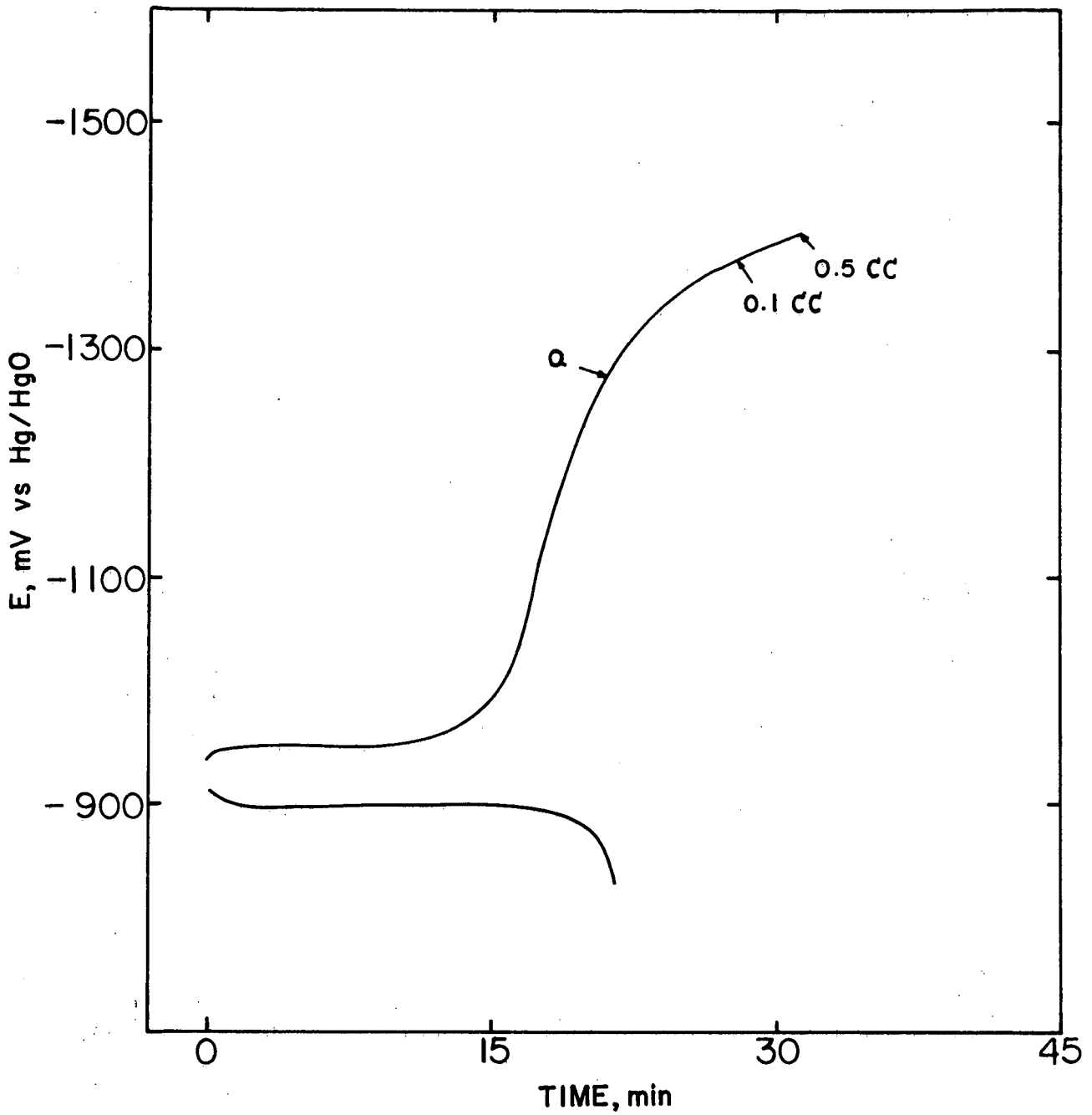

Fig. 22. Charge/discharge cycle of silver sinter-based Cd electrode SS Cd-2 (Ag 130, NaF compact, cycle No. 32, 7 mA/cm^2, 25% KOH, room temperature; a = first individual, small bubbles)

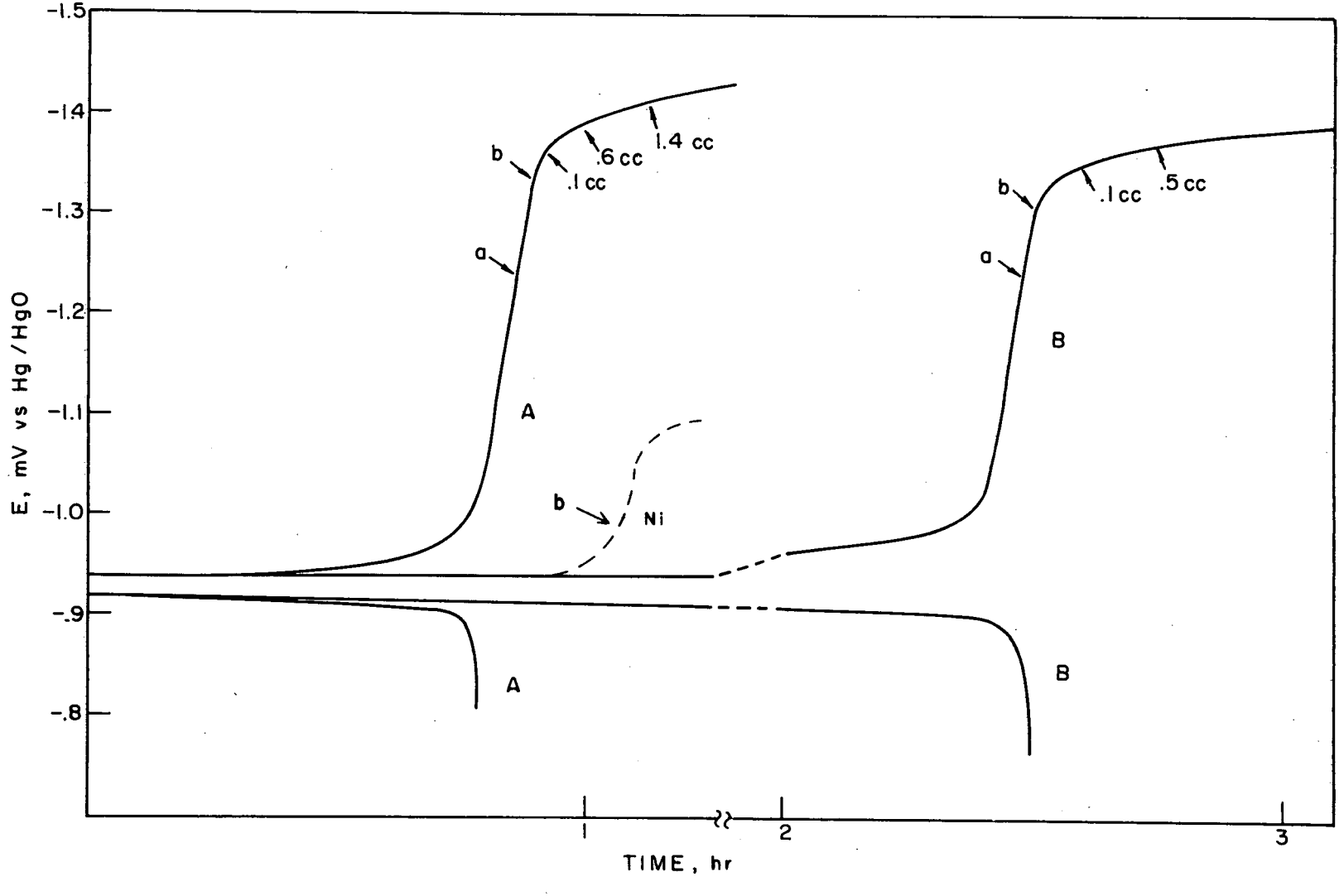

Fig. 22a. Cd impregnated Ag sinter, SSCd-1 (A = 40th cycle, i = 7.75 mA/cm^2; B = 43rd cycle, i = 3.1 mA/cm^2; a = first bubbles at active top center of electrode; b = first bubbles all over electrode)

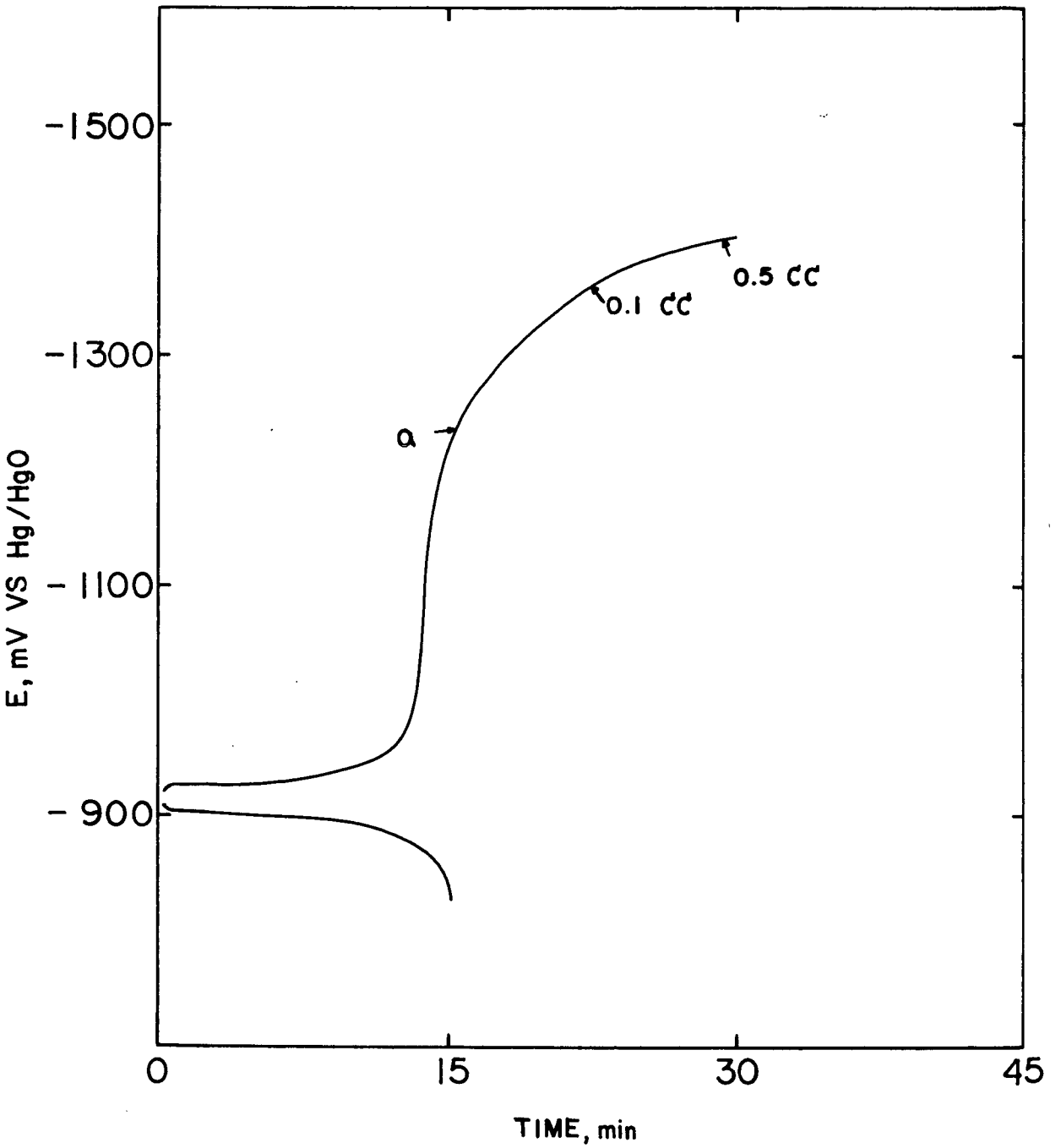

Fig. 23. Charge/discharge cycles of silver sinter-based Cd electrode SS Cd-3 (Ag 220, cycle no. 40, 7 mA/cm^2, 25% KOH, room temperature; a = first individual, small bubbles)

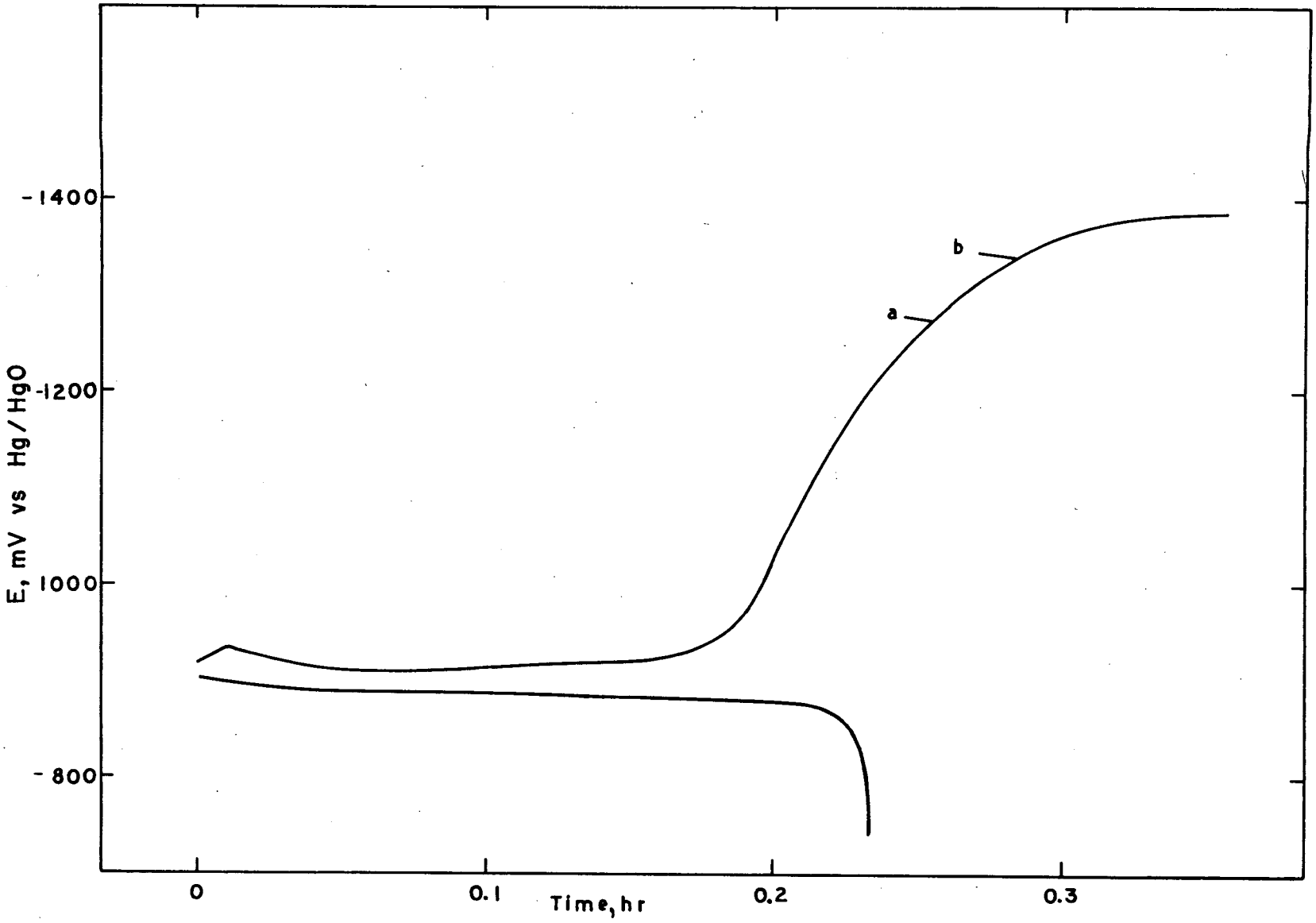

Fig. 24. Charge/discharge cycles of silver sinter-based Cd electrode SS Cd-12 (Ag 300, cycle no. 78, 7.9 mA/cm^2, 30% KOH, room temperature; a, first individual small bubbles; b, moderate gassing)

Table III. Capacity of Silver Sinter-Based Cd Electrodes
(Measured Capacity as Percent of Theoretical Capacity)

SS Cd-	1	2	3	4	5	6	7	8	9	10	11	12	13
Ag Powder	150	130C	220	130	150	220	220	220 mod.	220 mod.	220 mod.	300	300	300
Cycle No.													
1	70.0	42.0	54	42.5	49.3	28.5	38.8	74.6	67.6	74.5	72.0	74.5	70.0
5	46.2	21.0	29.0	27.5	33.2	18.8	26.8	53.5	50.4	53.7	44.5	48.8	45.5
						†	†						
10	34.5	13.0	21.0	20.0	22.4	19.5	22.0	38.0	40.3	40.5	30.8	34.2	31.5
20	23.8	9.0	15.5	12.5	13.7	9.8	11.2	23.2	26.6	25.4	18.5	22.6	18.5
		†	*										
30	18.3	7.0	12.0	8.1	9.5	7.1	8.4	18.3	20.9	20.3	16.3	16.5	14.0
	*	*					†						
40	25.1	13.0	8.0	7.0	7.2	6.0	6.7	15.5	17.7	16.5	11.4	14.1	11.6
				**		†							
50	15.3	4.2	-	20.0	6.3	5.4	4.5	13.4	14.0	14.1	9.9	12.1	11.0
					**				†	†			
60	11.2	2.6	-	15.0	17.9	4.7	-	12.3	14.0	16.5	9.0	10.9	8.9
Charge discharge rate limits	0.5-1	1-10	1-3	1.5-10	1-5	1.5-5	2-4	0.5-4	0.5-2	0.7-3	0.5-4	0.5-4	0.5-4

* Charged into H_2 evolution or potentiostated.

** Charge cut off shifted more cathodic.

† Current density reduced.

will serve as the basis for the following comparative discussion of electrode behavior, even though individual capacity values of the different electrodes may not be exactly comparable due to variations in operating conditions, such as current density and cutoff voltages. Significant changes during the cycling are indicated in the Table. More detailed information on the test behavior of each individual electrode was given in the Second Quarterly Report.

An important feature common to all silver-based electrode structures was the rapid decrease in capacity with increasing number of cycles. The rate of decrease was somewhat accentuated by cycling the electrodes at a constant current density, which results in an increasing charge and discharge rate as the electrode capacity decreases. Generally, a decrease in current density, a cathodic shift of the charge cutoff voltage, or charging into hydrogen evolution increased electrode capacity. After this initial increase, however, the capacity continued to decrease as before. This behavior is illustrated in Fig. 24a. Potentiostating the electrode at -1.2 V versus Hg/HgO overnight (H_2 evolution <0.1 cc) also restored part of the "lost" capacity.

The initial utilization of active material varied with the different electrode structures. For example, plates of type "220" showed an initial utilization of approximately 40 to 50% of the theoretical capacity. The modification of these structures by the use of $AgNO_3$ and Ag_2O resulted in a roughening of the internal surfaces, increasing the initial utilization to approximately 75% of the theoretical value. The very fine structures of type "300" also exhibited a high initial utilization.

The rate of decrease of electrode capacity as a function of the number of cycles was, however, remarkably similar for the wide variety of plaque structures. This is graphically illustrated in Figs. 25 and 26. Generally, under these conditions, the electrodes lost approximately half of their capacity after 5 to 10 cycles, and this value was again cut in half at approximately 20 to 30 cycles. A closer analysis of the cycling data showed that the capacity loss did not appear to be confined to either the charge or the discharge cycle. As Table IV shows, the capacity between two preset potential values changed continuously from charge to discharge and following charge, etc.

In order to obtain a reliable basis for comparison of silver sinter-based Cd electrodes with conventional nickel sinter Cd electrodes, we subjected the latter to the same test conditions. The upper voltage cutoff was set to approximately -1 V versus Hg/HgO to avoid H_2 evolution. The results are shown in Fig. 26a. The

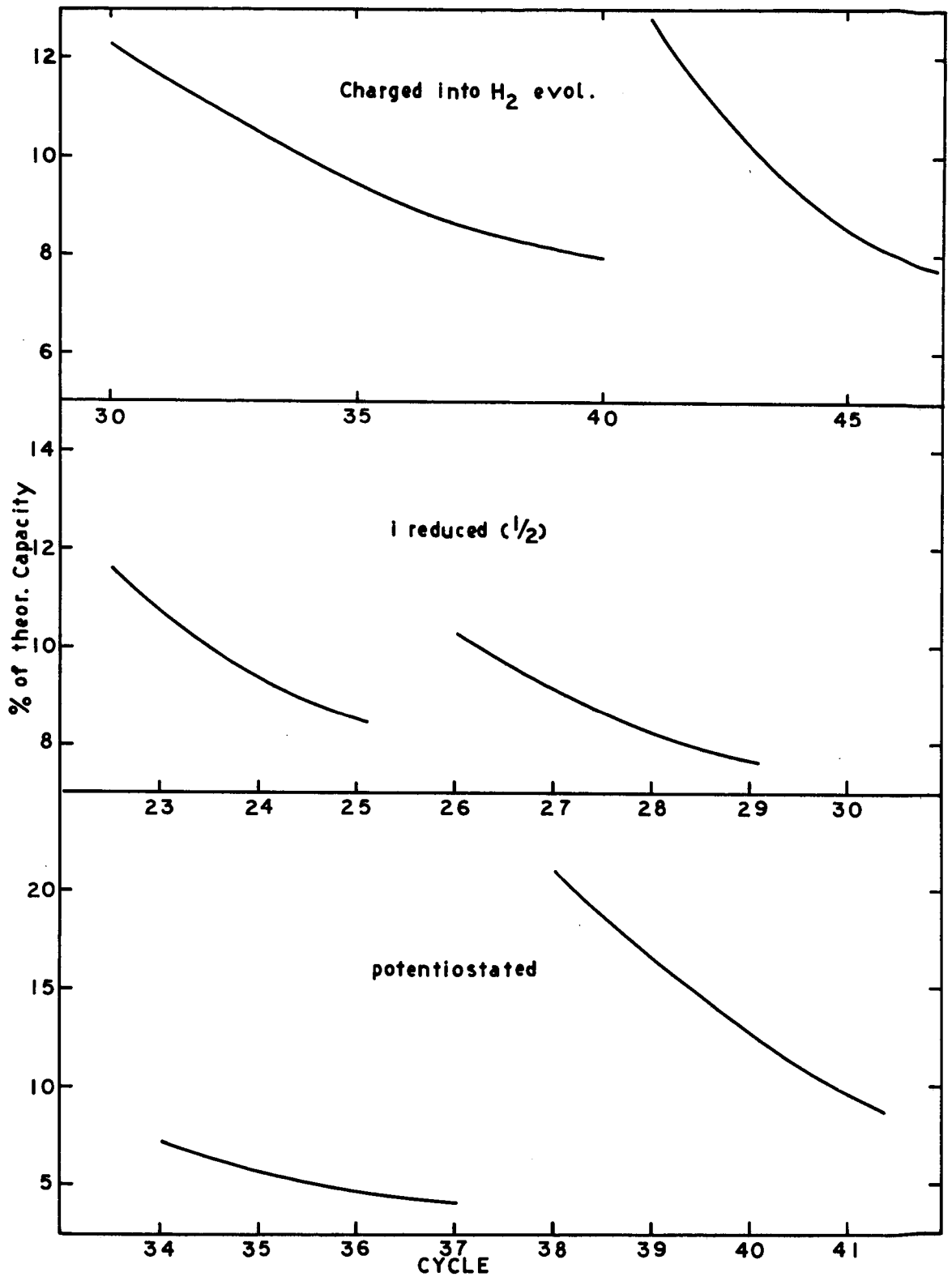

Fig. 24a. Effect of operating conditions on the capacity of Cd impregnated silver sinters

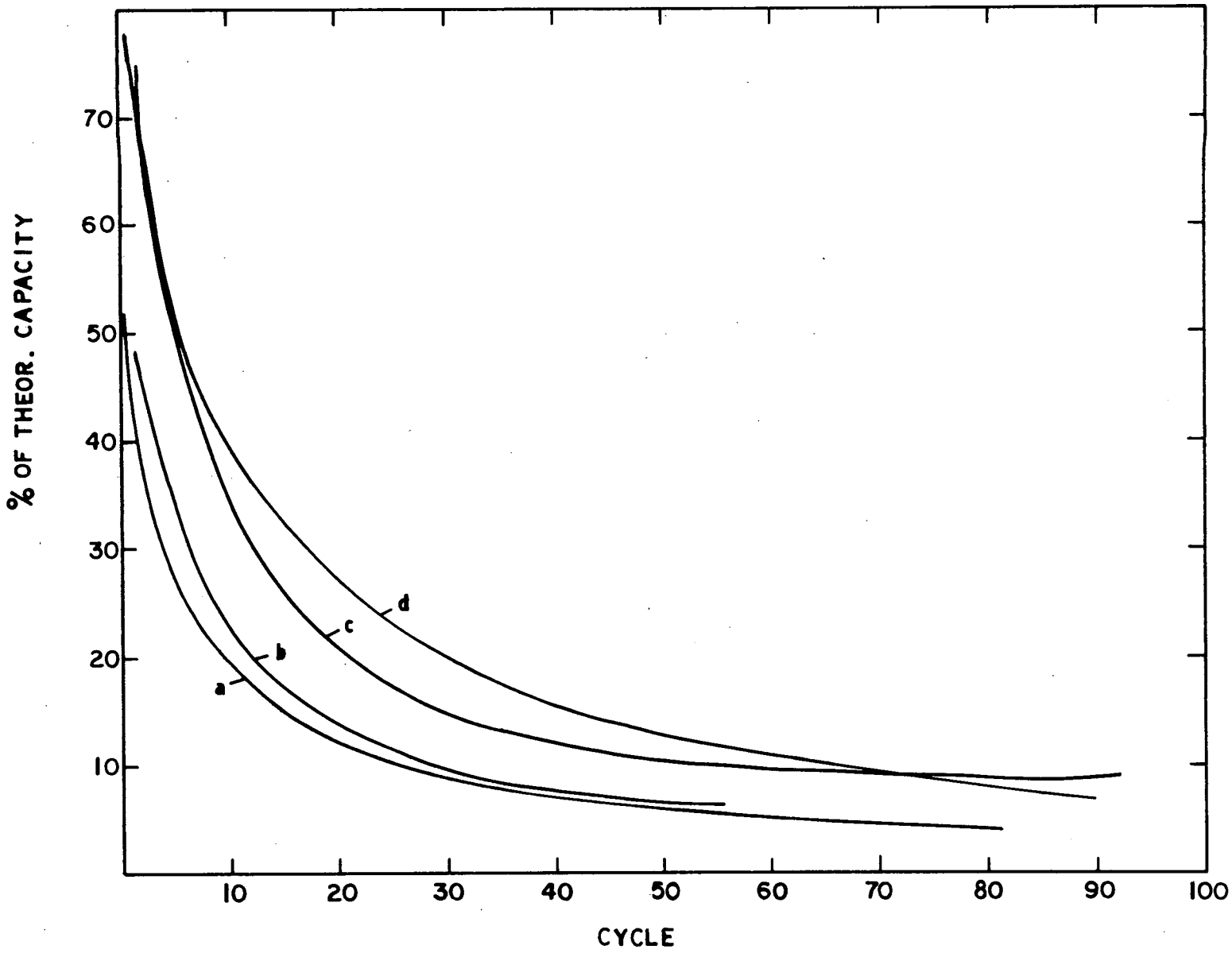

Fig. 25. Capacity change of-Cd impregnated silver sinters [a, types 130 and 220; b, type 150; c, type 300; d, type 220 modified (room temperature 25% KOH)]

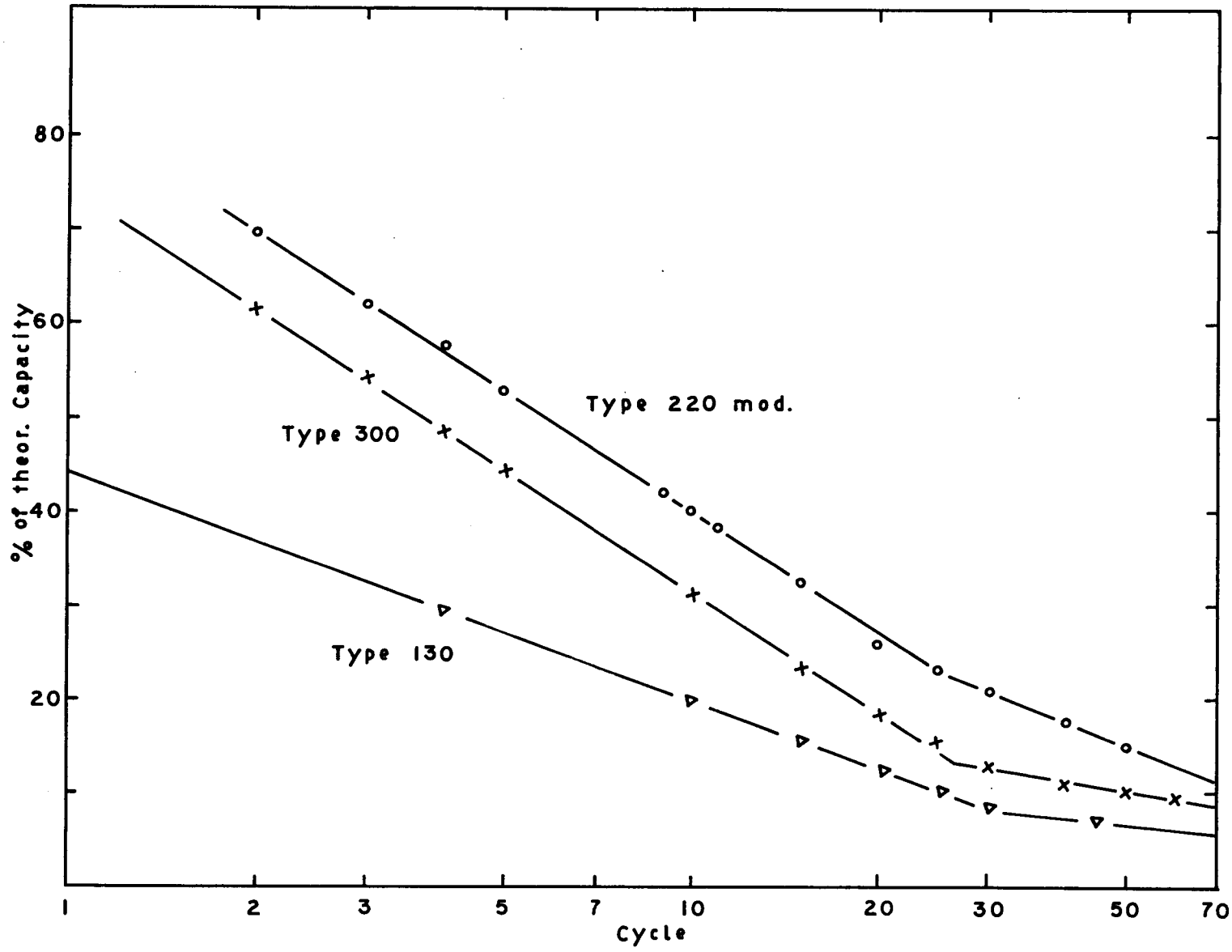

Fig. 26. Capacity change of Cd-impregnated silver sinters (room temperature)

Table IV. Charge and Discharge Times Between Preset Voltage Limits at Constant Current Density

	SS Cd-2		SS Cd-3	
Cycle No.	Charge, hr	Discharge, hr	Charge, hr	Discharge, hr
1	1.25	0.88	1.5ψ	1.18
2	0.83	0.68	1.05	0.90
3	0.64	0.56	0.82	0.75
4	0.52	0.49	0.72	0.67
5	0.47	0.42	0.65	0.62
10	0.30	0.28	0.47	0.45
11	0.28	0.26	0.45	0.43
12	0.27	0.25	0.42	0.41

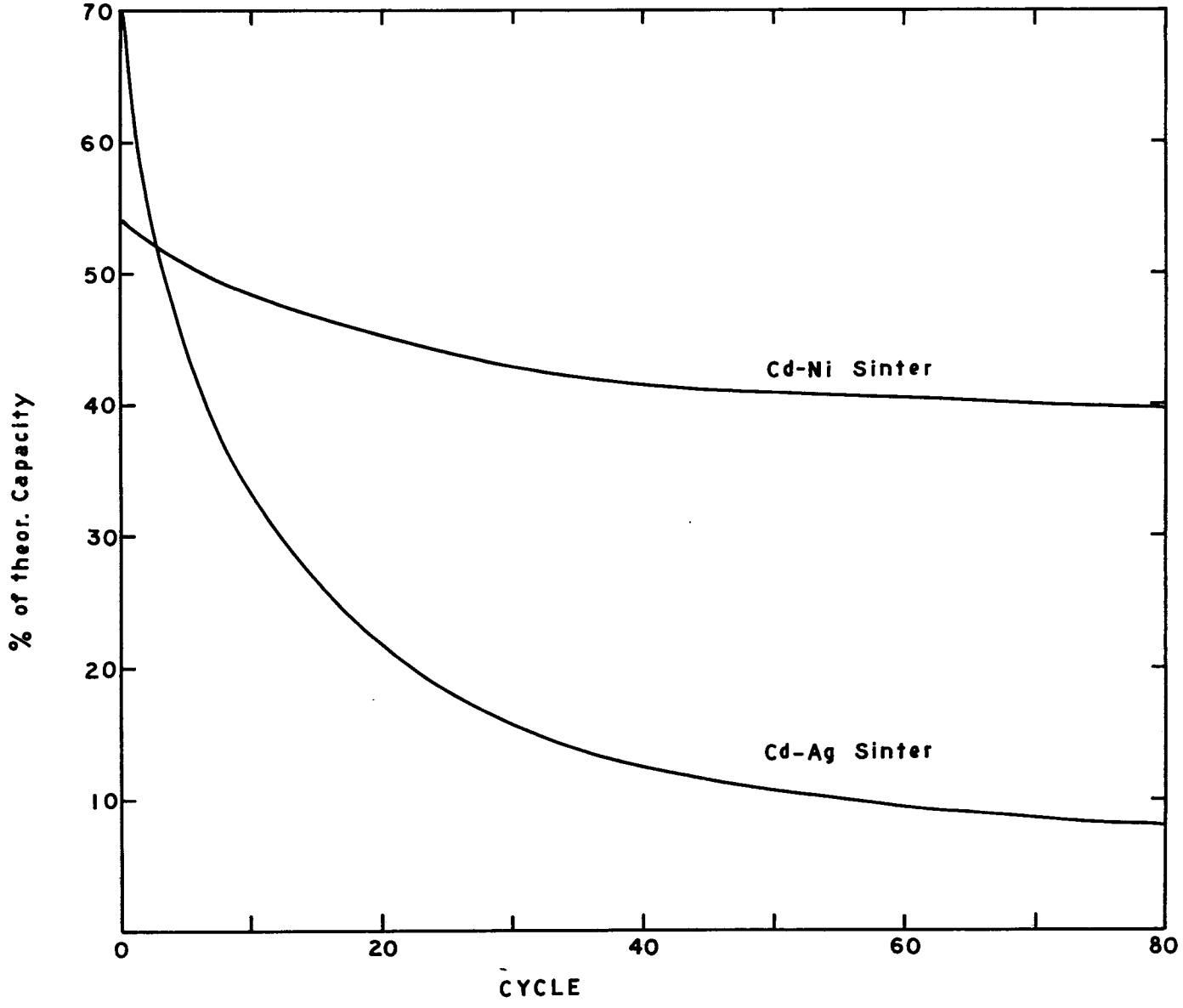

Fig. 26a. Capacity change of Cd impregnated Ag and Ni sinters (room temperature)

pertinent data for NS Cd-3 and NS Cd-4 are included in Table II. In analogy to some early testing of silver sinter-based electrodes, NS Cd-3 was not subjected to any prior formation cycling. This caused no significant difference; except for the first few cycles, these nickel sinter-based Cd electrodes showed only a very small change in capacity upon cycling. For example, the capacity of NS Cd-3 changed between cycle 25 to 225 only from 38.8% to 34% of its theoretical capacity.

This result has important implications. It proves that the testing procedure (flooded operation in an excess of electrolyte, cycling at relatively high rate between fixed potential values) cannot account for the observed differences in behavior between silver sinter- and nickel sinter-based cadmium electrodes.

To obtain further information which could explain the unexpected behavior of silver sinter-based Cd electrodes, we investigated the morphology of cycled structures by scanning electron microscopy. Figs. 27 to 32 show scanning electron microscope cross sections of various cycled electrodes. Especially noteworthy are the needle shaped crystals in the cycled electrodes SS Cd-4 and SS Cd-5 (Figs. 27 and 28). Fig. 29 shows a "220" type plaque after three cycles. There were few larger crystals in this structure. The internal silver surface was quite uniformly covered by a very fine crystalline mass. Cycled electrode SS Cd-8 is shown in Fig. 30. Large, regularly shaped crystals located throughout the sinter structure with no apparent needles were observed. In electrode SS Cd-12, the large regularly shaped crystals could be seen more clearly. It should be noted that cycling of this electrode was interrupted in the fully charged state. Even though needle shaped crystals are not apparent in this photomicrograph, a higher magnification showed that they were present in this structure (Fig. 31).

For comparison, Fig. 33 shows a cycled nickel sinter-based electrode (NS Cd-4). Crystalline and amorphous particles seem to be intermixed. No needle shaped crystals were detectable.

4. Conclusions

The silver sinters investigated here covered a wide variety of different structures with respect to both pore size and pore-size distribution. The initial utilization of active material depended on the plaque type. The rate of capacity decrease with the number of cycles was surprisingly independent of structure; it was considerably higher than with nickel-based Cd electrodes tested under the same conditions.

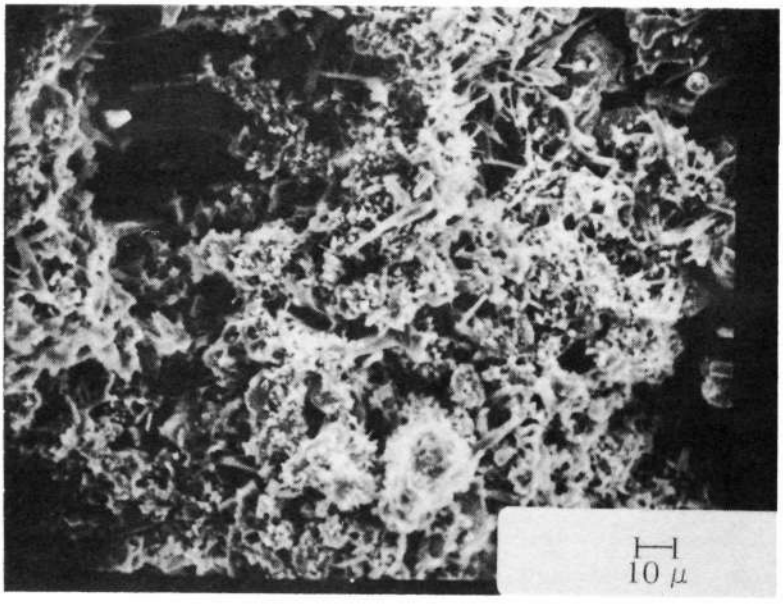

Fig. 27. Cycled Cd-impregnated Ag sinter 130 (SS Cd-4, >150 cycles, discharged)

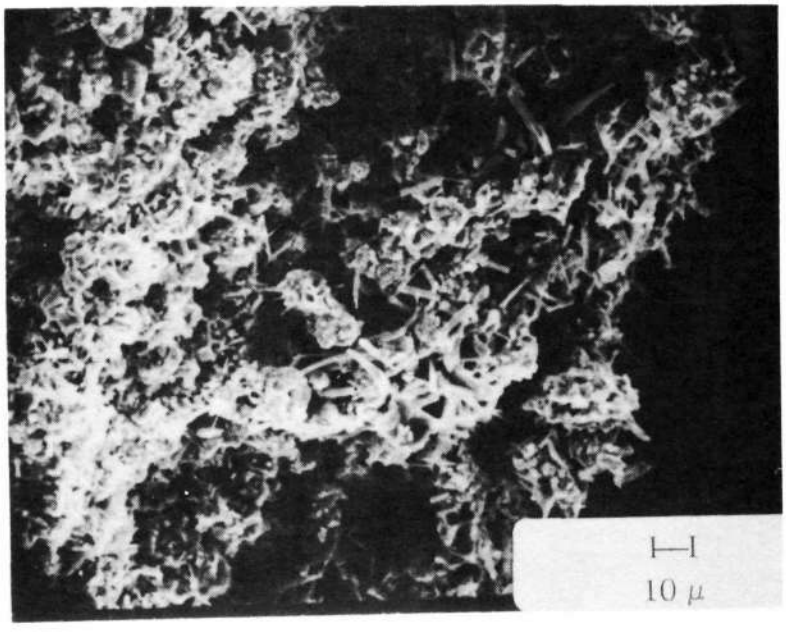

Fig. 28. Cycled Cd-impregnated Ag sinter 150 (SS Cd-5, >125 cycles, discharged)

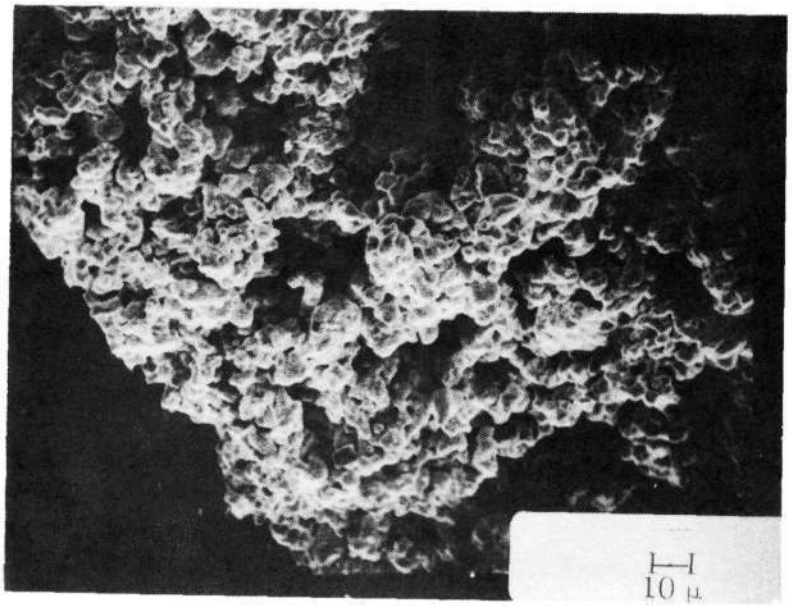

Fig. 29. Cycled Cd-impregnated Ag sinter 220 (three cycles, 80% discharged)

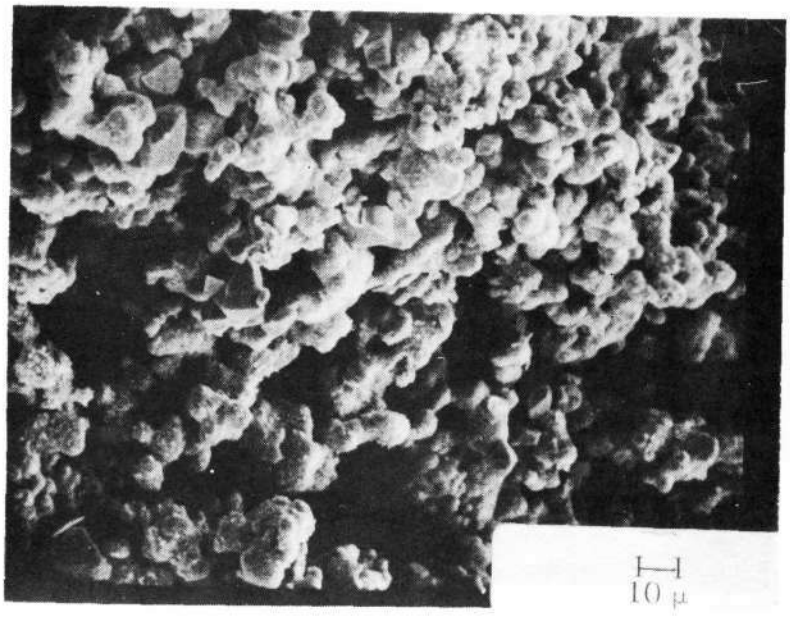

Fig. 30. Cycled Cd-impregnated Ag sinter 220, $AgNO_3$ modified (SS Cd-8, 133 cycles, 83% discharged)

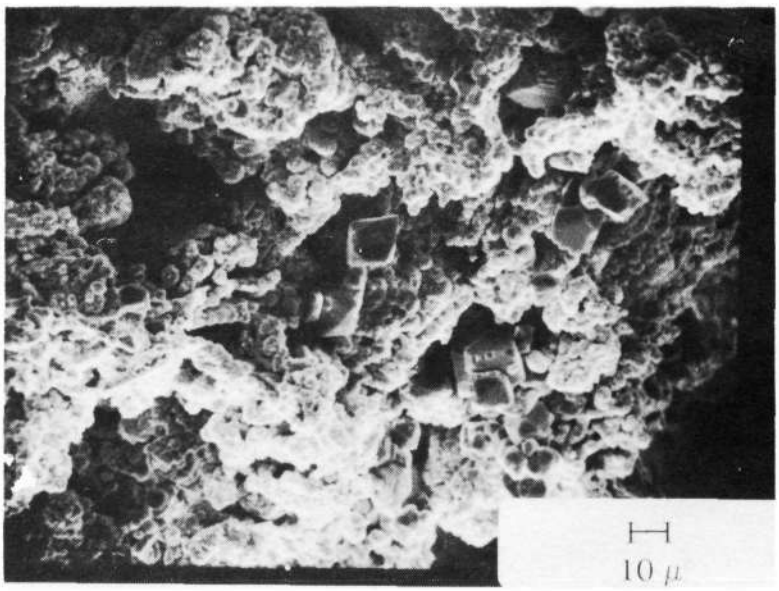

Fig. 31. Cycled Cd-impregnated Ag sinter 300 (SS Cd-12, 104 cycles, charged)

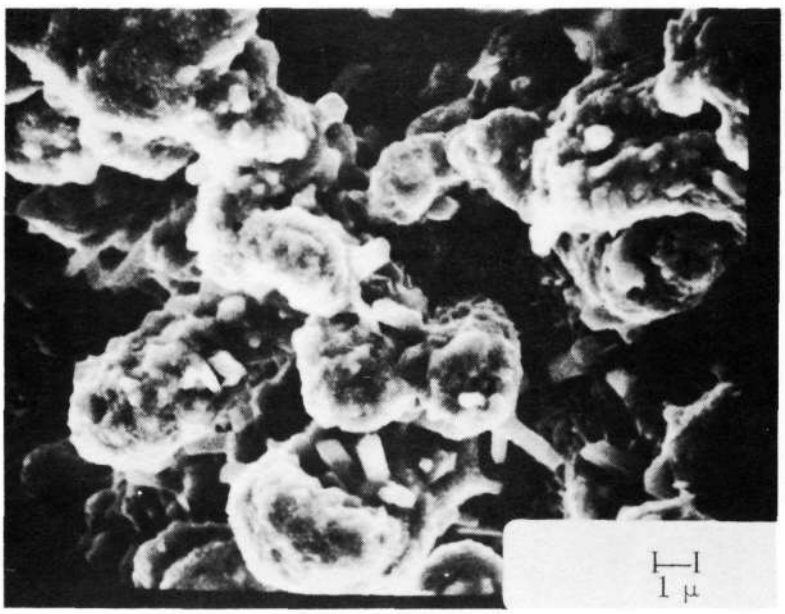

Fig. 32. Cycled Cd-impregnated Ag sinter 300 (SS Cd-12, 104 cycles, charged)

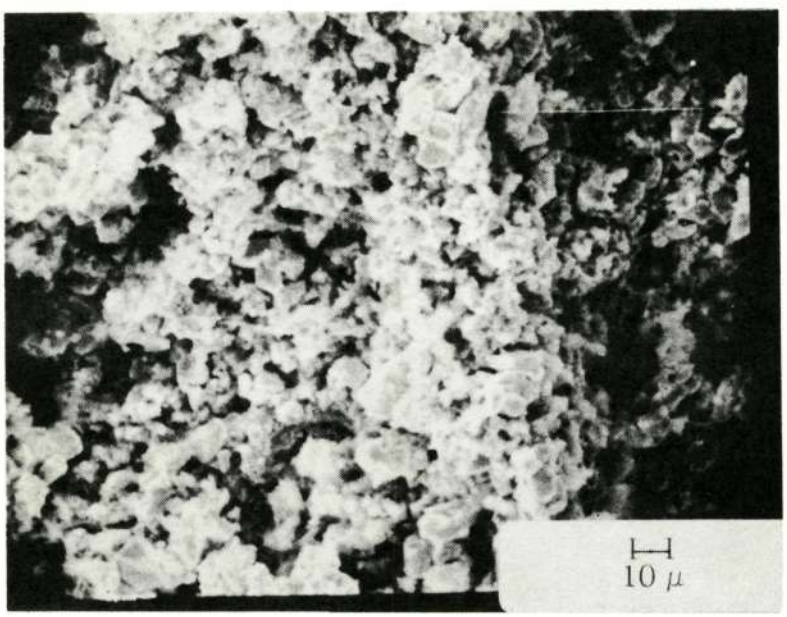

Fig. 33. Cycled Cd-impregnated Ni sinter (NS Cd-4, 73 cycles, 60% discharged)

Scanning electron micrographs of cycled electrodes showed the presence of needle shaped crystals in silver sinter-based Cd electrodes which could not be detected in nickel sinter-based electrodes. To establish the significance of this difference requires further investigation. The use of silver as the plaque material in addition to plaque structure may have a bearing on the electrochemical behavior of these silver sinter-based Cd electrodes. However, this requires further investigation.

D. Teflon-Bonded Cadmium Electrodes

1. Introduction

Teflon-bonded cadmium electrodes have found some interest in connection with the development of non-magnetic batteries,[9] (e.g., cadmium silver cells). However, no systematic investigations concerning their structure and electrochemical behavior have been carried out. In the following we report on an exploratory investigation of various preparation procedures and on the effect of silver powder and Teflon binder content. Silver powder is used as a conductive filler with the intent of increasing the electronic conductivity throughout the electrode structure.

2. Electrode preparation

Various procedures for the fabrication of Teflon-bonded cadmium electrodes were evaluated. The basic steps are: (1) the preparation of a paste by mixing the cadmium oxide or hydroxide and, in some cases, various amounts of silver powder (e.g., Handy and Harman Silpowder 150) with the specified amounts of Teflon in the form of a suspension (Teflon 30, Dupont) and sufficient water to obtain a suitable consistency; (2) distributing the paste evenly on both sides of an expanded metal substrate (Exmet 5 Ag 10 3/0 or 10 Cd 10 3/0); (3) drying and pressing of the electrodes (typically at $\sim$ 2500 lb/in.^{2}); and (4) sintering of the electrode typically for 10 min at 275 °C in a N_2 atmosphere. Electrodes prepared by pressing a presintered powder mixture of CdO and Teflon into a mold had less favorable mechanical properties. These exploratory experiments have been described in detail in previous reports.[9,10]

The cadmium hydroxide used was prepared by rapid addition of 8.5 N KOH (4% in excess of the stoichiometric amount) to a vigorously stirred 0.3M $Cd(NO_3)_2$ (Baker Reagent Grade) solution at 70 °C. The white precipitate was filtered, washed with triply distilled water to neutrality, and dried at 65 °C.

3. Electrochemical evaluation of Teflon-bonded structures

All electrodes were tested in electrochemical cells equivalent to the one described earlier. Normally the formation consisted of potentiostating the electrode at -1.2 V versus Hg/HgO for 12 to 24 hours. While sintered electrodes show a greenish brown to brown color from CdO, formed electrodes were always dark grey independent of their state of charge. The test regime consisted of full charge/discharge cycles between -1.2 and -0.75 V versus Hg/HgO at current densities corresponding to rates between C and C/2. Occasionally the charging cycle was allowed to continue beyond the -1.2 V (versus Hg/HgO) cutoff voltage and the gassing behavior of the electrodes was observed. Representative charge and discharge curves for silver containing electrodes are shown in Figs. 34 and 35. The basic shape of the potential-time curves is similar for all electrodes. The potential is fairly constant during the charging process, followed by a fairly rapid potential increase towards the end of the charging cycle. In some instances, the potential rise at the end of the charging cycle showed a plateau presumably reflecting the reduction of that $Cd(OH)_2$ which is not in good electronic contact with the screen.

Small individual gas bubbles at the electrode were initially observed at potentials above -1.2 V (versus Hg/HgO). At electrode TFE-1, significant gas evolution did not occur until -1.3 to -1.4 V. At electrode TFE-3, which contained a larger amount of silver as a conductive filler (~ 12% versus 5%), the gassing occurred approximately 50 mV less negative. All electrodes continue to accept charge well beyond the beginning of gas evolution. Electrode TFE-1 showed some light shedding at the end of cycling. Electrode TFE-3 showed surface disruption but practically no shedding. The high and continuously increasing value of the charging potential observed in some instances, as well as the additional charge acceptance beyond the start of gas evolution, appear to be due to lack of good electronic contact between the current collector grid and active materials, thus giving rise to an ohmic potential drop. A typical charge/discharge cycle of TFE Cd-1, an electrode which contained no silver at all, is shown in Fig. 36. The advent of gas evolution occurred at -1.28 V versus Hg/HgO, which was approximately 70 mV more cathodic than with silver containing Teflon-bonded electrodes. A scanning electron micrograph of this electrode after cycling showed distinct hexagonal crystals. (Fig. 37).

The useable capacity of all Teflon-bonded cadmium electrodes decreased with increasing cycle number. The actual delivered capacities did depend on the operating

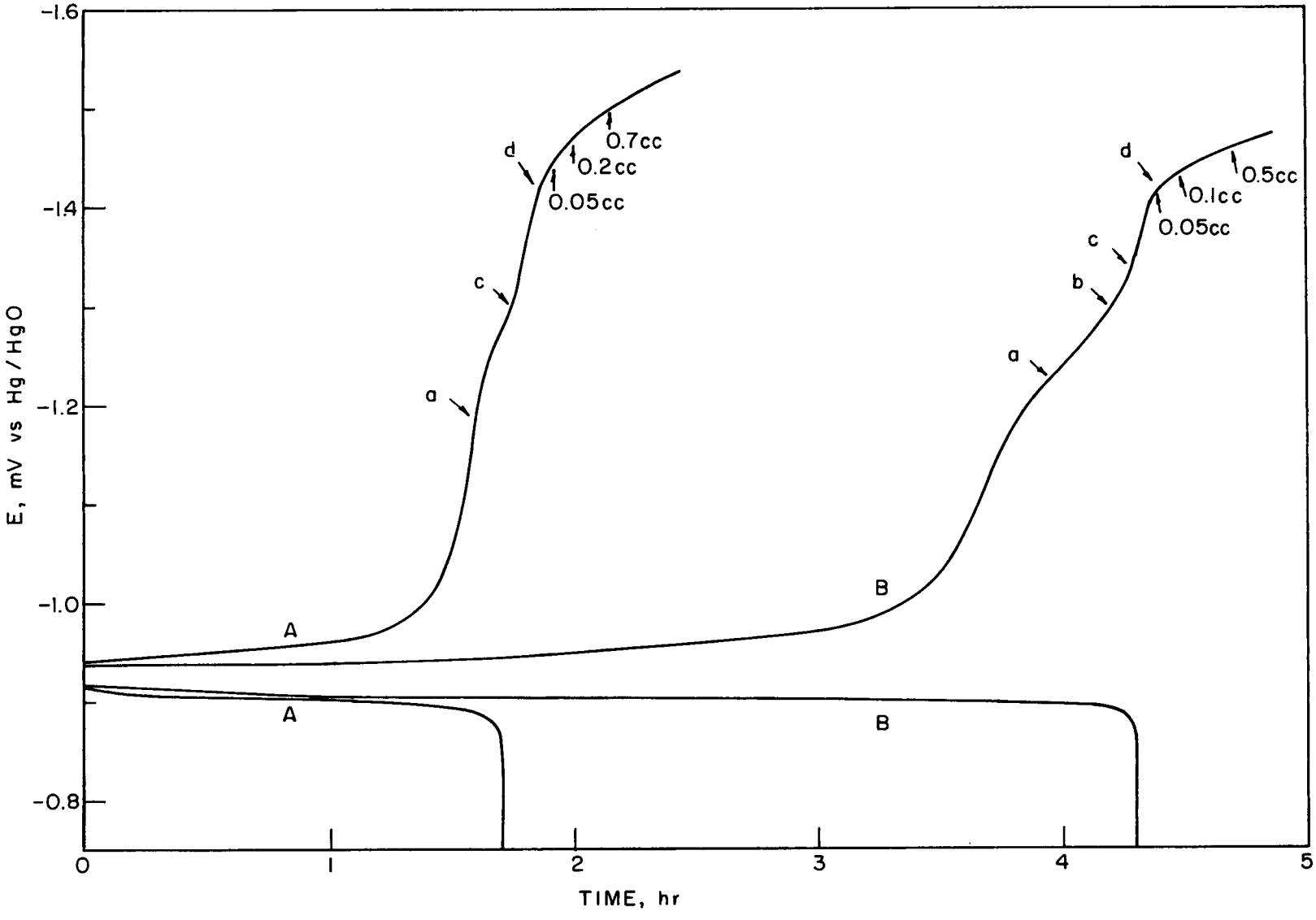

Fig. 34. Charge/discharge cycles of Teflon-bonded Cd electrode TFE-1 (25°C, A = 14th cycle 5.5 mA/cm^2, B = 16th cycle 2.75 mA/cm^2; a = individual small bubbles, b = regularly small bubbles, c = slow gassing, d = moderate gassing)

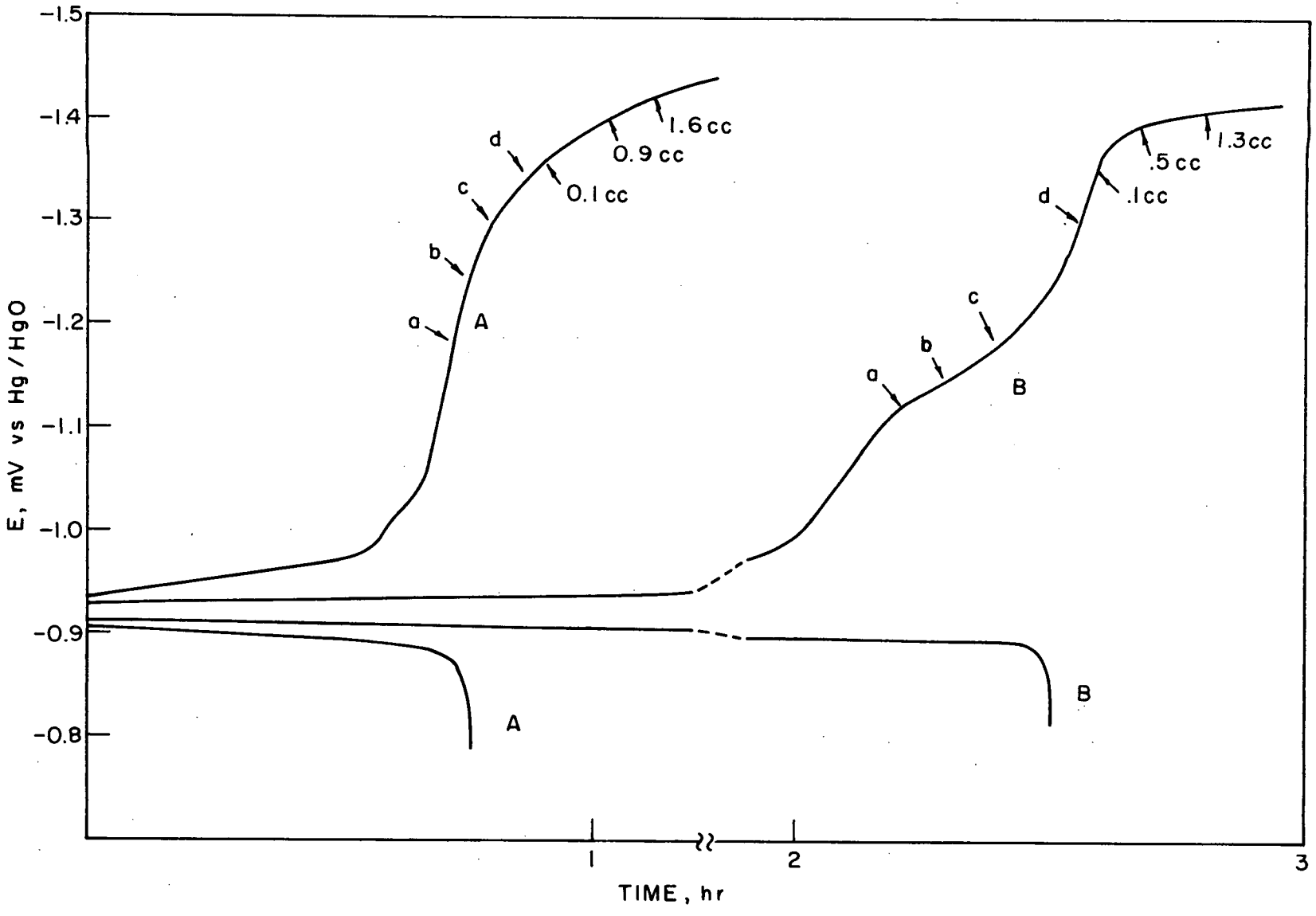

Fig. 35. Charge/discharge cycles of Teflon-bonded Cd electrode TFE-3 (A = 17th cycle, 8.3 mA/cm^2; B = 18th cycle, 4.15 mA/cm^2; a = first individual small bubbles, b = regularly small bubbles, c = weak gassing, d = moderate rate gassing)

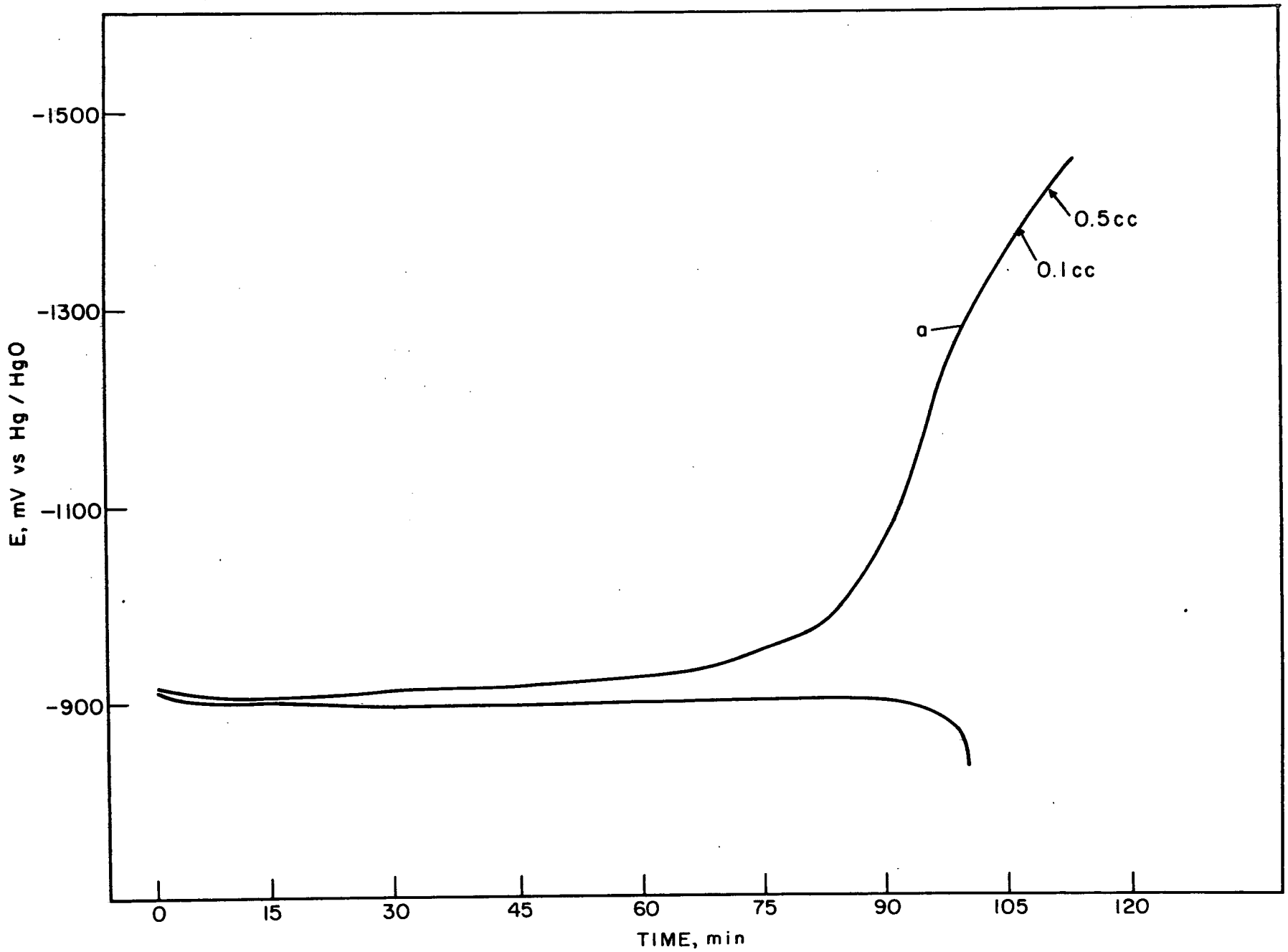

Fig. 36. Charge/discharge cycles of Teflon-bonded Cd electrode TFE Cd-1 (cycle no. 9, 5 mA/cm^2, 25% KOH, room temperature, a = first individual small bubbles)

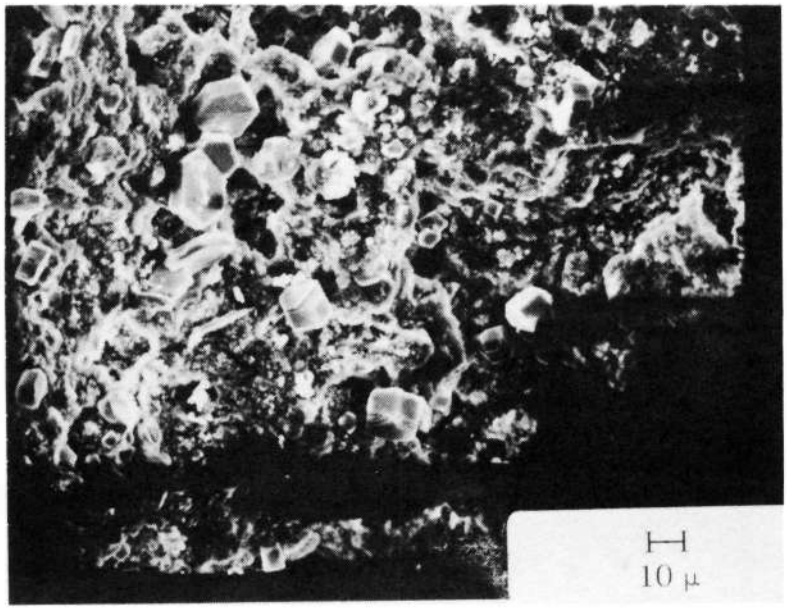

Fig. 37. Cycled Teflon-bonded electrode TFE Cd-1 (85 cycles, discharged)

conditions in much the same way as discussed in some detail in connection with cadmium impregnated silver sinters. So, for example, an increased capacity resulted by reducing the charge and discharge rate, by over-charging, or by potentiostatically holding the electrode at a potential cathodic to the plateau potential but below hydrogen evolution (e.g., between -1.0 and -1.2 V versus Hg/HgO).

The effect of electrode composition on capacity as a function of cycle number was more systematically investigated in a parametric study. The variables were: (1) Teflon content, (2) level of Ag filler, and (3) the substrate material (in some cases). The electrodes were cycled between -1.3 to -0.75 V versus Hg/HgO at approximately the 1-hr rate.

The capacities as a function of cycle numbers for the different electrodes tested are shown in Table V. The capacity change is also graphically illustrated for two extreme examples in Fig. 38. From the performance of the different electrodes, we can draw the following conclusions:

a. Increasing the Teflon content from 5 to 15%, has an adverse effect on electrode capacity. Mechanical stability is only slightly better at the higher Teflon content.

b. Increasing the silver powder content from 0 to 5 to 10% lowers electrode capacity.

c. The use of cadmium instead of silver as substrate material at otherwise equal electrodes improved capacity.

Thus, this parametric study indicates that the most desirable performance characteristics should be obtainable with Teflon-bonded electrodes on cadmium or silver screen at low Teflon content and containing no silver powder as conductive filler. In order to determine whether the difference in performance between electrodes containing Cd instead of Ag substrates can be explained by the participation of the Cd screen in the cycling, we examined the cycling behavior of the bare expanded Cd metal screen. To roughen the surface, the Cd screen was subjected to 260 full cycles at a relatively high rate (~ 10 C), followed by cycles at approximately a C/10 rate. The measured capacity was 0.0024 Ahr/in.^{2}. Thus, the participation of the Cd substrate can only contribute less than 5% to the measured electrode capacity. This result is of further importance since it shows that Cd substrates can be used in practical electrodes without appreciable degradation during cycling.

Table V. Capacities (% of Theoretical) of Teflon Bonded Electrodes (Pressed)

	% Ag Powder	% Teflon				Cycle No.
Ag screen	0	5	5	15	15	
		[.016]	[.015]			
		62.5	64.3	-	-	1
		39.4	49.2	-	-	10
		34.9	44.8	-	-	20
		32.9	41.5	-	-	40
		29.4	37.8	-	-	60
		28.3	34.0	-	-	100
		[.025]	[.018]			
Cd screen	0	81.0	67.0	-	-	1
		53.0	43.0	-	-	10
		42.0	38.0	-	-	20
		[.017]	[.016]	[.015]	[.017]	
Ag screen	5	61.7	71.8	45.0	54.8	1
		51.0	45.0	42.0	44.3	10
		42.5	38.3	33.0	33.0	20
		37.6	34.2	23.0	26.0	40
		32.2	30.8	21.7	27.3	60
		27.0	28.0	20.2	24.1	100
				[.0195]	[.0173]	
Cd screen	5	-	-	61.8	82.0	1
		-	-	47.9	55.0	10
		-	-	39.9	44.0	20
		-	-	44.5	46.0	40
		-	-	39.0	44.0	60
		-	-	38.7	33.6	100
		[.0117]	[.0131]	[.023]	[.027]	
Ag screen	10	27.1	26.0	27.9	23.8	1
		33.0	36.0	14.9	11.0	10
		31.0	31.0	12.7	8.8	20
		23.0	21.0	8.7	5.6	40
		15.4	21.0	8.4	5.0	60
		-	-	6.1	4.7	100

[ ] = electrode thickness in inches

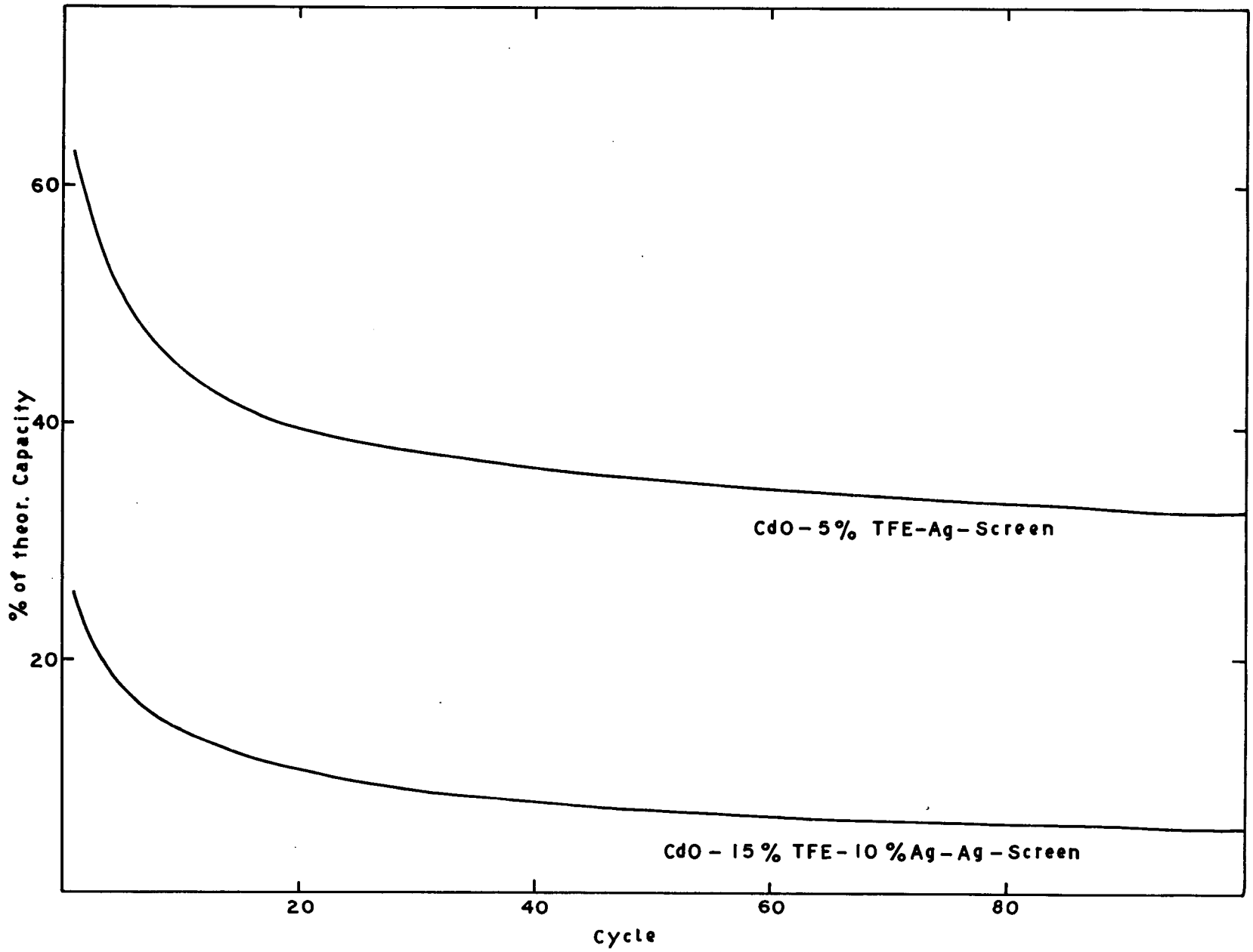

Fig. 38 Capacity as a function of full charge/discharge cycle

The results of this parametric study were somewhat unexpected, especially with respect to the negative effect of added silver powder on capacity retention upon cycling. It would be tempting to relate this behavior to that of cadmium impregnated silver sinters. At present it is, however, not appropriate to speculate on what, if any, effect silver might have or in which way it might influence the structure of Teflon-bonded electrodes. The negative effect of increased Teflon content appears to result from the increased hydrophobic character of the electrode and the isolation of some cadmium hydroxide.

E. Electrodeposited Sponge Cadmium

1. Cd sponge preparation

Our experiments were based on the results of an investigation by Henderson and Ladan[11] on the preparation and structure of electrodeposited cadmium sponge. Depending on experimental conditions (see Fig. 39), deposits of different morphology were reported. For a high electrochemical efficiency, the deposit must be present in a very fine state of subdivision. In addition, the deposit must be sufficiently porous to facilitate bulk transport to and from the electrode during cycling and, at the same time, should be very adherent to the substrate.

Henderson and Ladan defined in their experiments five types of deposits; I and II were crystalline; III was a dull grey non-adherent powder; IV was a non-adherent, dull black, brittle sponge; and V was a dull grey coherent sponge with good adherence to a "bright" cadmium substrate. Only type V appeared to be suitable for cadmium electrodes. The condition for the occurrence of each type are shown in Fig. 39.

The plating bath consisted of 100 g $CdCl_2$ and 130 g KCl in 1 ℓ of triply distilled water. The electrodeposition of cadmium was carried out at room temperature in a glass container. Two cadmium counterelectrodes were located parallel and equi-distant to the substrate, for which expanded cadmium metal and cadmium sheet (5 and 10 mil) were used with various surface pretreatments. Table VI summarizes the results. The morphology of the deposits varied between spongy and crystalline. The surface treatment of the substrate and thus the creation of suitable nucleation sites appeared to be of central importance. An example of a crystalline Cd deposit is shown in Fig. 40. Such deposits have a relatively low surface area and correspondingly low efficiencies when subjected to charge and discharge cycles. Fig. 41 shows a high surface area sponge with a dark grey appearance (sample No. 9).

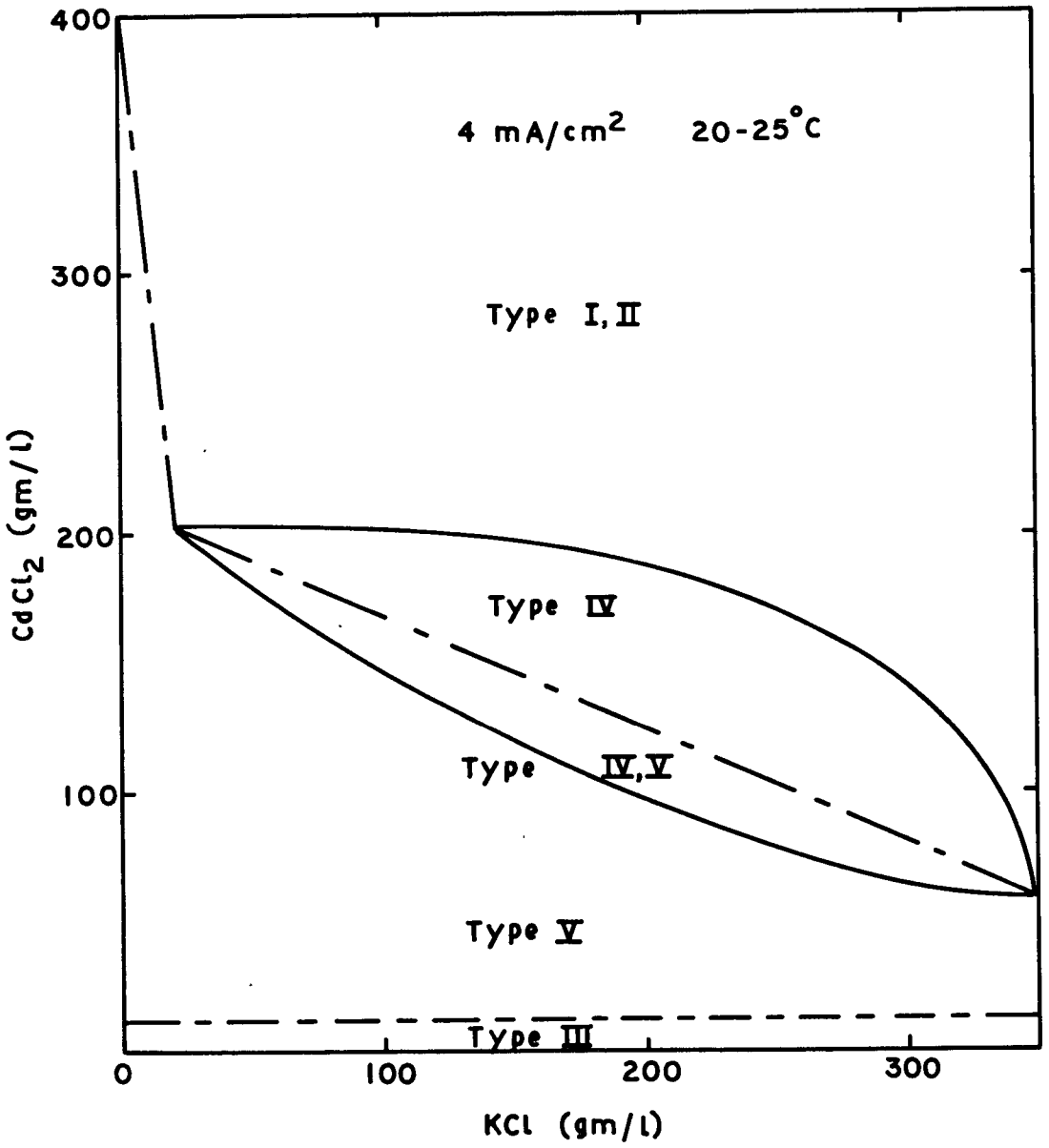

Fig. 39. A plot of $CdCl_2$ concentration versus KCl concentration showing the areas within which each of the five types of deposit was observed

Table VI. Electrodeposition of Sponge Cadmium on Cadmium (Solution: 100 g $CdCl_2$ + 130g CdCl/ℓ, Room Temperature)

Sample No.	Surface Preparation	i, mA/cm^2	Time, min	Deposit Morphology
1 Cd screen	Reduced in 30% KOH H_2O rinse	10	6	Crystalline
2		35	15	
3		5	45	
4 Cd sheet		30	20	Fine crystalline
5		30	35	Small area of sponge rest crystalline
6		30	50	Variable both types
7	Detergent wash H_2O rinse	30	20	Crystalline
8	Hand polished with alumina H_2O rinse	10	60	Good sponge poor adherence
9		60	60	Good sponge poor adherence
10		10	60	Crystalline
11		10	-	Variable results
12	Rinsed in KOH-ethyle alcohol misture (50-50 w/25% KOH)	20	120	
13	Anodic-cathodic treatment in 25% KOH	20	120	

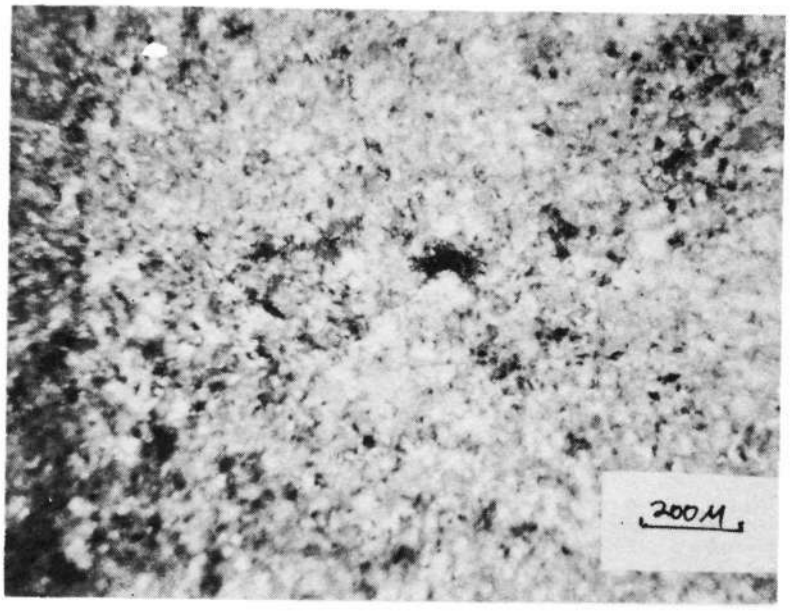

Fig. 40. Electrodeposited crystalline deposit

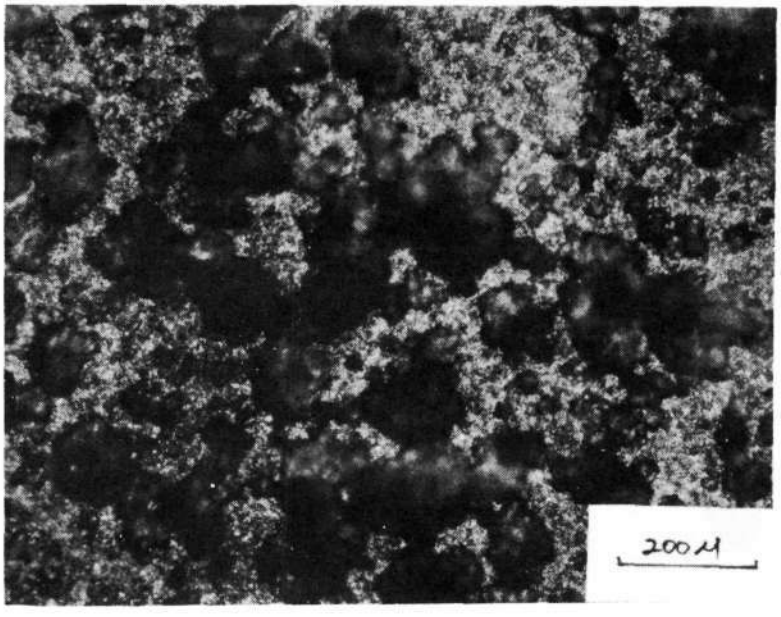

Fig. 41. Electrodeposited Cd sponge

2. Electrochemical evaluation

A cadmium deposit of similar appearance to the one shown in Fig. 41 was subjected to electrochemical testing. The electrode was cycled at room temperature between -1.24 V and -0.75 V versus a Hg/HgO reference electrode. Fig. 42 shows a typical charge/discharge cycle. At the end of charge, we observed a large potential change to hydrogen evolution. The advent of gas evolution occurred at approximately -1.3 V versus Hg/HgO.

The utilization and the change in capacity as a function of the number of charge/discharge cycles is shown in Table VII. As in our previous tests, we found a decrease in capacity with cycling. Extending the charge cycle to hydrogen evolution or holding the electrode potentiostatically at -1.2 V versus Hg/HgO increased the capacity considerably. The mechanical stability of the plated sponge was only moderately good, showing significant shedding during cycling.

Table VII. Capacity of Electrodeposited Cd-Sponge Electrode ES Cd-1, (Room Temperature, 25% KOH Cycled Between -840 mV to -1270 mV vs Hg/HgO Reference)

No. of Cycles	Discharge Time, hr	Capacity, % of Theoretical
1	3.04	54.5
2	2.90	52.0
5	1.04	37.0
10	0.86	31.0
45	0.98	17.0
		Full charge
50	1.79	32.0
60	1.19	21.0
100	1.02	18.5
175	0.95	16.0
Potentiostated to -1.2 vs Hg/HgO for 60 hr		
178	2.85	51.0
180	2.00	36.0
183	1.68	30.2

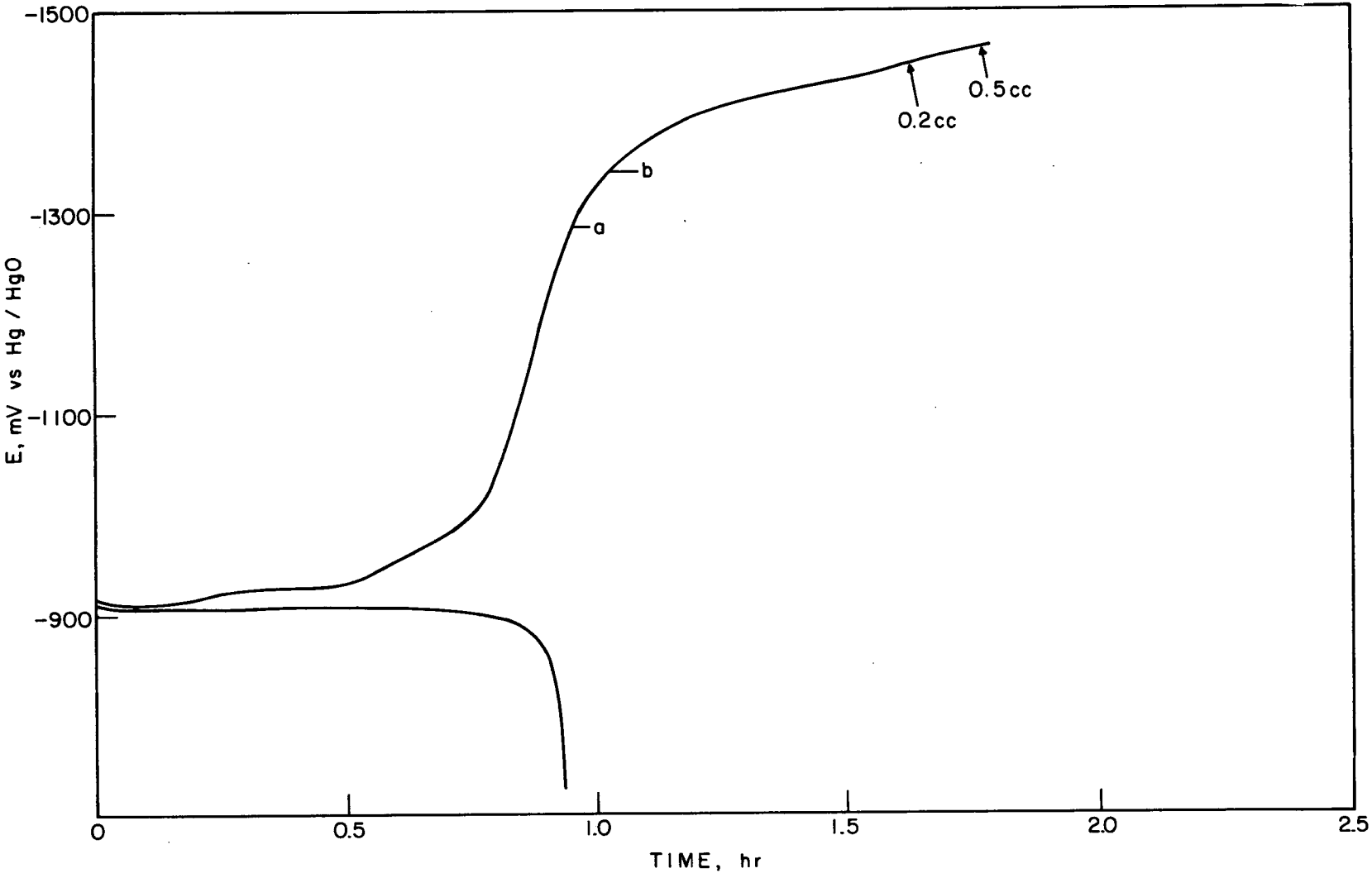

Fig. 42. Charge/discharge cycles of electrodeposited Cd sponge electrode ES Cd-1 (cycle no. 50, 5 mA/cm^2, 25% KOH, room temperature; a, first individual, small bubbles; b, moderate gassing)

F. Cadmium Sinter Based Structures

1. Preparation of Cd sinters

A feasibility study of manufacturing procedures for Cd sinter-based structures was carried out using high purity Cd (59 Cominco American) of different particle size. This material came from the same production lot (HPM 1185) and was classified according to ASTM screen fractions. We characterized the material further as shown in Table VIII.

Table VIII. Cadmium Powder Characteristics

Screen Size	Fischer Average Particle Diameter, μ	Bulk Density, g/cc	Packed Density, g/cc
-100	41	2.35	2.99
-200	30	2.66	3.51
-325	14	2.48	3.46

Scanning electron microscope pictures of Cd-200 and Cd-325 powders are shown in Figs. 43 and 44. The powders were irregularly shaped, especially in the case of Cd-325, and covered with a wide range of particle sizes.

In an effort to obtain cadmium plaques, we investigated the sintering of cadmium powders in argon, in hydrogen-helium mixtures, in the presence of a flux, and in the form of Cd-NaF compacts. These experiments have been described in detail previously.[10] Only two modified procedures of sintering cadmium powders in the form of Cd-NaF compacts resulted in plaques with sufficient mechanical strength to be tested as electrodes:

a. Cd-NaF compacts of 1-1/4 in. diameter were obtained by pressing a mixture of 60 vol % NaF and 40 Vol % of -325 Cd powder at 20,400 lb/in.^{2} The compact was heated in an inert atmosphere slightly above the melting point of Cd. After leaching, a mechanically sound structure of porous cadmium remained. A fractured cross section is shown in the scanning electron micrograph of Fig. 45. It is worth noting the extremely rugged internal surface of this structure.

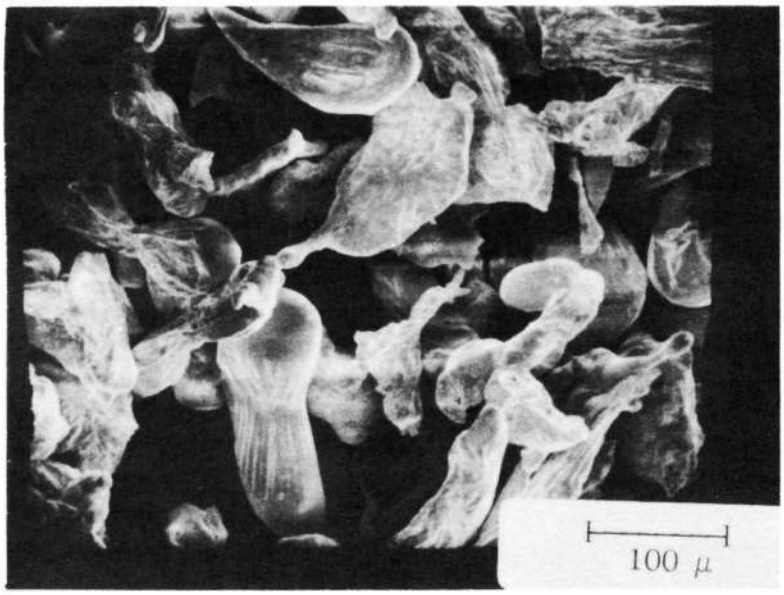

Fig. 43. Cadmium powder, Cominco-200

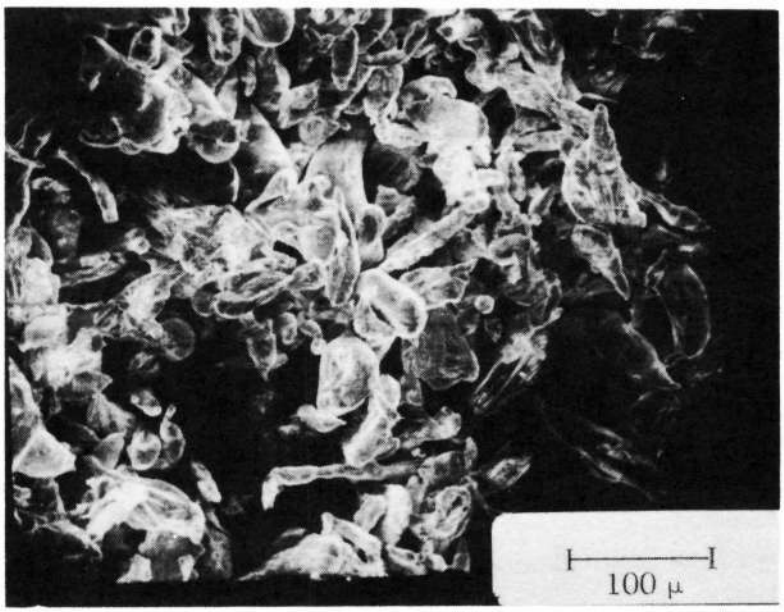

Fig. 44. Cadmium powder, Cominco-325

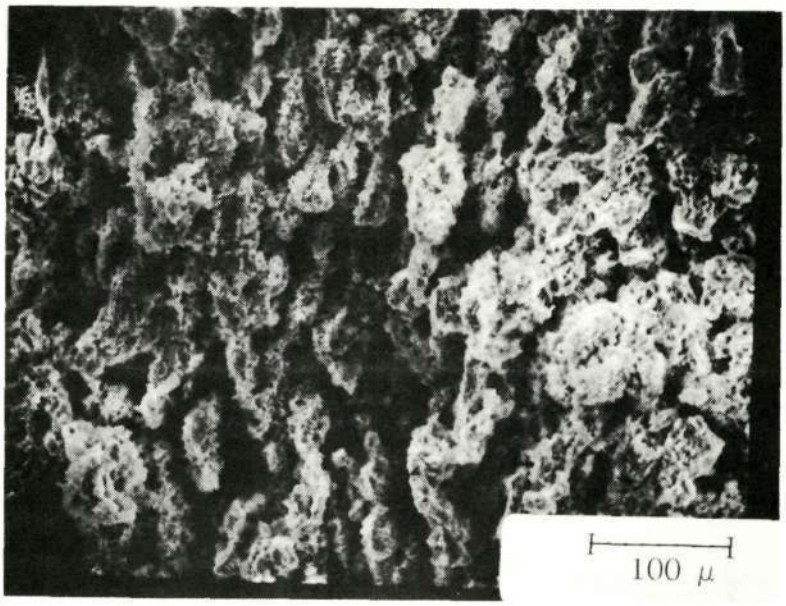

Fig. 45. Cadmium sinter (preparation method a)

b. This procedure is characterized by the addition of an inorganic salt which will melt below the desired sintering temperature and can act as a flux by dissolving the cadmium oxide. To explore this approach, the eutectic melt of 50 mol% KNO_3 and 50 mol% $NaNO_3$ (MP 220 °C) was ground to a fine powder and 5% by weight was added to the NaF-Cd mixture. After thorough blending, the mixture was compacted (18,500 psi for 5 min) and sintered at 290 °C for 20 min. The resulting structure, after leaching, exhibited reasonable mechanical strength. A scanning electron micrograph of a cross section is shown in Fig. 46. The actual structure of the cadmium sinter was masked by cadmium hydroxide crystals which precipitated upon leaching.

2. Electrochemical evaluation of Cd-sinter structures

A cadmium sinter plaque obtained by leaching of NaF-compact [preparation method (a)] was impregnated with cadmium hydroxide equivalent to a theoretical capacity of 0.125 Ahr and cycled at room temperature in 25% KOH. The capacity of this electrode (CdS-1) as a function of cycle number is shown in Table IX. The measured capacity continuously increased as a larger part of the cadmium sinter structure participated in cycling. After approximately 130 cycles, a maximum capacity was reached corresponding to over 50% utilization based on the total plate weight. After that, the capacity remained fairly constant until the electrode slowly disintegrated. This type of electrode disintegration should not be a significant problem in the constrained configuration of an actual battery. Typical charge and discharge cycles of this electrode are shown in Fig. 47. The charge and discharge plateaus are fairly flat, the charge plateau being followed by a large potential change prior to the end of charge. The advent of gas evolution occurred at -1.3 V versus Hg/HgO. After cycle 49, the cell was cooled to 5 °C. A typical cycle at that temperature is also shown in Fig. 47. There is little difference in shape between the cycles at 23 °C and 5 °C. However, at the same current density, the capacity at 5 °C is only approximately 2/3 of the value at 23 °C. The advent of hydrogen evolution at 5 °C occurs at approximately -1.4 V versus Hg/HgO

Fig. 48 represents a scanning electron micrograph of the electrode CdS-1 after cycling. It shows the wide-size distribution of the $Cd(OH)_2$ crystals.

Additional cadmium sinter structures with silver substrates were prepared using procedure (a). The electrochemical behavior was analogous to the one described

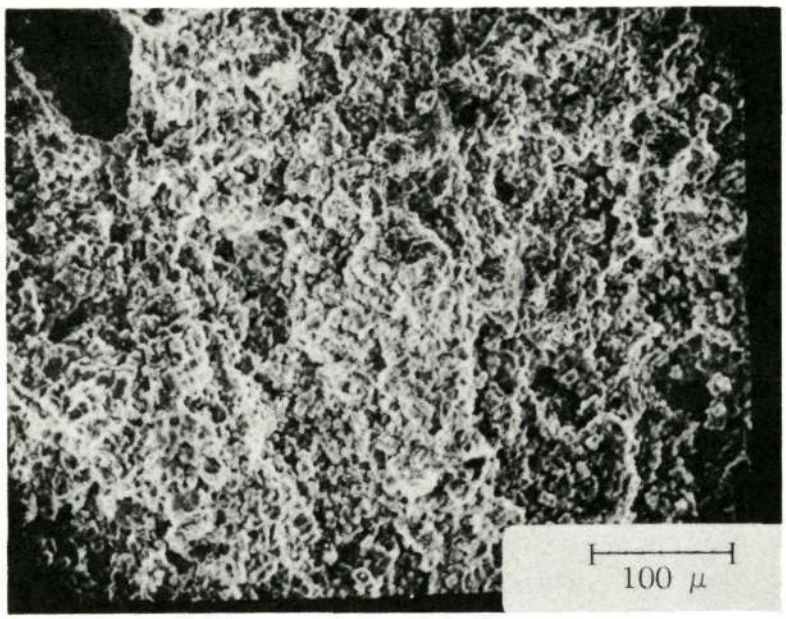

Fig. 46. Cadmium sinter (preparation method b)

Table IX. Capacity of Cd Sinter Based Cd Electrode Cd S-1 (Room Temperature, 25% KOH, 7.4 cm^2, 40 mil)

No. of Cycles	Discharge, hr	Capacity, Ahr	Comments
1	1.70	0.340	25.6 mA/cm^2; cycled from -850 mV to -1250 mV vs Hg/HgO
5	1.68	0.336	
10	1.50	0.300	
20	1.58	0.316	
30	1.84	0.368	
40	1.94	0.388	
50	1.08	0.216*	
60	2.15	0.430	
100	2.62	0.524	
120	2.74	0.548 Utilization 49% of plate weight	
130	2.80	0.560	
140	1.71	0.513	38.5 mA/cm^2; cycled as above
160	1.71	0.513 Electrode swollen, shedding	
180	1.47	0.442	
195	1.34	0.402 Electrode disintegrating	

* at 5°C.

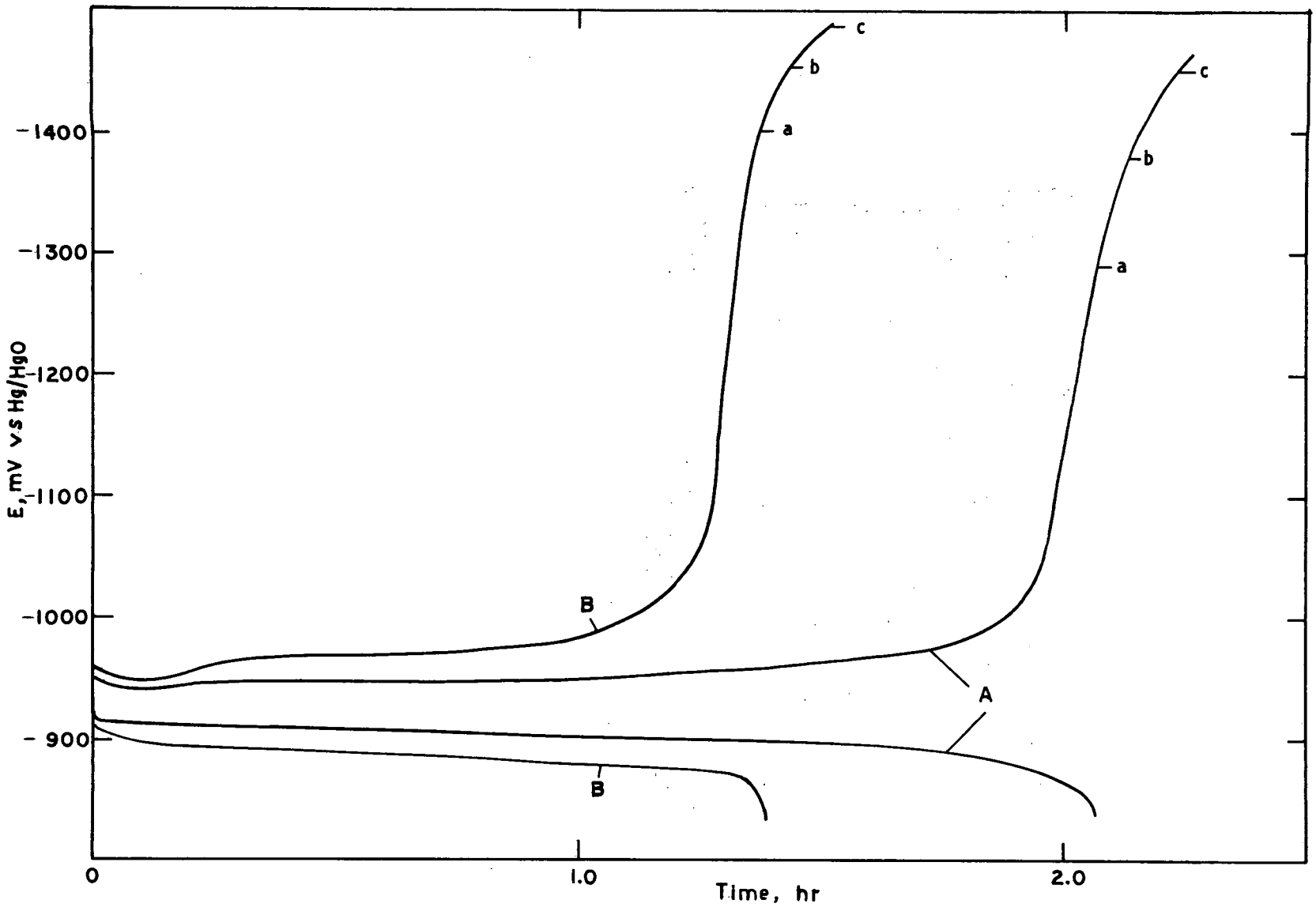

Fig. 47. Charge and discharge cycles of Cd sinter electrode Cd S-1 (25.3 mA/cm^2, 30% KOH; A, cycle 49 at 25°C; B, cycle 51 at 5°C; a, advent of gas evolution; b, moderate gassing; c, strong gassing)

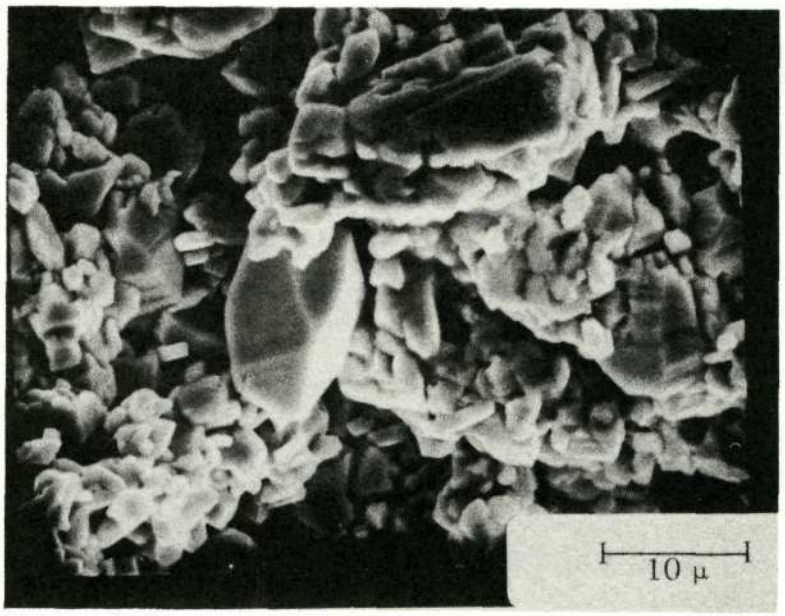

Fig. 48. Cycled Cd-sinter electrode Cd S-1 (196 cycles, discharged)

above. These cadmium sinters were tested without any impregnation with active material and thus the measured capacities were lower. Some problems regarding the adherence of the cadmium sinter to the expanded silver substrate were encountered. A typical structure is shown in Fig. 49. Here the electrode structure was sandwiched between two positive electrodes and subjected to full charge/discharge cycles at approximately the 1-hr rate. The maximum in capacity corresponds to 22% of the theoretical capacity based on the total electrode weight.

G. Discussion

We developed methods for preparation and examined the electrochemical behavior of the following electrode structures:

1. Cd impregnated Ag sinters,
2. Teflon-bonded cadmium hydroxide on Ag and Cd substrates,
3. Cd sinter structures on Ag and Cd substrates,
4. Electrodeposited sponge Cd on Cd substrates.

In order to judge and compare the feasibility of these structures for use as practical battery electrodes, we have to apply the following main considerations: (1) charge and hydrogen overvoltage characteristics, (2) capacity change during cycling, and (3) ease of manufacture.

Common to all structures are:

1. Fairly flat charging curves (potential versus time) and a large potential change at the end of charge.

2. An advent of hydrogen evolution (defined by the first appearance of small bubbles at the electrode surface) at highly cathodic potentials (-1.25 to -1.3 V versus Hg/HgO). The advent potentials for pure cadmium structures were approximately 50 mV more cathodic than at electrodes containing silver. The advent of hydrogen evolution at conventional nickel-based cadmium electrode structures occurred at below -1 V versus Hg/HgO.

With respect to capacity retention upon cycling, significant differences were observed between the various electrode structures. A comparison of the cycle behavior is given in Fig. 50. The cycle regime for this test consisted of full charge/discharge cycles between preset potentials at rates between C/2 and 2C in a flooded

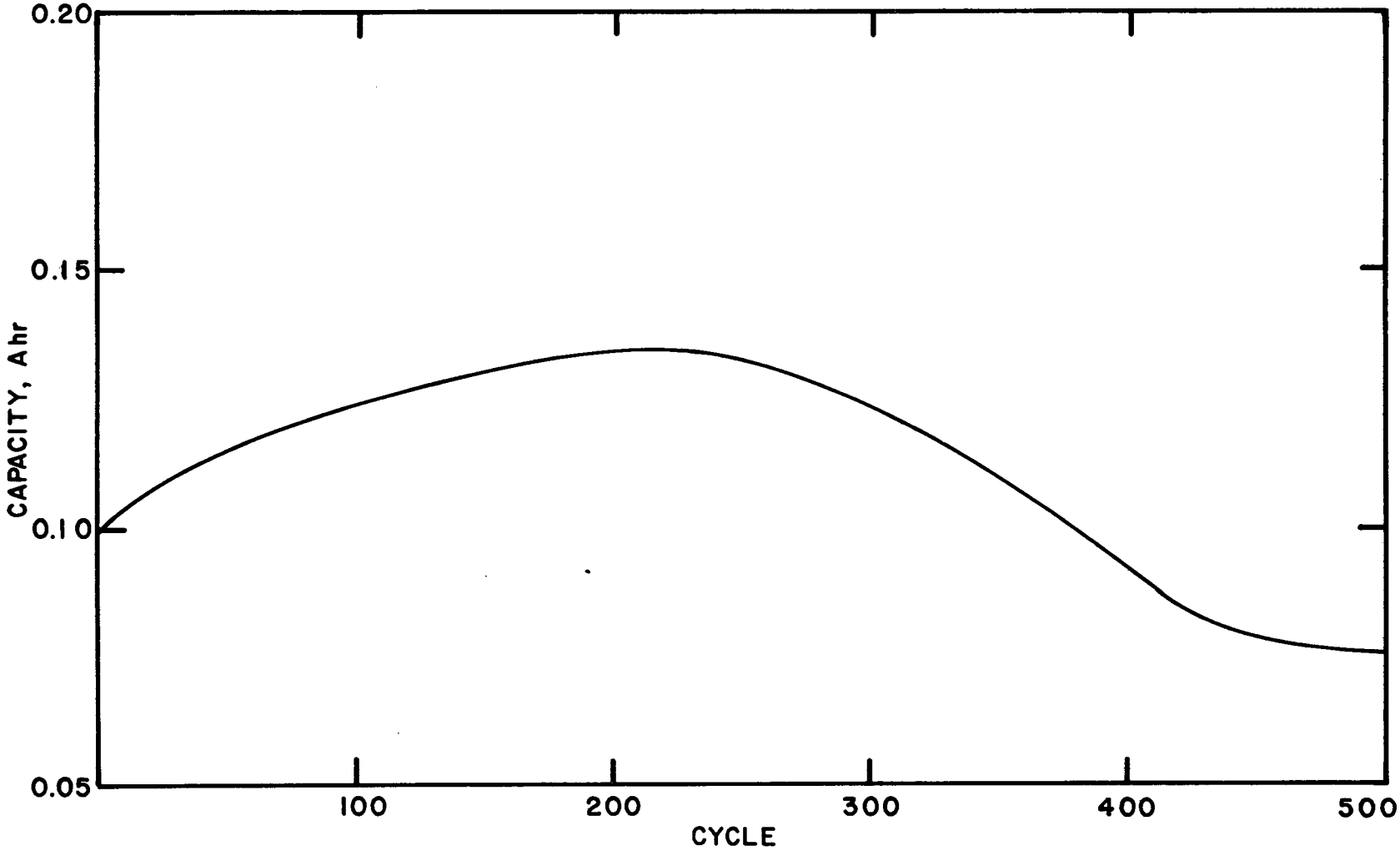

Fig. 49. Capacity of unimpregnated Cd Sinter Cd S-4, full charge/discharge cycles at rates between C and C/2 (8 cm^2, 0.035 in., room temperature, 30% KOH)

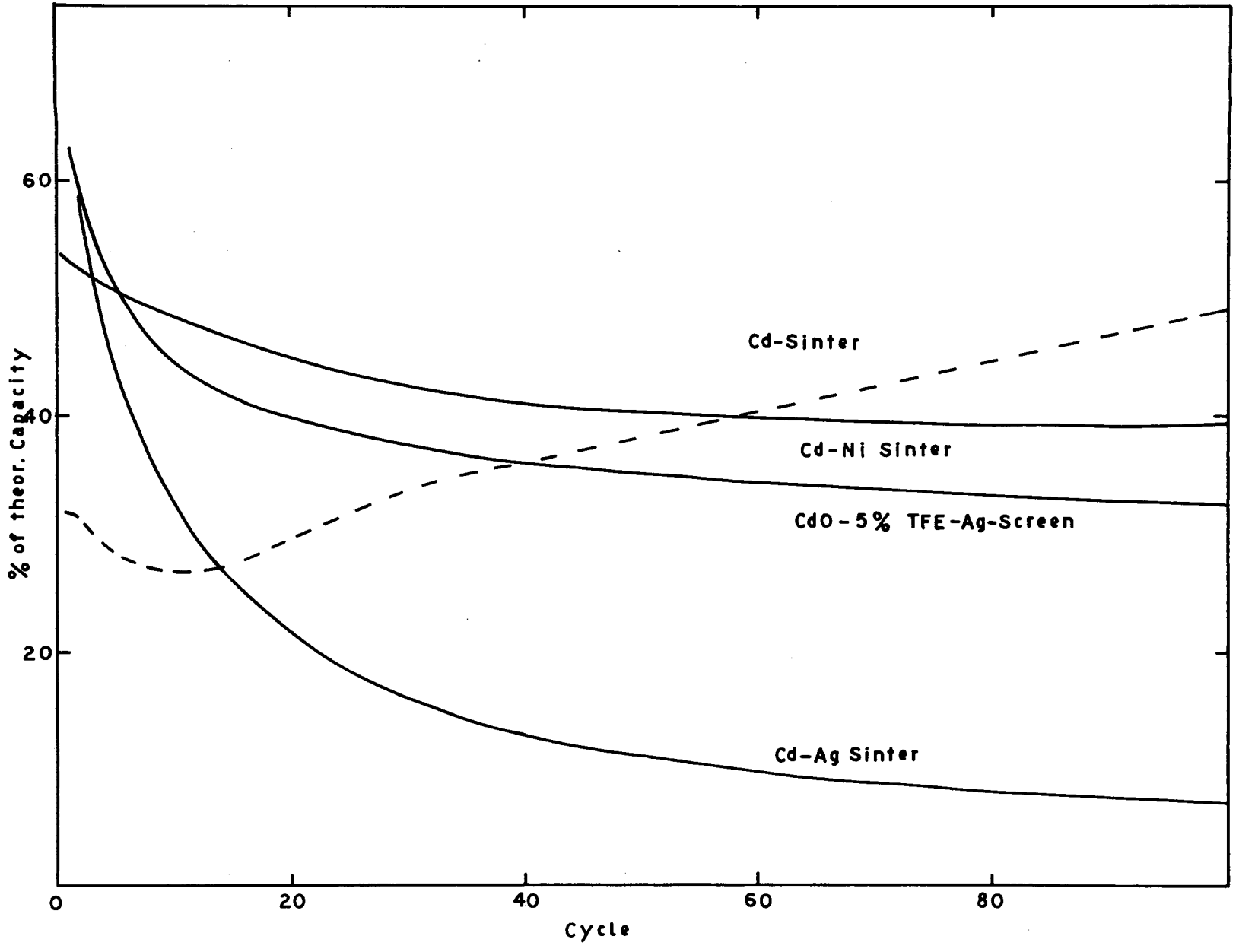

Fig. 50. Cycle behavior of various negative electrode structures

condition. This constituted very severe testing conditions, and in order to obtain a known reference we tested conventional nickel sinter-based cadmium electrodes under identical conditions.

The cadmium impregnated silver sinter showed, at the present state of development, a relatively large loss of usable capacity with increasing number of cycles (a behavior which cannot be satisfactorily explained with the available data).

The cadmium sinter structures showed initially an increasing capacity characteristic with a flat maximum and a following slow capacity decay. This was a consequence of the increasing participation of the cadmium sinter structure in the cycling.

Suitable Teflon-bonded cadmium electrodes (low binder content, no Ag powder filler) showed a capacity-cycle characteristic which is very similar to the one obtained with conventional cadmium impregnated nickel sinters. The main capacity decay occurred within the first 20 cycles. Beyond this the capacity decreased only very slowly.

3. No specific manufacturing difficulties are envisioned for the fabrication of cadmium impregnated silver sinters or Teflon-bonded electrodes. The preparation of cadmium impregnated silver sinters would involve practically the same procedures as the manufacture of conventional cadmium impregnated nickel sinters. The fabrication of Teflon-bonded cadmium electrodes involves the uniform distribution of the paste onto a screen substrate, followed by pressing and sintering. These processes can easily be automated.

The presently used procedure to prepare cadmium sinters appears to be less suitable for scale-up.

H. Conclusion

Based on these considerations at the present state of development, we judged Teflon-bonded cadmium electrodes as the best choice for practical high hydrogen overvoltage electrodes.

IV. ELECTRODE TESTING

A. Introduction

Cadmium hydroxide impregnated silver sinters show at the present state of development a considerably more rapid decay in capacity upon cycling when compared to conventional nickel sinter electrode structures. The cadmium sinter structures appear promising; however, there are open questions, especially with regard to ease of manufacture and cycle life. Thus, at the present state of development, Teflon-bonded cadmium oxide electrodes appear to be most suitable for the testing at various temperatures and charge rates. A suitable manufacturing procedure has been developed, and they show a capacity-cycle number characteristic very similar to nickel sinter-based Cd electrodes.

The selected test conditions were:

1. Temperature: 0, 25, 50°C
2. Charge rate: C, C/3, C/10, (C/30)
3. Discharge rate: C/2

The measured parameters were:

Positives: Electrode Potential
Capacity
O_2 Evolution Rate

Negatives: Electrode Potential
Capacity
Advent of H_2 Evolution

The tests were carried out at 3 different loadings for positive electrodes and 2 loadings for negative electrodes.

B. Experimental

1. Electrode preparation

a. Negative plates

Teflon-bonded cadmium electrodes on expanded cadmium substrate were prepared as previously described. A paste consisting of cadmium hydroxide, water, and 5% Teflon (in the form of a dispersion, Teflon 30, DuPont) was evenly distributed onto a cadmium screen (10 Cd 3/0). After partial drying the electrodes were pressed at 2,500 lb/in.^{2}, completely dried in vacuum at 150°C, and sintered for 10 min at 275°C in an inert atmosphere.

The electrodes were formed potentiostatically at ~1.2 V versus Hg/HgO for 48 hr and conditioned by 20 to 25 full charge/discharge cycles between -725 and -1324 mV versus Hg/HgO in order to obtain a fairly stable capacity. The electrode data are summarized in Table X.

b. Positive plates

The plaque was prepared by sintering a dry layup of carbonyl Ni powder (INCO Ni 287) for 20 min at 900°C in H_2 atmosphere. It was impregnated by the high temperature electrochemical impregnation process using a solution of 2 M $Ni(NO_3)_2$, 0.3 M $NaNO_2$ (pH4, 104°C) and a current density of 0.5 A/in.^{2} for times between 30 and ~120 min. The plates were formed by C/2 charge/discharge cycles (100% overcharge) to a stable capacity. The plaque and plate data are summarized in Table XI.

2. Electrode testing

In order to allow simultaneous constant current test cycling, the size of the individual electrodes was adjusted to obtain equal capacities. The electrodes were assembled in Plexiglas cells described earlier. The electrolyte was 30% KOH. The cells were immersed into a thermostated water bath controlled by a portable unit (Blue M Electric Co.) capable of controlling temperatures between -15 to 100°C. Potentials were measured versus Hg/HgO reference electrodes and continuously monitored using a multipoint recorder (Esterline Angus).

The cycling of the electrodes was controlled by two Tyco-built battery cyclers. Positive electrodes were cycled between 0 V versus Hg/HgO and full O_2 evolution. During charge, the volume of O_2 evolved as a function of time was

Table X. Teflon-Bonded Cadmium Electrodes

Electrode	Thickness (mils)	Theoretical Capacity ($Ahr/in.^3$)	Cycle No.	Capacity (Ahr)	Capacity (% of Theoretical)
TF Cd-T1	32	10	1	0.135	56
			10	0.105	44
			20	0.090	37
TF Cd-T2	25	12	1	0.180	81
			10	0.118	53
			20	0.094	42
TF Cd-T3	18	8	1	0.150	67
			10	0.095	43
			20	0.084	38
TF Cd-T4	18	8	1	0.145	66
			10	0.090	41
			20	0.077	35

Table XI. Positive Electrodes

Electrode	Plaque Thickness (mils)	Plate Thickness (mils)	Theoretical Capacity ($Ahr/in.^3$)	Formed Capacity ($Ahr/in.^3$)
Ni-1	26.7	26.9	3.5	3.8
Ni-2	26.8	28.1	5.1	4.6
Ni-3	26.9	31.2	7.5	7.9

quantitatively measured. Negative electrodes were cycled between -0.7 and 1.35 V versus Hg/HgO. The advent of gas evolution, defined by the first formation of small bubbles at the electrode surface, was determined visually. To facilitate the observation, the thermostated bath containing the cells was placed on a light table. An overall view of the experimental arrangement is shown in Fig. 51.

C. Results and Discussion

1. Negative plates

The test results of the Teflon-bonded Cd electrodes are summarized in Table XII and in Figs. 52 through 56.

The shape of the current potential curves of all electrodes tested is very similar. As a characteristic example we will examine the behavior of electrode T2 in more detail. Fig. 52 shows the change of electrode potential upon charge at different rates using the same time scale. The advent potential for hydrogen evolution changed only slightly with charge rate. For example, the gas advent at the C/10 rate occurred at a potential of only about 50 mV less than at the C rate.

With Teflon-bonded cadmium electrodes the potential change at the end of charge was occasionally more or less discontinuous, as illustrated in the reproduction of a charging curve (Fig. 53). This behavior appeared to be typical, especially for low rate charging, and was observed at all temperatures. A tentative explanation may be that during charging the metallic cadmium grows from the electronically conducting matrix into the electrode making contact with pockets of previously isolated cadmium hydroxide. At the end of charge, that is, in the region where the potential increases, small changes in accessibility of active material will result in relatively large fluctuations of potential. On the charge plateau, however, this effect would not lead to any visible potential changes since the negative electrode potential is practically independent of state of charge.

The effect of temperature on the potential time behavior is illustrated for the two extreme charge rates (C/10 and C) in Figs. 54 and 55. Fig. 54 shows a continuous increase in capacity with rising temperature. Except for the higher hydrogen overvoltage at 0°C, the shape of the charging curves showed little difference. The high rate charge shown in Fig. 55 exhibited an unexpected behavior. Here the potential change towards the end of charge is less abrupt at 50°C and further the capacity is again decreased at the higher temperature. This behavior is illustrated in Fig. 56, which shows the average charge capacity at the different rates as a

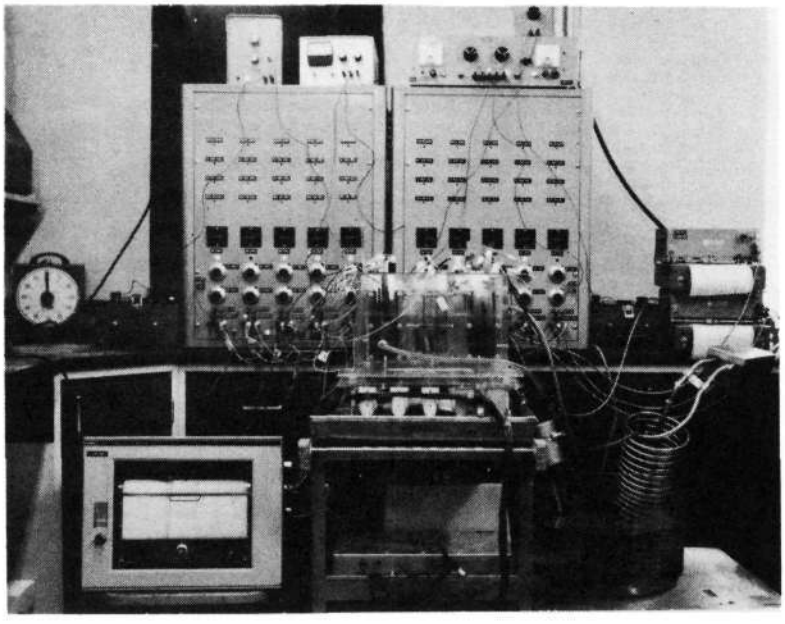

Fig. 51. Arrangement for electrode testing

Table XII. Test Results of Teflon-Bonded Cd Electrodes

		T1	T2	T3	T4	T1	T2	T3	T4	T1	T2	T3	T4	T1	T2	T3	T4
Temp., °C	Charge Rate	Charge Capacity† in mAhr				Total Charge in mAhr				H_2 Advent ‡ -V versus Hg/HgO				Discharge Capacity‡‡ in mAhr			
0	C	27	29	25	44	33	33	30	45	1.37	1.39	1.43	1.30	31	31	28	45
	C/3	36	36	31	50	42	44	35	55	1.36	1.35	1.41	1.32	39	40	35	56
	C/10	45	42	39	60	45	45	42	60	1.32	1.34	1.38	1.27	49	45	37	56
25	C	57	67	32	38	64	72	38	45	1.31	1.27	1.30	1.27	64	69	39	44
	C*	63	73	37	38	87	99	78	72					70	79	49	44
	C/3	56	73	38	41	62	74	38	49	1.25	1.21	1.25	1.23	64	69	40	45
	C/10	53	67	47	46	54	75	51	51	1.25	1.22	1.26	1.22	69	66	44	48
50	C	46	46	23	24	67	66	45	45	1.26	1.28	1.29	1.34	58	56	38	37
	C/3	69	75	55	56	80	80	80	80	1.26	1.23	1.29	1.30	70	78	55	54
	C/10	88	111	67	83	135	135	135	135	1.25	1.25	1.28	1.29	90	110	60	60

*Final Test

†Capacity to -1.3 V versus Hg/HgO

‡First small gas bubble at electrode surface

‡‡C/2 rate

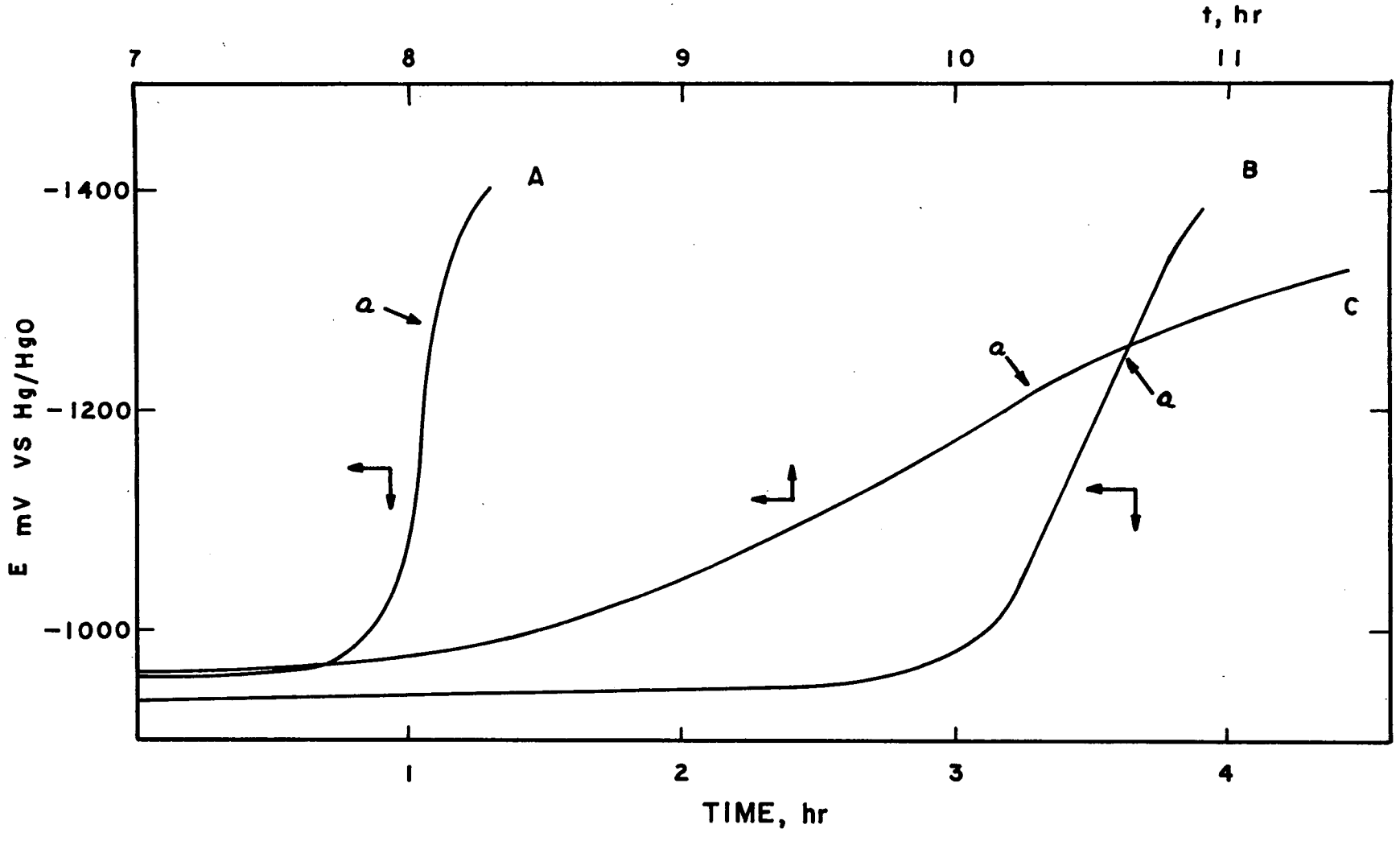

Fig. 52. Potential change of electrode T-2 during charge [A = C rate, B = C/3 rate, C = C/10 rate, 25°C, 30% KOH; a = advent of H_2 evolution (no iR correction)]

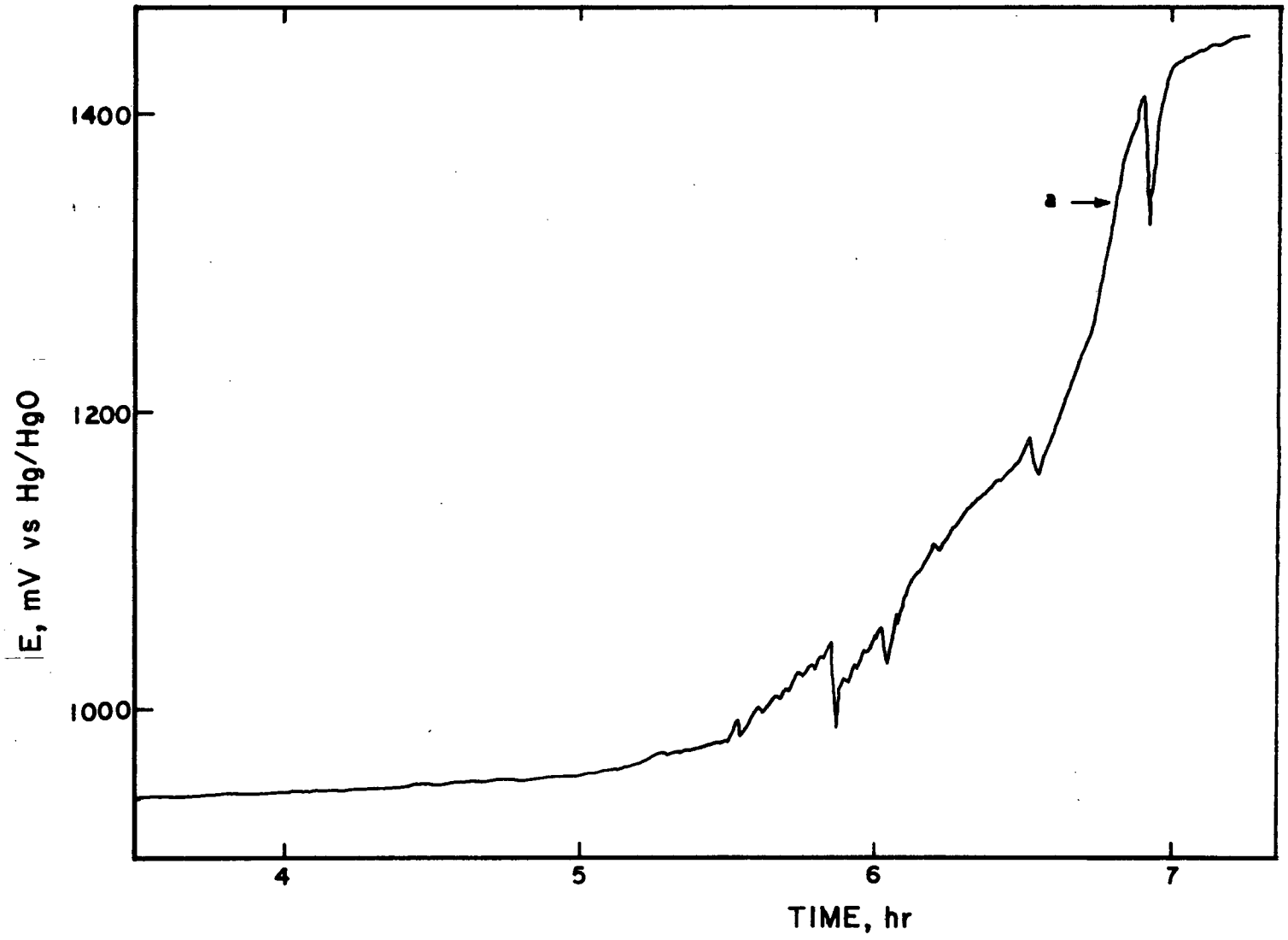

Fig. 53. Typical potential-time trace during charge of a Teflon-bonded Cd electrode (T-1) at low rate (C/10), 6 mA, 0°C, 30% KOH; a = advent of H_2 evolution

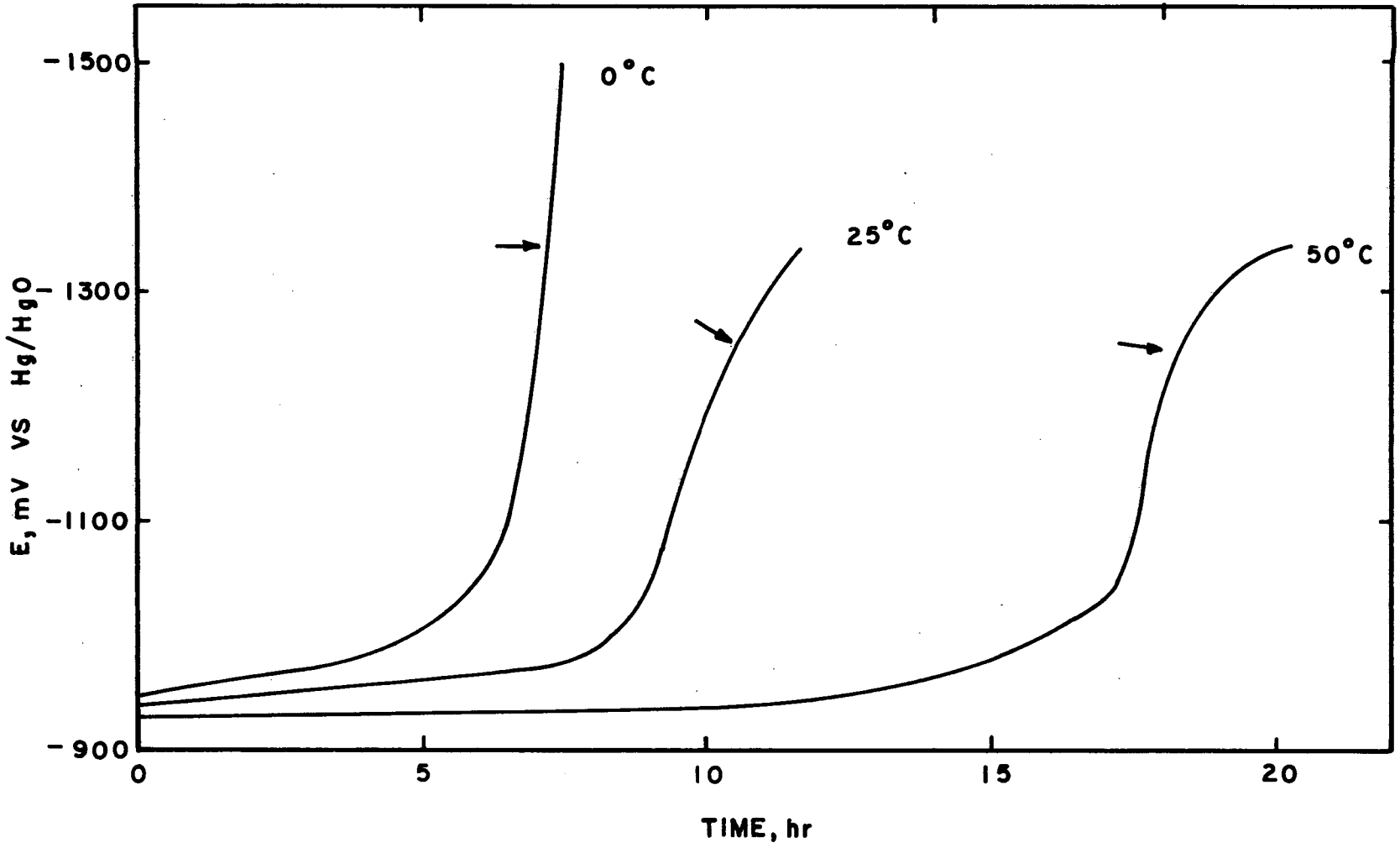

Fig. 54. Potential change of electrode T-2 during charge at C/10 rate, 6 mA, 30% KOH (no iR correction), arrow = advent of H_2 evolution

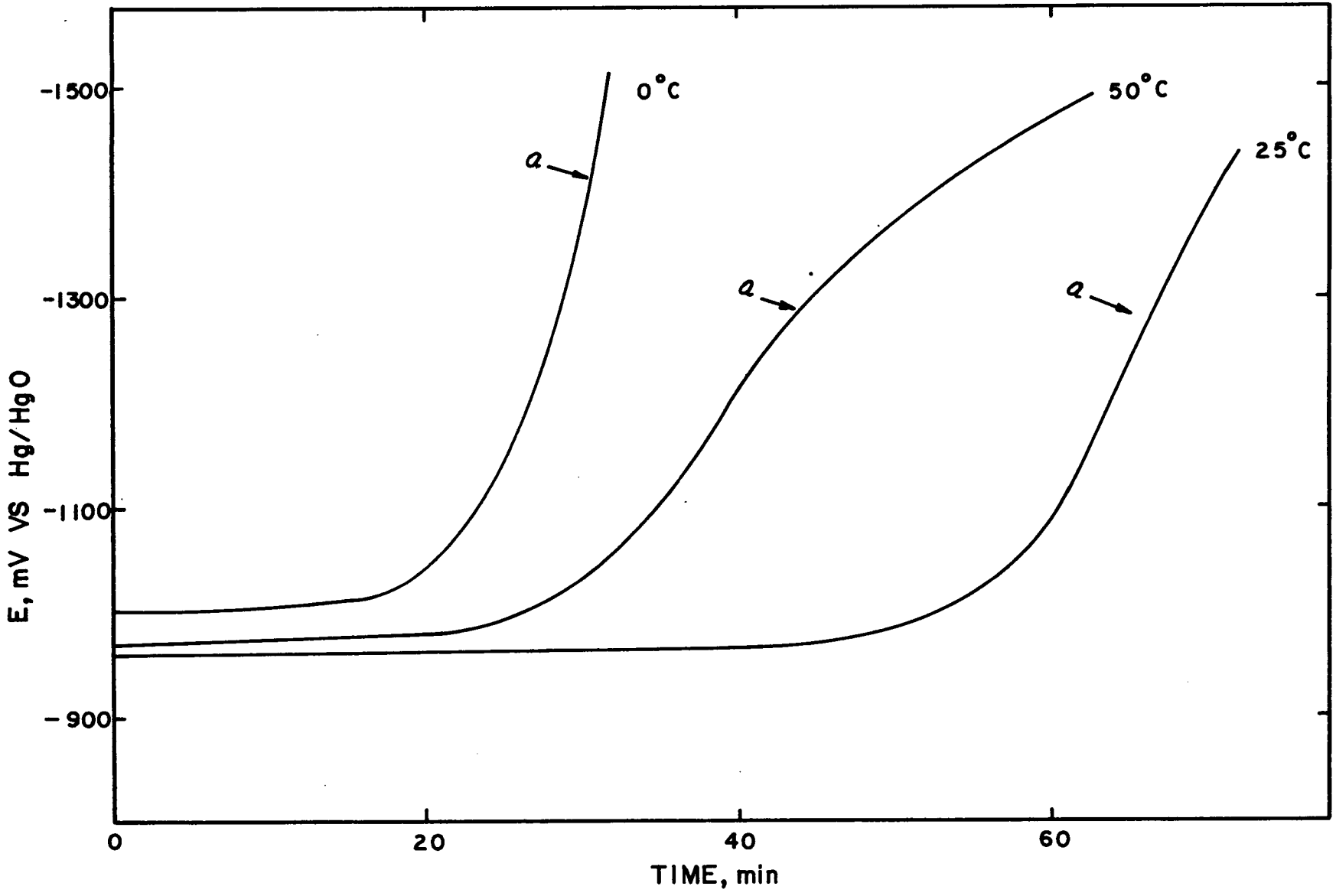

Fig. 55. Potential change of electrode T-2 during charge at C rate, 60 mA, 30% KOH (no iR correction), arrow = advent of H_2 evolution

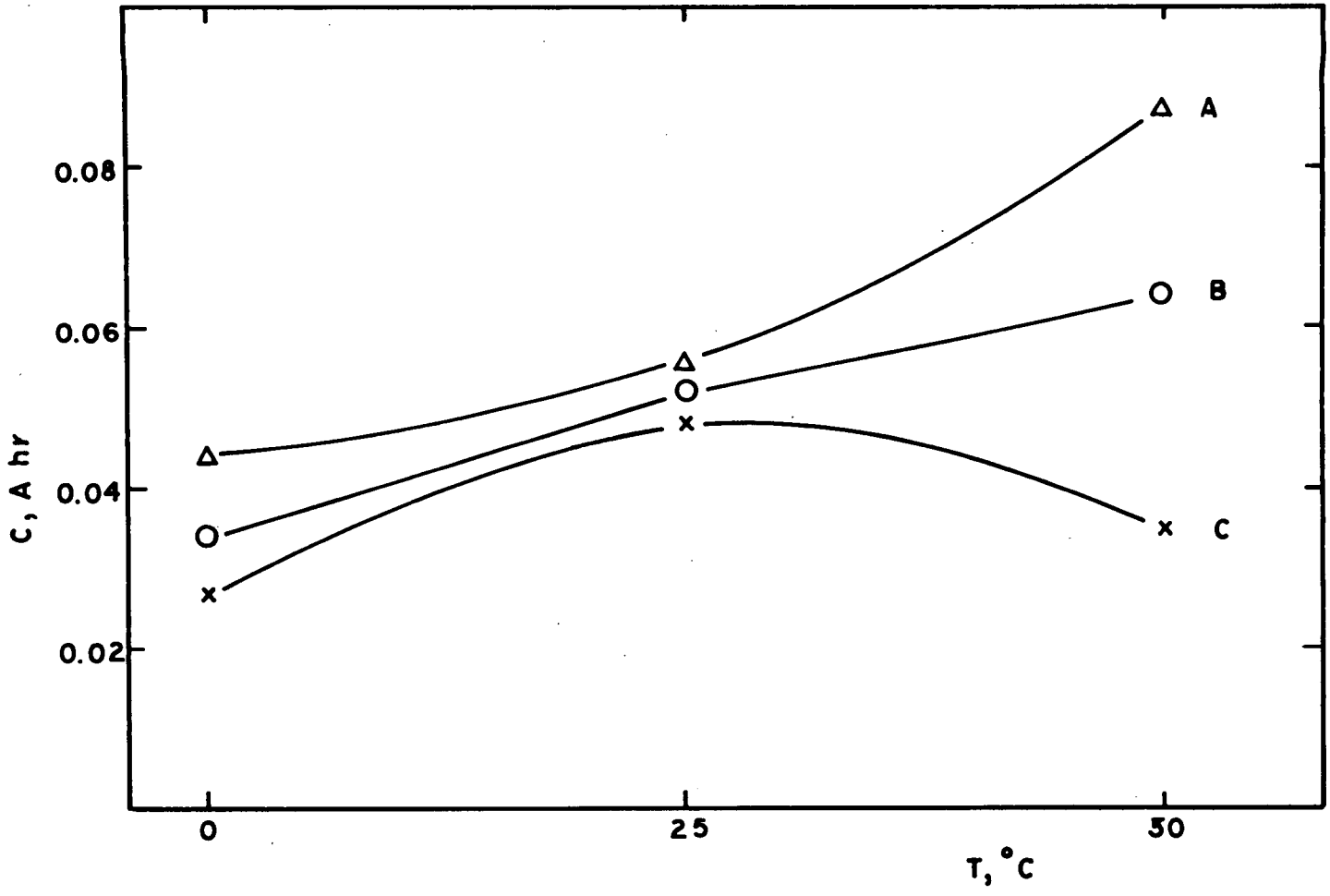

Fig. 56. Average charge capacity (to -1.3 V versus Hg/HgO) of Teflon-bonded Cd electrodes (A ≈ 10-hr rate, B ≈ 3-hr rate, C ≈ 1-hr rate)

function of temperature. The discharge capacities also followed a similar pattern. Especially two features shall be pointed out: (1) the electrodes appear to be more rate sensitive at 50°C than at 25 or 0°C, and (2) at the 1-hr charge rate a lower capacity was found at 50°C than at 25°C.

The agreement of the control measurements at 25°C (which were carried out after the runs at 50°C), with the original values obtained at the start of the test, appears to exclude the possibility that systematic changes with time could be responsible for this type of behavior.

Recent investigations of the cadmium electrode mechanism[13] have established that the major mechanism, especially at elevated temperatures, involves a soluble intermediate species in both the charging and discharging reactions, which means it can be described as a dissolution precipitation process on discharge and a plating process on charge. Further, it was found that for a given electrode structure the average cadmium hydroxide crystallite size was larger at higher temperature and at lower discharge rate.[14] Since, in our case, the discharge rate was kept constant at the 2-hr rate for all measurements, it should not contribute as a major factor. Due to the decreased surface to volume ratio, the anticipated effect of larger cadmium hydroxide crystallites on the charge behavior would be an increased rate sensitivity and a lowered capacity. At an elevated temperature this is counteracted in part by a higher cadmium hydroxide dissolution rate and by accelerated transport processes. Thus, these two main effects are already sufficient to qualitatively explain the observed electrode behavior. It must be understood, however, that the detailed processes occurring during charge and discharge in a porous Teflon-bonded Cd electrode are more complex and that little data exists at higher temperatures. The interaction of the above mentioned processes also suggests that this effect should be strongly dependent on structure, and it would be valuable to compare the present results with similar experiments on conventional negative plates.

Fig. 57 shows the first and second charge cycle at 25°C following electrode testing at 50°C. Here the temperature was lowered in the discharge state of the electrode. The potential time curve A reflects the charging of the cadmium hydroxide formed during the high temperature discharge. Similar effects have been observed at conventional nickel sinter-based Cd electrodes.[14]

The charge and discharge capacities of all electrodes tested are given in Table XII. From Table XII it can be further seen that the potentials for the advent of hydrogen evolution change only slightly with rate and temperature. The difference

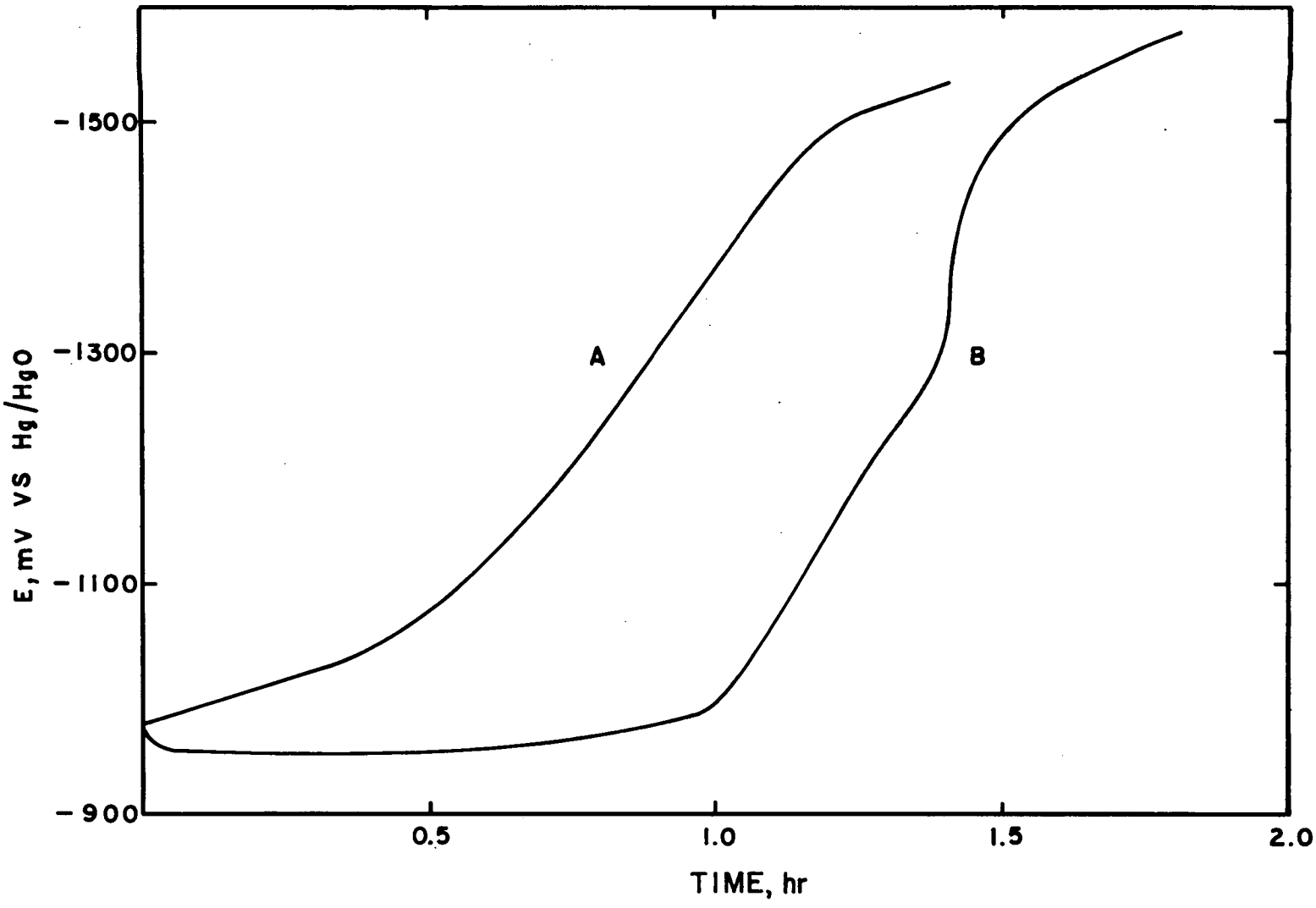

Fig. 57. Charging curves of electrode T-2 at 25°C following electrode testing at 50°C
[A = first charge at 25°C, B = second charge; 60 mA, 30% KOH (no iR correction)]

between the 1- and 10-hr rate is approximately 50 mV at 0°C and 20 mV at 50°C. The average advent potential for hydrogen evolution was measured as -1350, -1250, and -1275 mV at 0, 25, and 50°C, respectively. The nearly constant advent potentials are well suited for practical application since they allow the use of a uniform cutoff voltage on charge without the need for temperature compensation.

2. Positive plates

The reversible potential of the nickel hydroxide electrode is slightly more positive than the potential of the reversible oxygen electrode. Therefore, oxygen evolution is a parasitic process during charging of positive plates. The objective of this test was to determine the rate of oxygen evolution at different electrode loading, temperature, and charge rates. The results are summarized in Table XIII and in Figs. 58 through 66. The electrodes Ni-1 and Ni-2 were measured in duplicate and, except for the capacities, average values are reported.

The charge/discharge potentials (measured at half capacity) were practically independent of current density and temperature. The plateau potentials of oxygen evolution, however, showed a pronounced decrease with rising temperature. The change with charge rate was approximately 35 mV per factor of ten. This suggests already a higher fraction of the charge current diverting into O_2 evolution at lower charge rates and at higher temperatures. The capacities measured by a C/2 rate discharge after considerable overcharge also decreased, with lower charge rates and higher temperature. The rate dependence is especially pronounced at 50°C.

In addition, we measured directly the amount of oxygen produced. Figs. 58 through 66 give, for the three different electrode loadings, the rate of O_2 evolution as a function of time at the different charge rates and temperatures. The advent of O_2 evolution occurred in all cases quite early. However, below room temperature the rate of O_2 evolution is quite small up to a high state of charge of the positive plate. Furthermore, below room temperature the absolute rate of O_2 generation during the major part of the charging process is only slightly lower at the lower charge rate. The consequence is that the fraction of the total charge current going into O_2 evolution increases as the charge rate decreases. At 0°C we measured also the O_2 formation rate during a 30-hr charge. It was found to be equal to the results obtained at the C/10 rate when related to the state of charge of the electrode.

At 50°C a considerable fraction of the charging current is diverted into O_2 evolution. This fraction increases dramatically with decreasing charge rate. Even

Table XIII. Results of Positive Plates

Electrode No.		1	2	3	1	2	3	1	2	3	1A	1B	2A	2B	3		
Temp., °C	Charge Rate	Charge Potential* mV versus Hg/HgO			O_2 Plateau mV versus Hg/HgO			Discharge Potential* mV versus Hg/HgO			Capacity† m Ahr					% Over Charge	Δ E‡ mV
0	C	460	447	434	590	577	571	350	360	358	190	177	190	210	182	40	132
	C/3	448	440	453	563	548	558	331	347	333	240	235	256	223	230	90	109
	C/10	442	449	443	545	540	538	353	368	358	160	160	170	175	170	60	103
	C/30	456	462		520	537	533	368	375	368	158	144	172		173	75	71
25	C	455	456	450	551	539	532	374	370	375	168	168	174	200	172	>20	87
	C/3	474	457	445	548	536	520	399	385	365	170	170	168	185	155	35	76
	C/10	485	468	450	542	544	480	392	378	360	163	168	170	163	177	75	54
50	C	450	445	457	472	480	490	362	355	357	172	172	193	212	180	80	30
	C/3	452	448	454	458	455	460	365	365	362	118	118	138	177	174	70	6
	C/10	437	441	447	437	441	447	340	340	342	100	88	106	120	110	150	0

*Potential at half capacity

†From discharge at 2-hour rate

‡Difference between average O_2 evolution potential and average charge potential

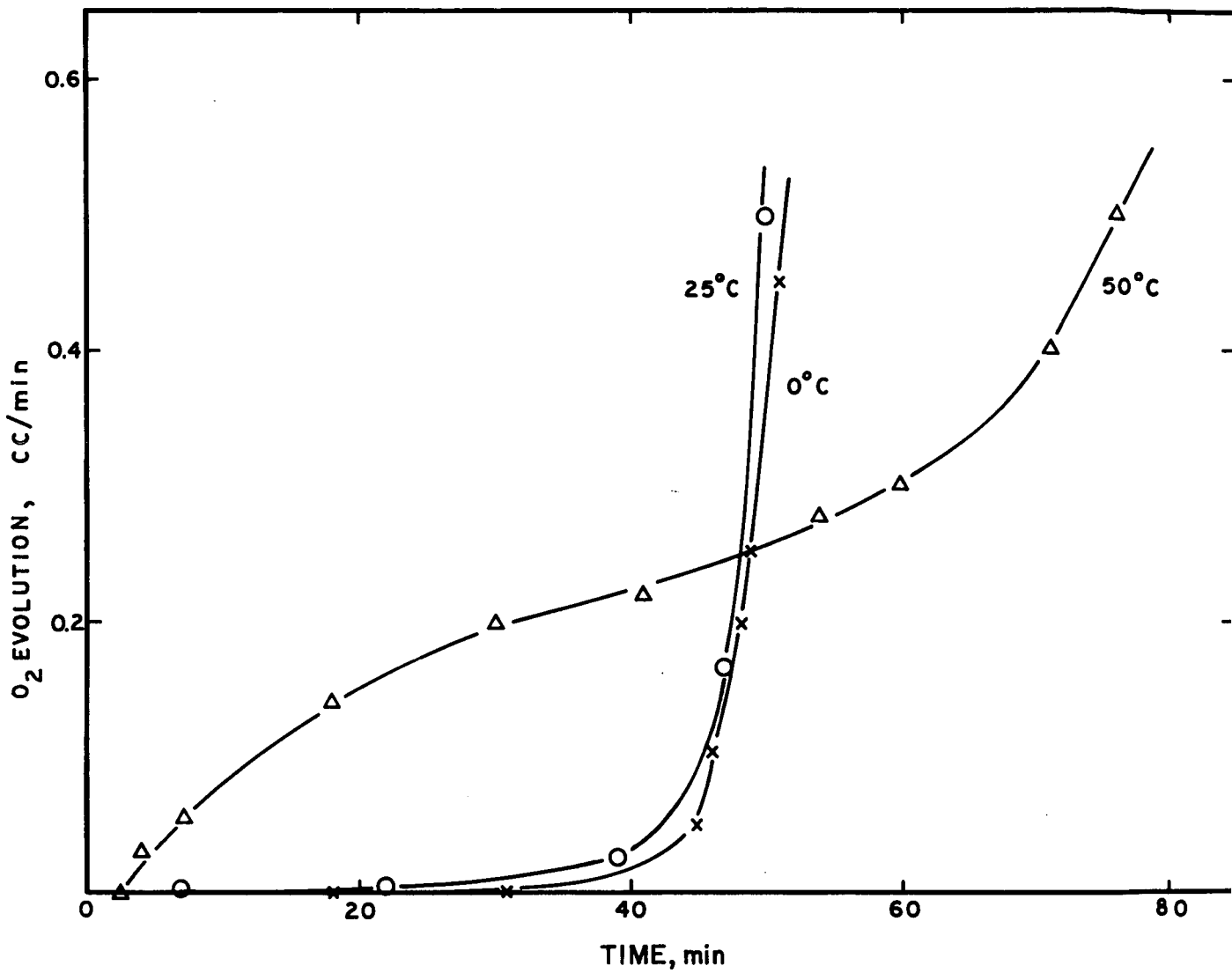

Fig. 58. O_2 evolution rate at electrode Ni-1 during charge at the 1-hr rate (200 mA, $\cong$ 0.69 cm^3O_2/min) 30% KOH

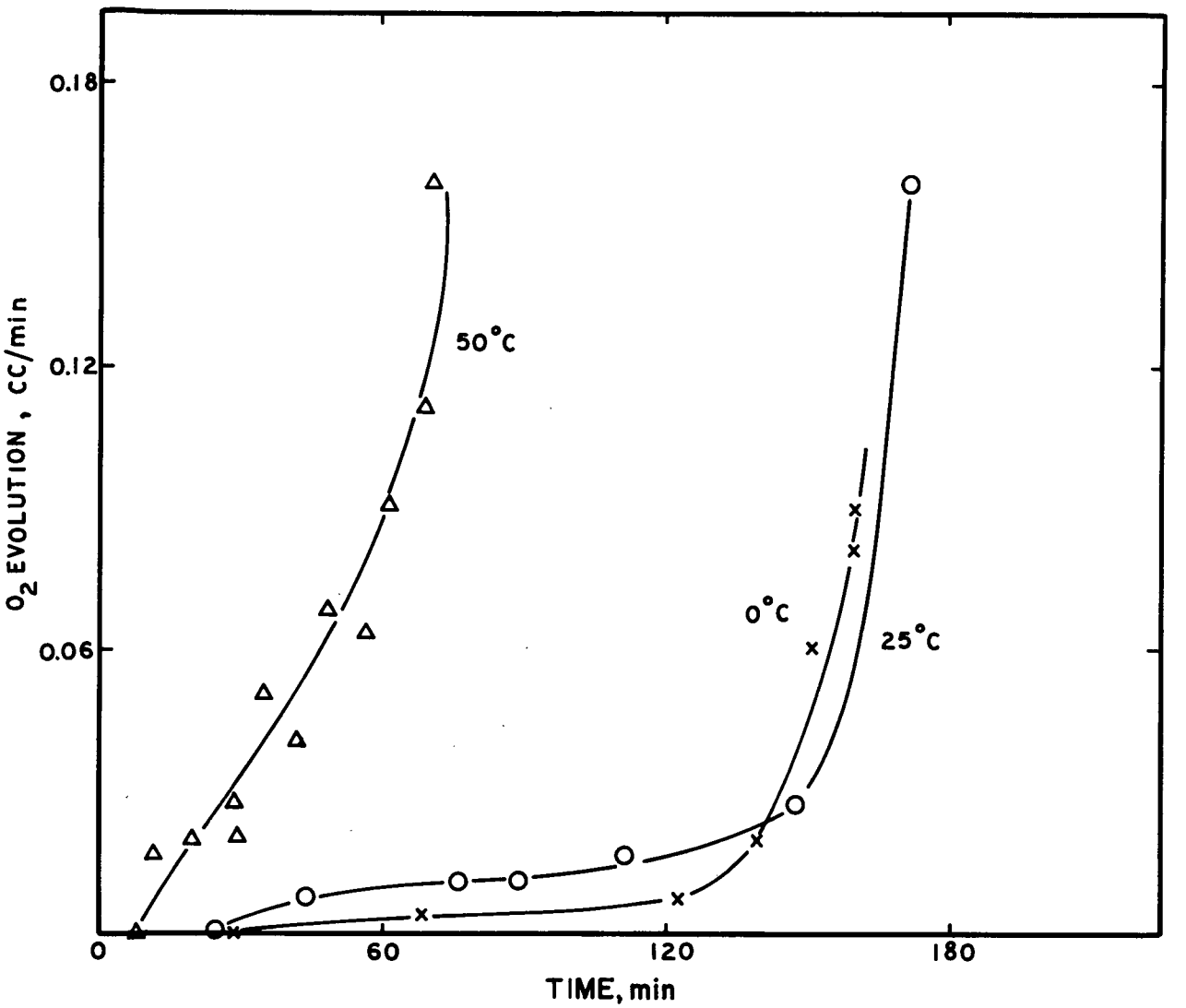

Fig. 59. O_2 evolution rate at electrode Ni-1 during charge at the 3-hr rate (67 mA, $\cong$ 0.22 cm^3O_2/min) 30% KOH

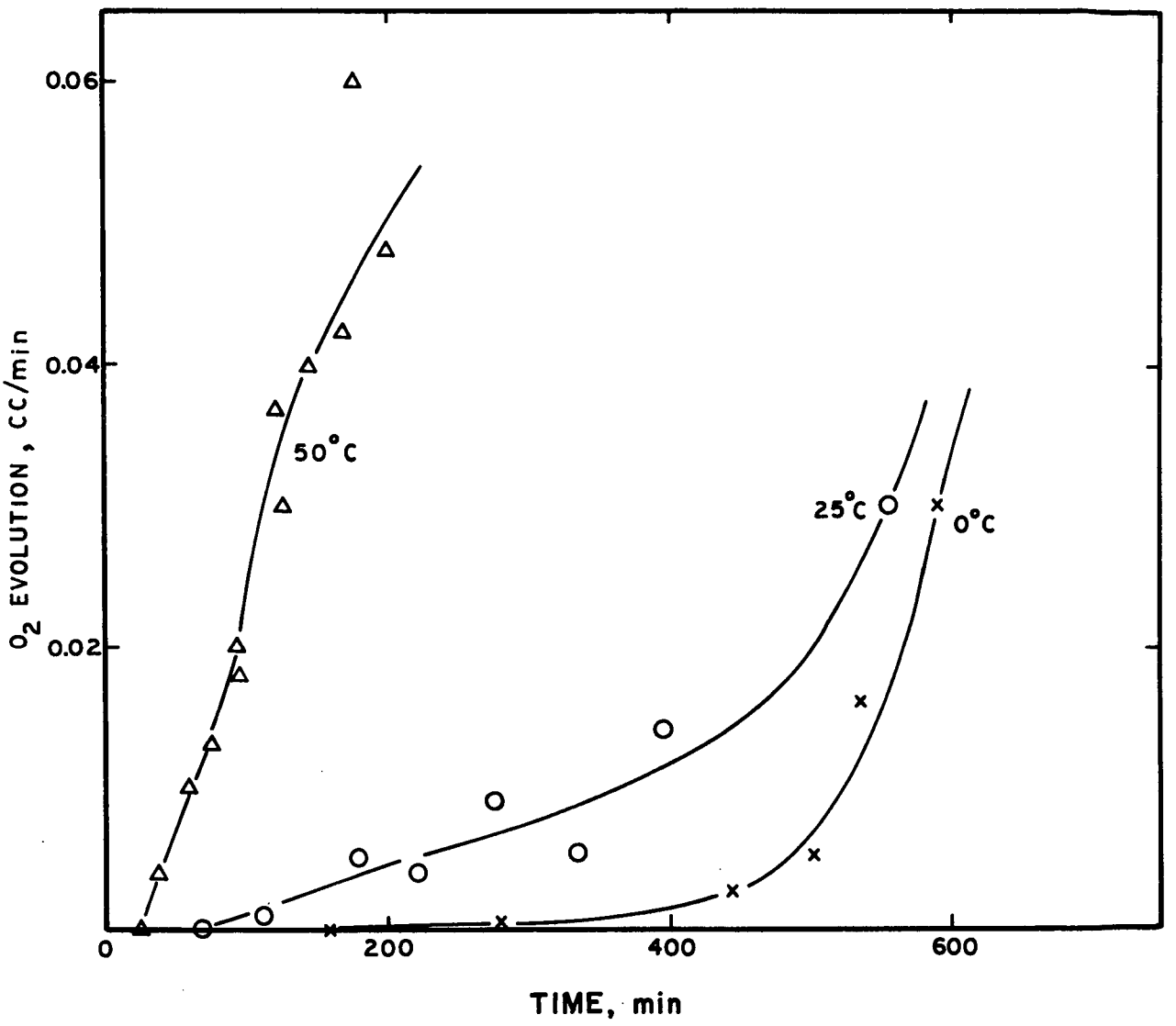

Fig. 60. O_2 evolution rate at electrode Ni-1 during charge at the 10-hr rate (20 mA, $\cong$ 0.069 cm^3O_2/min) 30% KOH

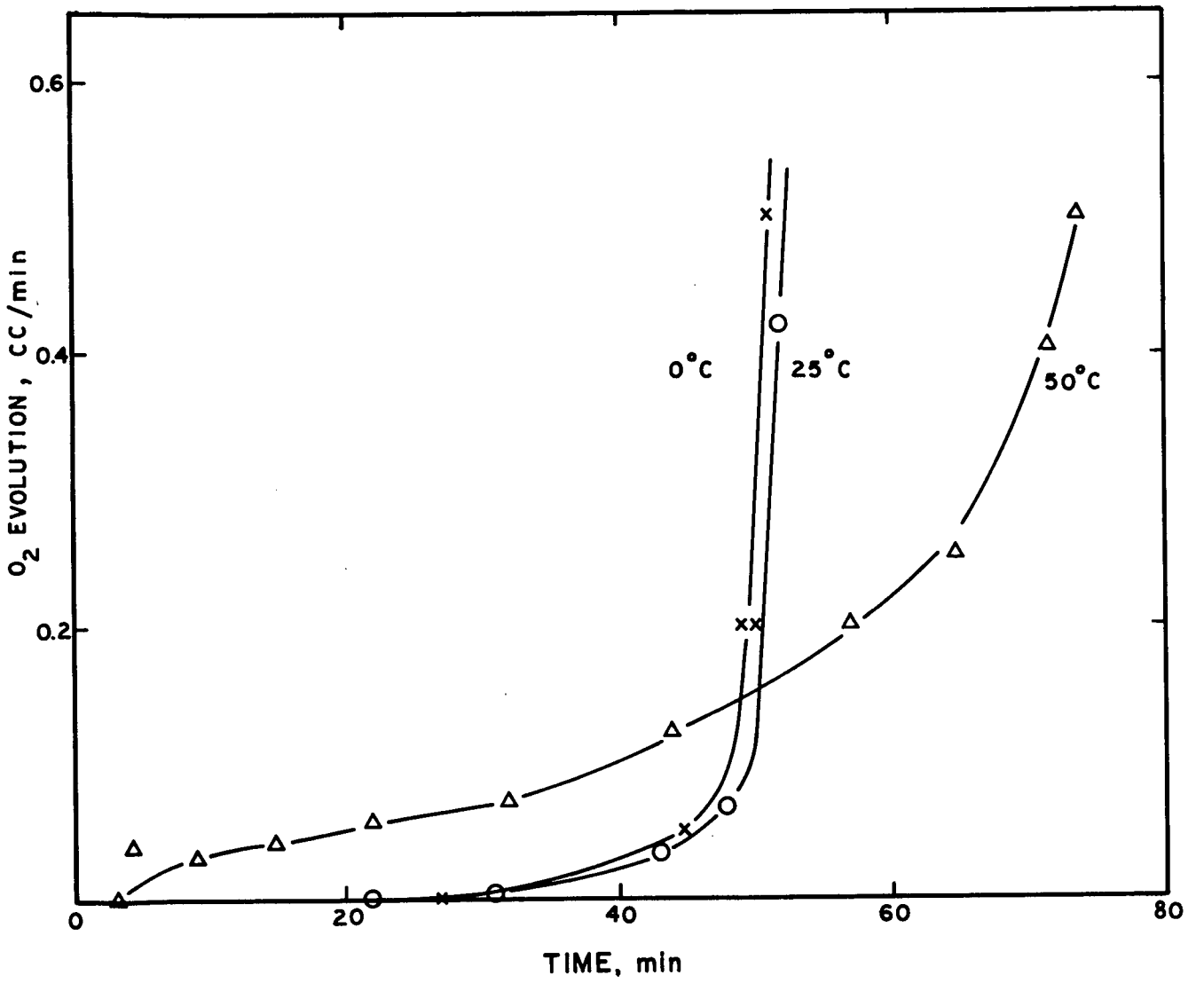

Fig. 61. O_2 evolution rate at electrode Ni-2 during charge at the 1-hr rate (200 mA, $\cong$ 0.69 cm^3O_2/min) 30% KOH

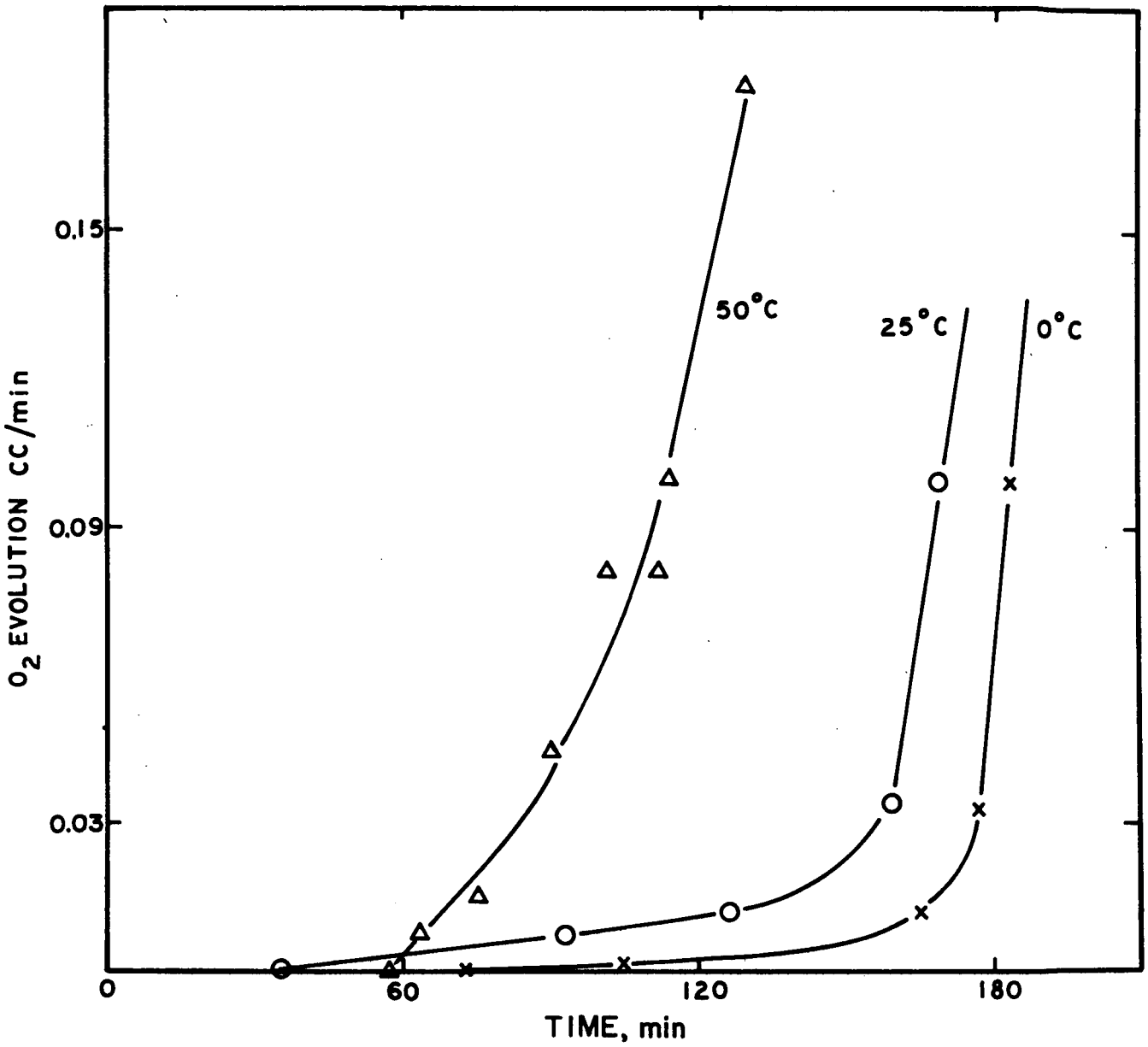

Fig. 62. O_2 evolution rate at electrode Ni-2 during charge at the 3-hr rate (67 mA, $\cong$ 0.22 $cm^3 O_2$/min) 30% KOH

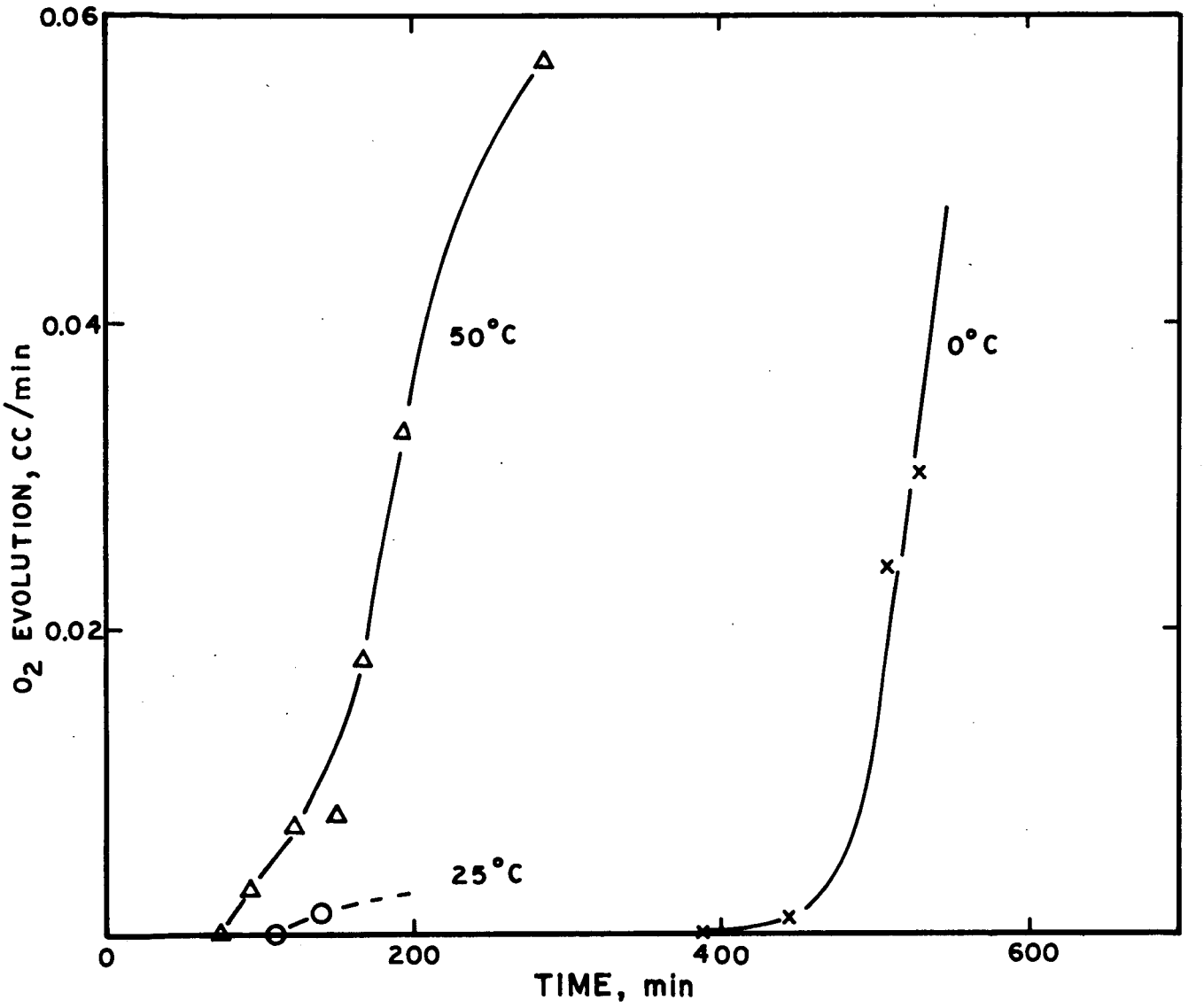

Fig. 63. O_2 evolution rate at electrode Ni-2 during charge at the 10-hr rate (20 mA, $\cong$ 0.069 cm^3O_2/min) 30% KOH

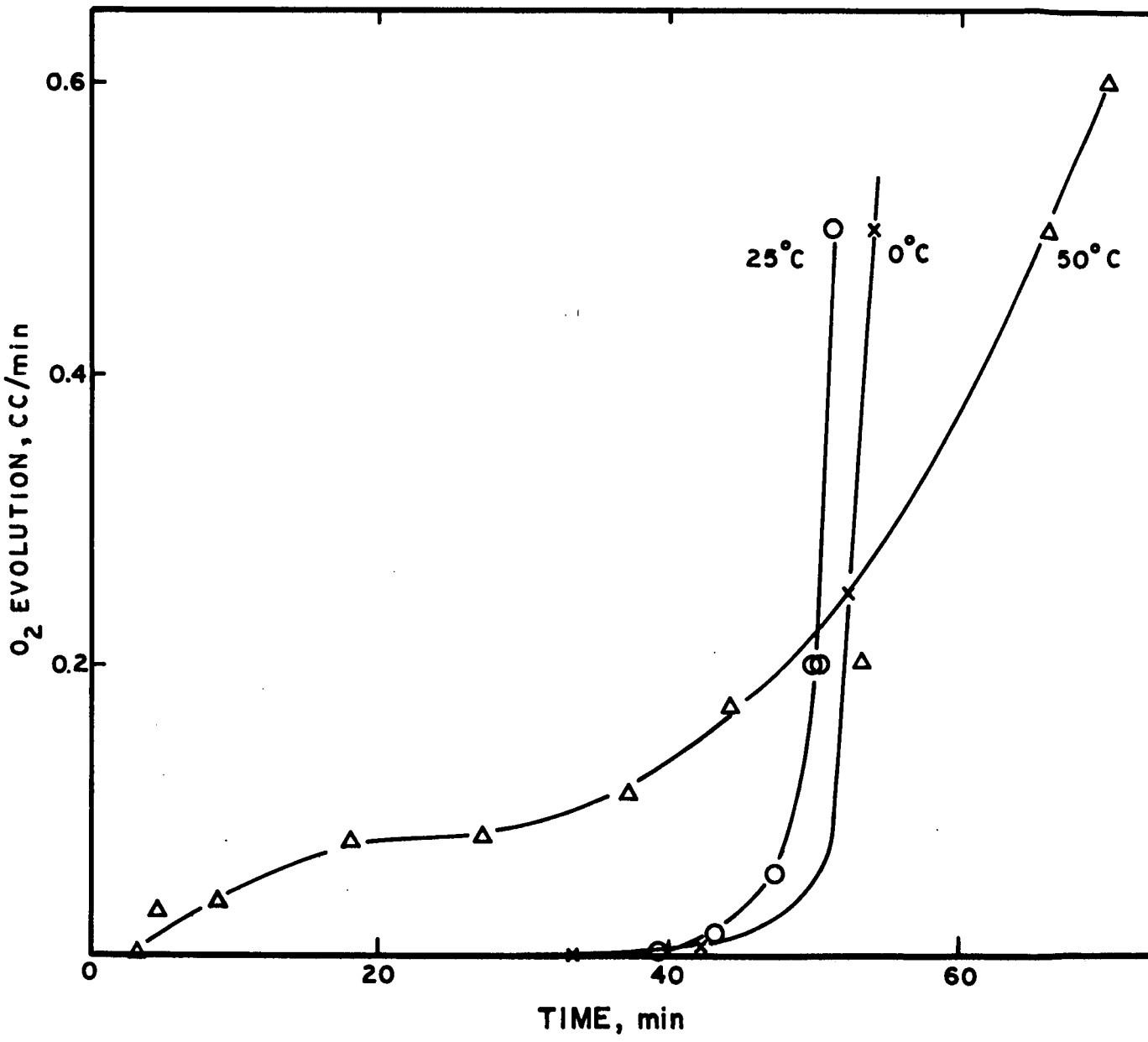

Fig. 64. O_2 evolution rate at electrode Ni-3 during charge at the 1-hr rate (200 mA, ≅ 0.69 $cm^3 O_2$/min) 30% KOH

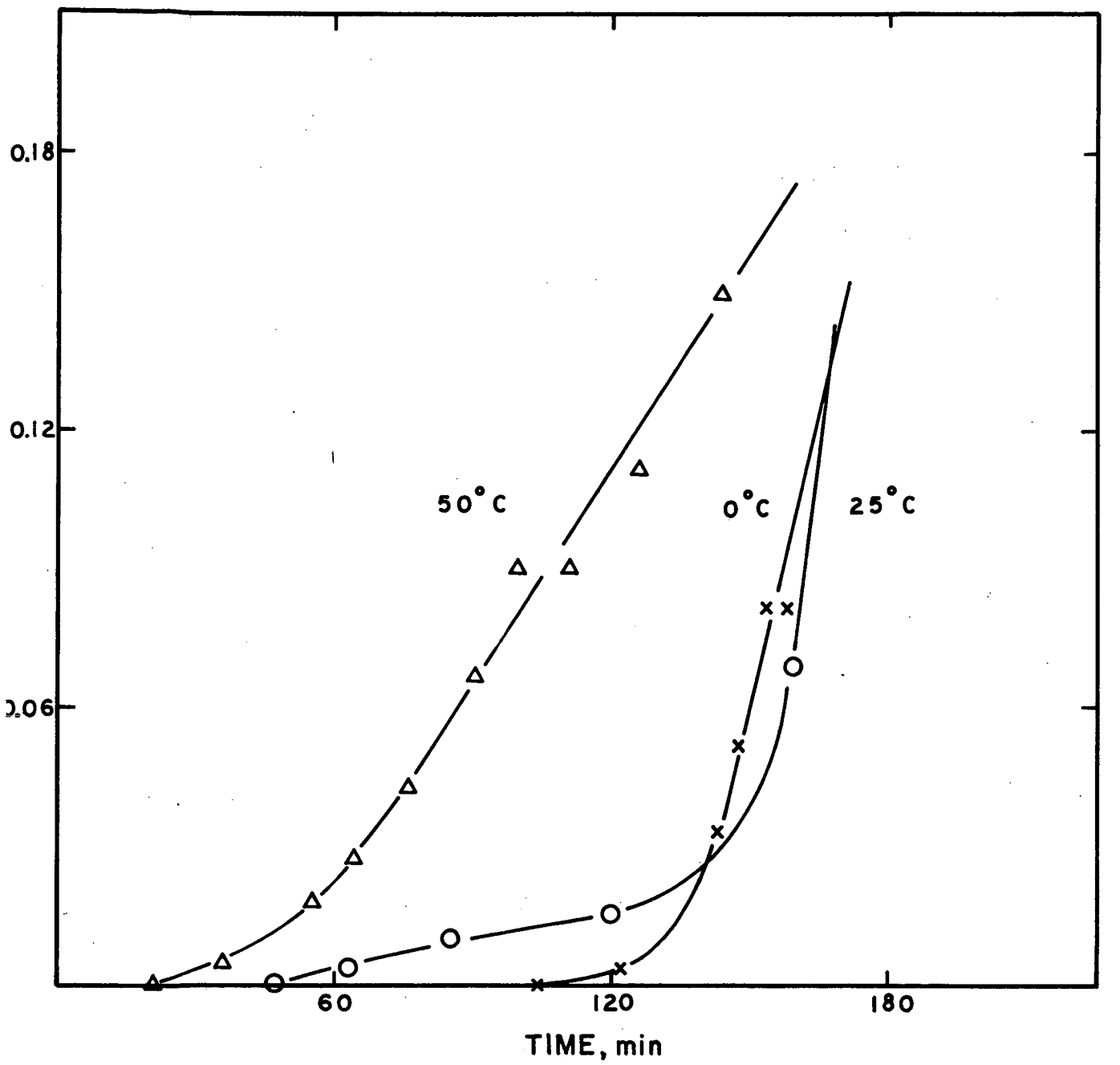

Fig. 65. O_2 evolution rate at electrode Ni-3 during charge at the 3-hr rate (67 mA, $\cong$ 0.22 cm^3O_2/min) 30% KOH

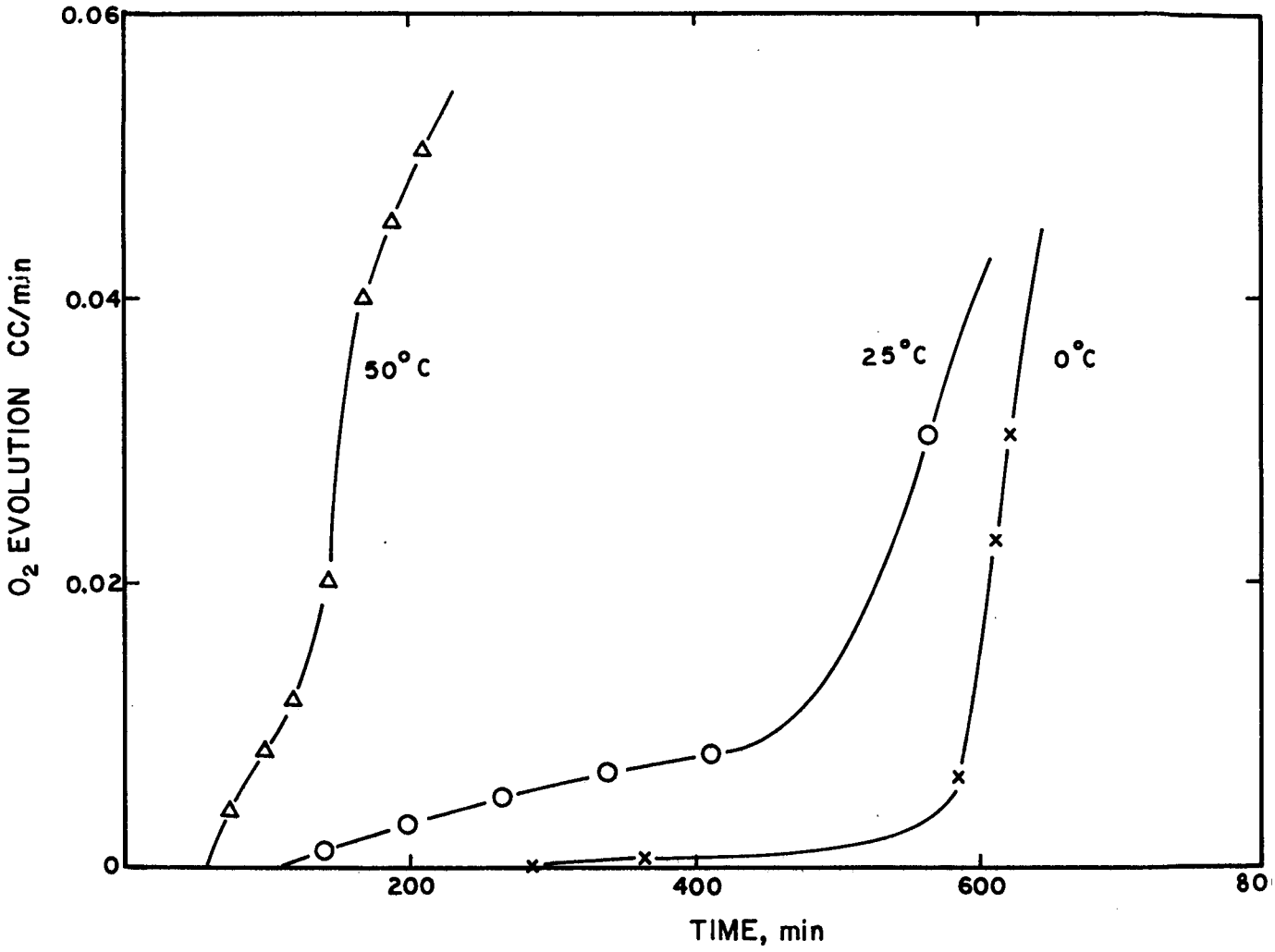

Fig. 66 O_2 evolution rate at electrode Ni-3 during charge at the 10-hr rate (20 mA, $\cong$ 0.069 cm^3O_2/min) 30% KOH

at the 1-hr rate, the electrode begins almost immediately to gas, and a half-charged electrode accepts only approximately 2/3 of the current for the charging process. At the C/10 rate a 25% charged electrode generates O_2 at a rate equivalent to half the charge current. Even after extended overcharge, only 50% of the total electrode capacity can be obtained on discharge.

The O_2 evolution rate as a function of charge input at room temperature is shown for the various charge currents in Fig. 67. This behavior is typical also for the other temperatures. The advent of O_2 evolution and the absolute rate of O_2 evolution during the major part of the changing process is independent of charge rate. The increase of O_2 evolution rate towards the end of charge occurs, however, earlier at the higher charge rates. For example, if we use the charge input at the C/10 charge rate as reference, that is, as 100%, an equal O_2 evolution rate (e.g., 0.04 cm^3/min) would be observed at approximately 85% state of charge at the C/3 rate charge and at 70 to 75% state of charge at the C rate charge. These percent values are fairly independent of temperature and electrode loading.

The observed behavior of nickel hydroxide electrodes on charge results from the superposition of the two competing processes: (1) the conversion of the nickel hydroxide from the reduced form into the oxidized form, and (2) the evolution of oxygen at the plate. The O_2 evolution reaction exhibits a Tafel behavior with a slope of approximately 35 mV/decade. The reaction is also strongly temperature dependent, and we calculated from our measurements an activation energy of approximately 24 Kcal/mole. In contrast to this, the charge potentials of the active nickel hydroxide mass are nearly independent of charge rate and of temperature.

If we compare the quantitative O_2 evolution data obtained at the differently loaded electrodes, we find the following: (1) the advent of oxygen evolution shows a trend to move towards higher states of charge with decreasing loading, and (2) a comparison of the state of charge obtained by extrapolating the ascending part of the rate-time curve to the abscissa, or a straight comparison of the state of charge at a given O_2 evolution rate (say 20% of the total charge current), identifies the medium loading of 5 Ahr/$in.^3$ as the best electrode from a gassing point of view.

This finding might be explainable by the combination of two counteracting effects. At a given charge rate the current density is higher at the higher loaded plate. This appears to lead to a slightly higher potential which would result in an accelerated O_2 evolution rate ~ 10 mV and would double the O_2 evolution rate. At

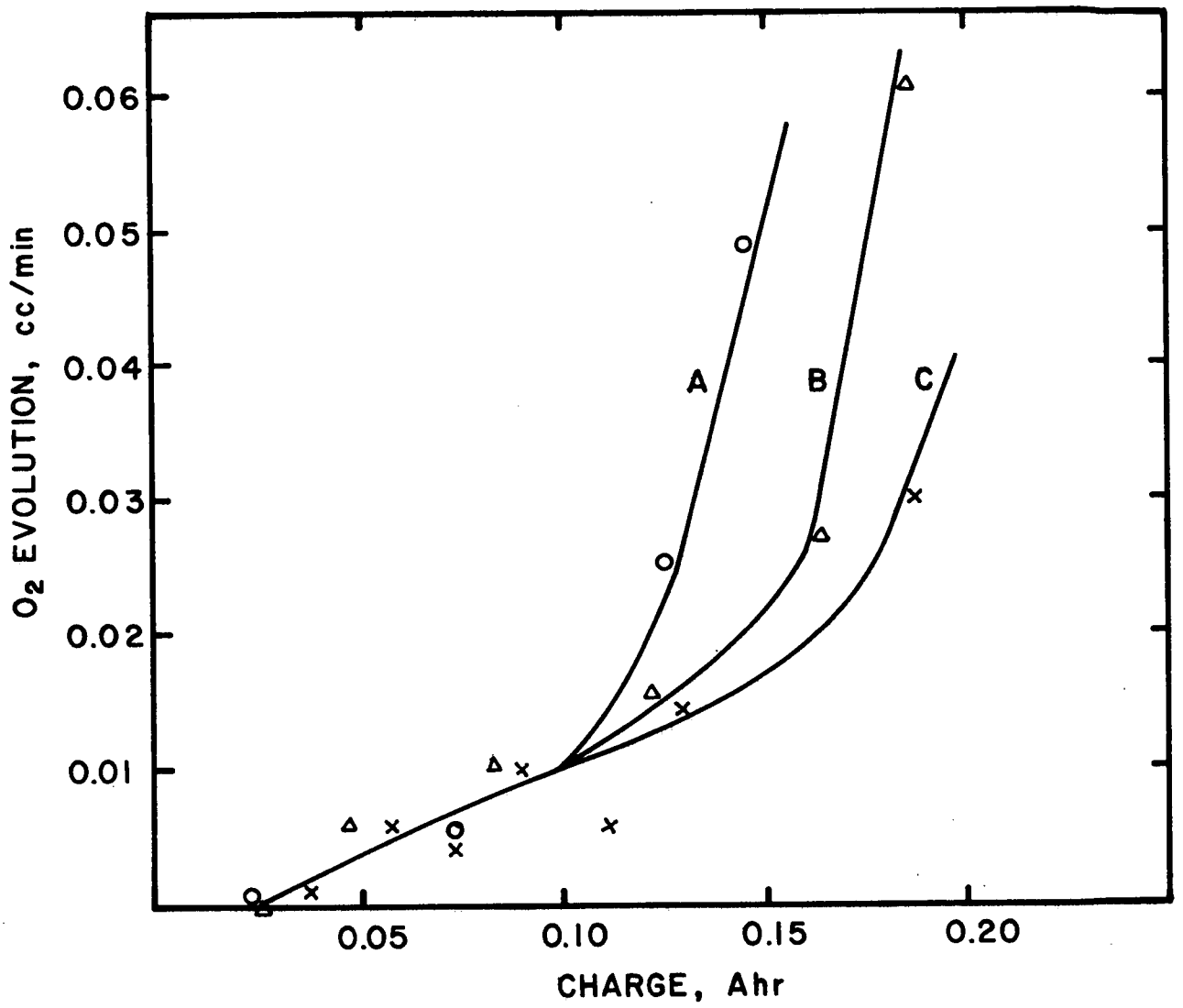

Fig. 67. O_2 evolution rate at electrode Ni-1 at various charge rates (25°C, 30% KOH; A = Crate, B = C/3 rate, C = C/10 rate)

the low-loaded electrode this effect appears to be counteracted, possibly, by a facilitated O_2 evolution on exposed Ni plaque. For practical battery application one will have to compromise between optimal charge acceptance and energy density which requires highly loaded plates. The results emphasize further the necessity of high charge rates (may also be in the form of pulse charging), especially if the cell is to be operated at elevated temperatures.

D. Conclusion for a Negative Limited NiCd Cell Design

1. Teflon-bonded cadmium oxide electrodes show good performance over the tested range of temperature and rate.

2. The advent potential of hydrogen evolution is slightly more negative at the lower temperature. A safe cutoff voltage is -1.25 V versus Hg/HgO (~ 1.75 V cell potential). This voltage can be applied to the whole temperature range without necessity of temperature compensation.

3. High charge rates are possible and safe, also at low temperatures. The effect of charge rate on capacity appears to be small at room temperature larger at 0°C and largest at 50°C. Lower charge rates result in higher capacity. Two-level charging appears to be most suitable. Thinner electrodes are less rate sensitive. At C/10 charge the average capacity at 0°C was 87% of the capacity at 25°C.

4. Positive plates start to evolve oxygen quite early (at approximately 30% and 5 to 10% state of charge at 0°C and 50°C, respectively).

Therefore, some oxygen evolution will occur in a negative limited cell. (The maximum rate is approximately 10% of conventional sealed cells at C/10 charge rate and less at higher charge rate. For operation at 50°C, an O_2 recombination capability equivalent to a C/10 rate appears to be necessary.)

5. For lower temperature operation (25°C and below), a negative to positive ratio of 1: 1.5 appears to be sufficient from the view point of O_2 evolution. For high temperature operation (50°C), a negative to positive ratio of in excess of 1: 2 appears to be necessary (depends on operating condition.)

These conclusions may be modified by the test results of complete cells.

V. NEGATIVE LIMITED NiCd CELLS

A. Introduction

The objective of this phase of the program was to demonstrate feasibility of the sealed negative limited cell design. To meet this objective we proposed to build and test 6 complete cells of approximately 4-Ahr capacity. These experimental cells were designed to allow a detailed analysis of this behavior in order to pinpoint possible problem areas. Therefore, the cells were equipped with a reference electrode, a thermocouple, and a pressure gauge.

B. Cell Design

Each cell contains 7 negative and 14 positive electrodes. The electrode size is 4 $in.^2$ (2 × 2 in.) with a nominal thickness of 20 mil for negative and 26 mil for positive plates. The theoretical capacity per plate is 1 Ahr and 0.5 Ahr for the negative and positive plates, respectively. According to our experience, the utilization of the negative plate is approximately 40 to 50% of the theoretical capacity, whereas positive active material can be nearly completely utilized. Thus, under actual operating conditions a negative to positive capacity ratio of approximately 1:2 will result.

As separator material we use Nylon 2505 from Pellon. In addition, each cell stack contains a nickel oxide reference electrode and a iron-constantan thermocouple. The cell cases consist of high impact polyphenylene oxide and were supplied by JPL. They were hermetically sealed using an epoxy cement. Also, each cell contains a pressure gauge (30 in. vacuum to +30 psi) and a control pressure release valve.

C. Cell Manufacture

1. Negative plates

The negative plates were manufactured in individual units of 4 × 4 in. and cut to yield four plates of 2 × 2 in. The electrode substrate consists of expanded Cd (Exmet Cd 10-3/0) with silver ribbon tabs. To assure good electrical contact, the silver ribbon was woven into the cadmium substrate and spotwelded to it. A paste consisting of 9.6 g CdO (Fisher analytical grade), 0.5 g Teflon in the form of a dispersion (Teflon 30, Dupont), and 5 mil distilled water was evenly distributed on 16 $in.^2$ of substrate and pressed between aluminum foil at 800 psi. This was followed by drying at 150°F for 1/2 hr. These plates were sintered at 250°C for 20 min, cut, wrapped with 1 mil Dynel (Webril), and pressed at 2000 psi. The plates were then formed potentiostatically at -1.2 V versus Hg/HgO reference for 24 to 48 hr, followed by complete discharge, washing in distilled water, and drying.

2. Positive plates

The plaque was prepared by the slurry coating of a nickel screen with carbonyl Ni powder (Inco Ni 287). The sintered plaque had a thickness of 24 mil and an apparent porosity of 78% corresponding to a powder porosity of 83%. Tabs consisting of 1/4-in. wide and 4-mil thick nickel strips were pressed into the plaque at 5000 psi and spotwelded. The plates were impregnated in a solution of 2 M $Ni(NO_3)_2$, 0.3M $NaNO_2$ (pH 4, 104°C) at a current density of 0.5 $A/in.^2$ for 45 to 50 min. Then the electrodes were rinsed thoroughly with distilled water and dried. The theoretical capacity was 0.125 $Ahr/in.^2$ The plates were formed by 6 cycles at the C/2 rate with 100% overcharge. Before measurement of their actual capacity, the plates were scrubbed and washed.

3. Cell assembly

The plates were assembled as shown in Fig. 68. The negative electrode tabs were silver soldered into a silver plated copper terminal while the positive tabs were spotwelded to a nickel bus. An NiO_x reference electrode was attached to the side of the electrode package. The thermocouple was enclosed in a sealed Teflon tube and its junction was located in the center between the reference electrode and the electrode stack. The terminal and the thermocouple were sealed into the cell case cover (high impact polyphenyleneoxide) with an epoxy cement (Allbond Allaco, Inc.) The plate assembly was designed to result in a tight fit in the cell

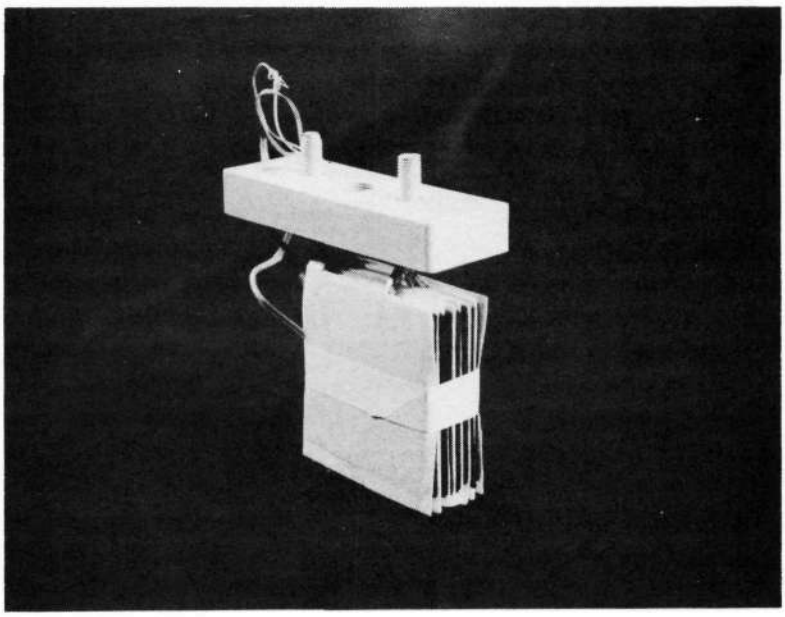

Fig. 68. Assembled plate stack of experimental negative limited NiCd cell

case. On one side an empty space resulted, since the supplied cases were wider than the electrode assembly. To reduce the gas volume this space was filled with inert plastic (Lucite). Then the cell assembly was turned upside down and the cover sealed to the case using the same epoxy mentioned above.

The pressure gauge-valve assembly was mounted in the threaded hole in the center of the cover using a viton o-ring for sealing. The gauge range extended from vacuum to 30 psi. Typically, the open volume of the complete cell, including the pressure gauge, was 28 to 30 cm^3.

The fill level with electrolyte had to be determined experimentally. It was necessary not only to know the absolute amount of electrolyte, but also the corresponding degree of saturation of the cell. We therefore used the following procedure: The cell was filled under vacuum with electrolyte and then the excess was drained. This state was defined as a 100% wet cell. By evacuation, various amounts of water were removed to obtain different electrolyte fill levels. The resulting difference in electrolyte concentrations were considered acceptable for these experimental cells. The electrolyte levels for the cells are listed in Table XIV, along with other pertinent cell characteristics. A completed cell is shown in Fig. 69.

Table XIV. Cell Characteristics

Cell No.	Capacity, Ahr				Positive Precharge % of pos. cap.	Electrolyte			Cell Resistance Ω
	Negative Theoretical	Positive as Formed	Cell			Total cc	Level %	Conc. wt%	
			Initial	Stable†					
1	7.1	6.1	3.7	2.6	0	17.0	66	46	0.003
2	7.1	7.5	3.8	2.5	0	18.0	69	45	0.003
3*	6.5	6.9	3.4	2.5	7	18.5	70	43	0.0045
4	7.4	7.4	3.8	2.6	7	15.2	69	43	0.005
5	7.2	6.7	4.2	2.5	0	20.2	80	35	0.003
6	7.4	5.8	3.3	2.6	0	22.4	85	33	0.002

*Cell No. 3 contains only 6 negative and 12 positive plates

†After ~30 cycles

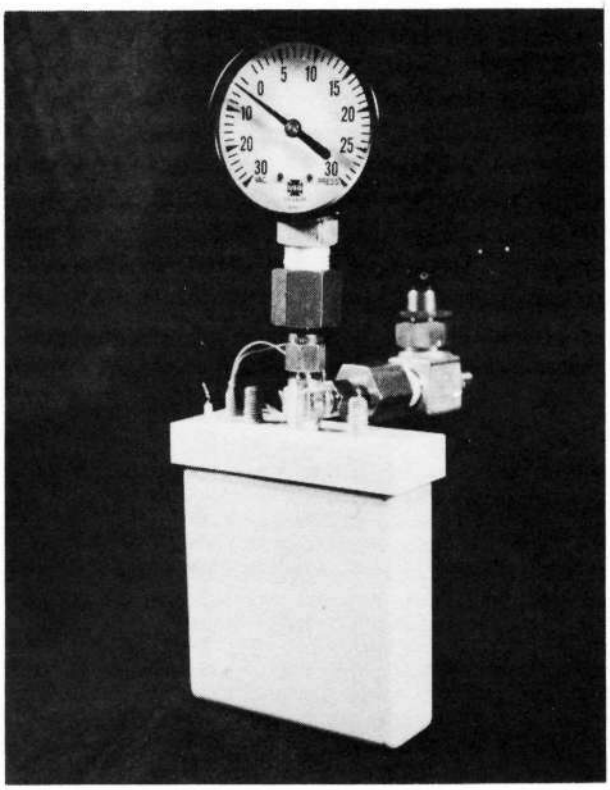

Fig. 69. Experimental negative limited Ni-Cd cell

D. NiCd Cell Test

1. Test procedures

Prior to the actual test regime the cells were evacuated, sealed, and cycled for 25 to 30 full cycles at rates between C and C/2 in order to obtain a stable capacity. Fig. 70 shows the cells and the Tyco-built battery cycler with voltage cut-off control during the pretest cycling.

This was followed by a readjustment of the electrolyte level to the values shown in Table XIV. In cells 3 and 4, approximately 7% positive precharge was introduced by overcharging the cell. The precharge level was calculated from the amount of hydrogen evolved ($\sim$200 cm^3). Then the cells were evacuated again and resealed. For the actual testing the cell temperature was kept constant by a temperature-controlled water bath.

The experiments were carried out at various temperatures and charge rates, while the discharge current was kept constant at 1.5 A corresponding to a nominal C/2 rate. Three consecutive cycles were recorded at each condition. The measured parameters included: (1) cell voltage (2) negative potential versus reference electrode, (3) charge input, (4) delivered capacity, (5) temperature difference between cell center and constant temperature bath, and (6) O_2 pressure in the cell.

2. Results and discussions

A typical charge/discharge cycle of a negative limited cell is shown in Fig. 71. The simultaneous recording of the negative plate potential versus a NiO_x reference electrode clearly demonstrates the potential shift at the full charge of the cadmium electrode.

After precycling, the capacities of all six cells were nearly identical. The utilization of the negative plates corresponded to values between 35 and 40% of their theoretical capacity. This compares very well with the test data obtained for individual cadmium electrodes.

The delivered capacities of the experimental cells at various temperatures are summarized in Table XV. The shown values represent averages of data from 3 to 6 consecutive cycles.

These results show that the charge rate had practically no influence on the delivered capacity. The change in temperature from 25 to 0°C caused the average capacity to decrease slightly ($\sim$15%). The electrolyte fill level appeared, however,

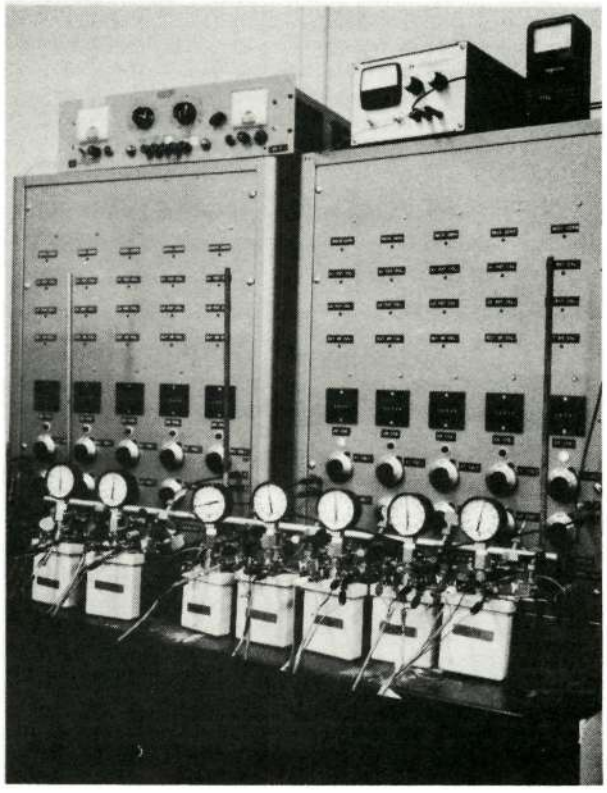

Fig. 70. Negative limited NiCd cells on test

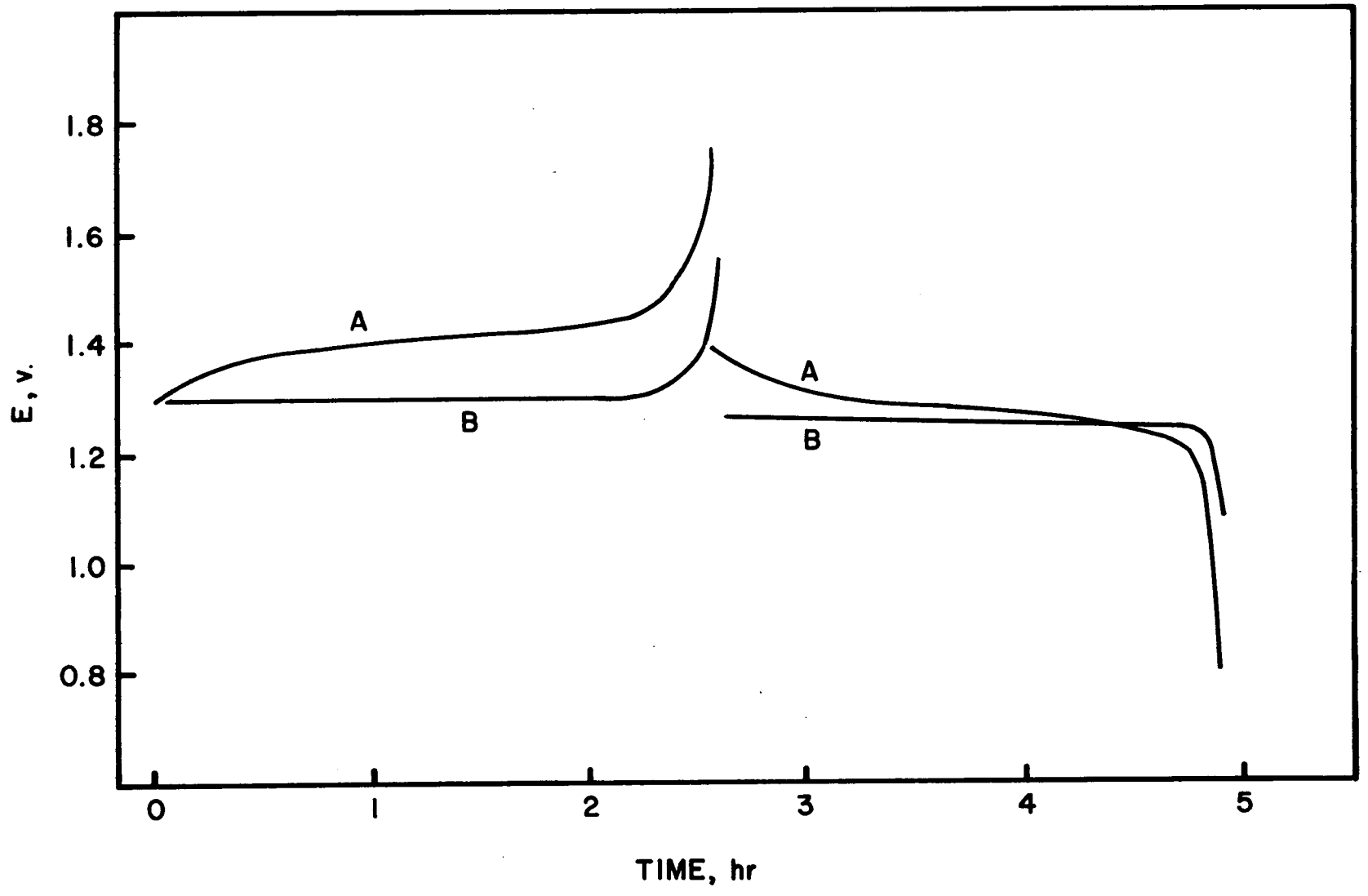

Fig. 71. Charge/discharge cycle of negative limited NiCd cell, 1.3A, room temperature [A = cell voltage, B = negative plate potential versus NiO_x reference (Trace A and B 3-min offset)]

Table XV. Capacity of Experimental NiCd Cells

Temperature	Delivered Capacity at 1.5 A, Ahr						
	25°C		0°C		35°C	25°C	
after charge at	1.0 A	0.5 A	1.0 A	0.3 A	1.5 A	1.0 A	0.4 A
Cell No. 1	2.57	2.44	2.22	2.28	2.52	2.39	2.40
2	2.31	2.12	1.78	1.87	2.04	1.84	2.04
3	3.08	2.87	2.31	2.00	2.26	2.34	2.52
4	3.04	3.15	2.37	2.24	–	2.89	2.79
5	2.73	2.63	2.45	2.48	–	2.59	2.89
6	3.05	3.26	2.65	2.63	–	3.27	3.49

to effect the capacity. The average values for the wetter cells 5 and 6 are approximately 20% higher than those of cells 1 and 2, which had a lower electrolyte level. The capacities of cells 3 and 4 showed intermediate values. Here, however, the increased capacity resulted from overcharging during precharge adjustment. As expected, the positive precharge had no effect on capacity changes as a function of rate and temperature. A comparison of the initial and final capacity values at 25°C shows little change during testing.

Towards the end of the low rate charge at 25°C, cell voltage oscillations were observed. They were caused solely by the negative electrode. Fig. 72 shows a typical example of the negative electrode potential in the last phase of the charging process. These potential fluctuations were different in the various cells. At a given cell, however, they were quite reproducible in consecutive cycles. They may be of the same origin as the potential fluctuations observed and discussed during the testing of Teflon-bonded cadmium electrodes. Here they could, however, also be caused by oxygen arriving at the cadmium electrode in the small bursts (bubbles). Again, one would only expect to see any effect of this kind during the potential change at the end of the charging process.

During a charge/discharge cycle, characteristic changes in gas pressure and temperature occurred in the cells. The pattern was quite similar in all cases, and typical examples are shown in Figs. 73 through 77. During charge the O_2 pressure in the cell decreased, passed through a minimum, and increased again towards

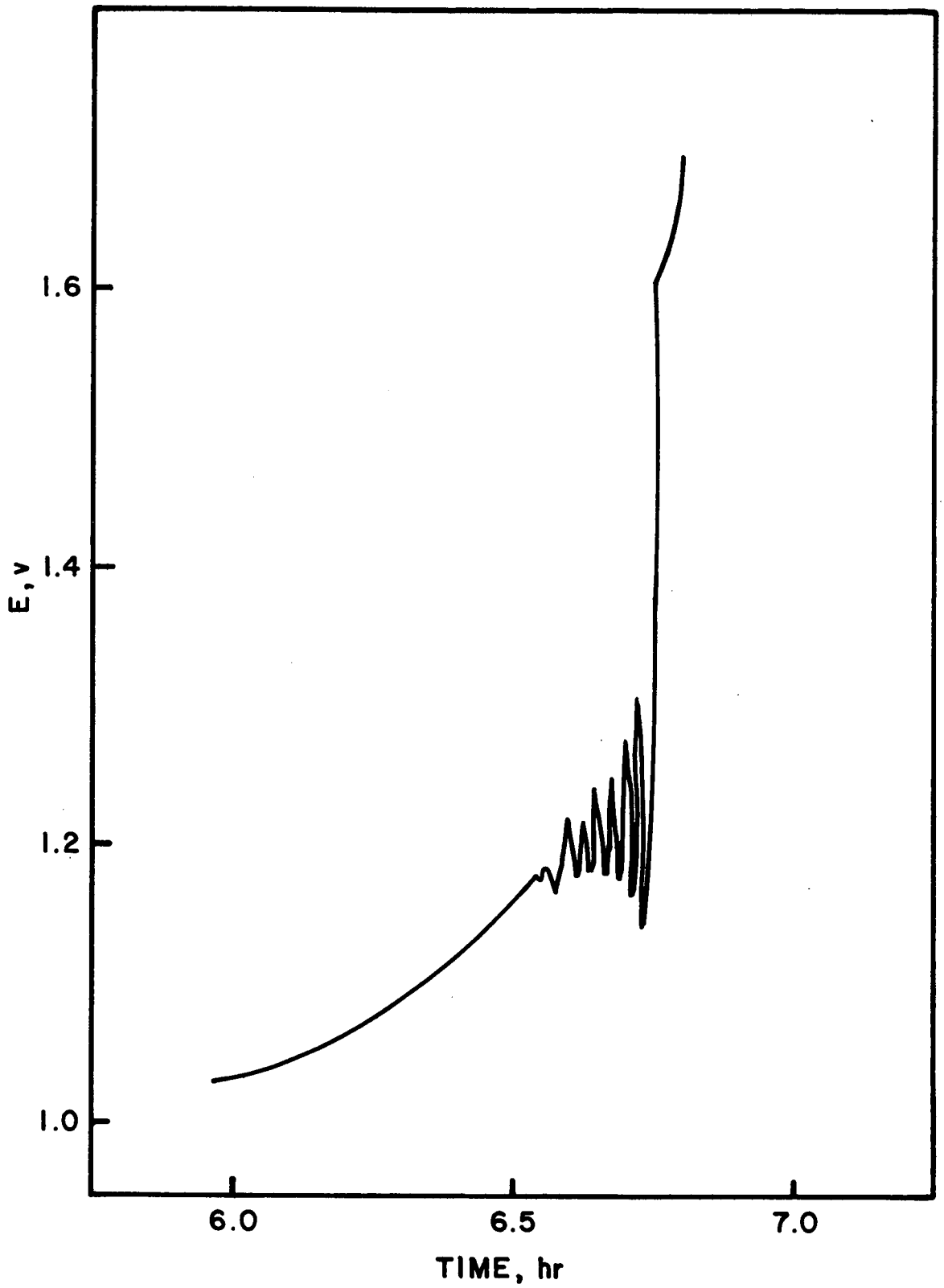

Fig. 72. Negative potential versus NiO_x reference at low rate charge (cell No. 1, 25°C, 0.5A)

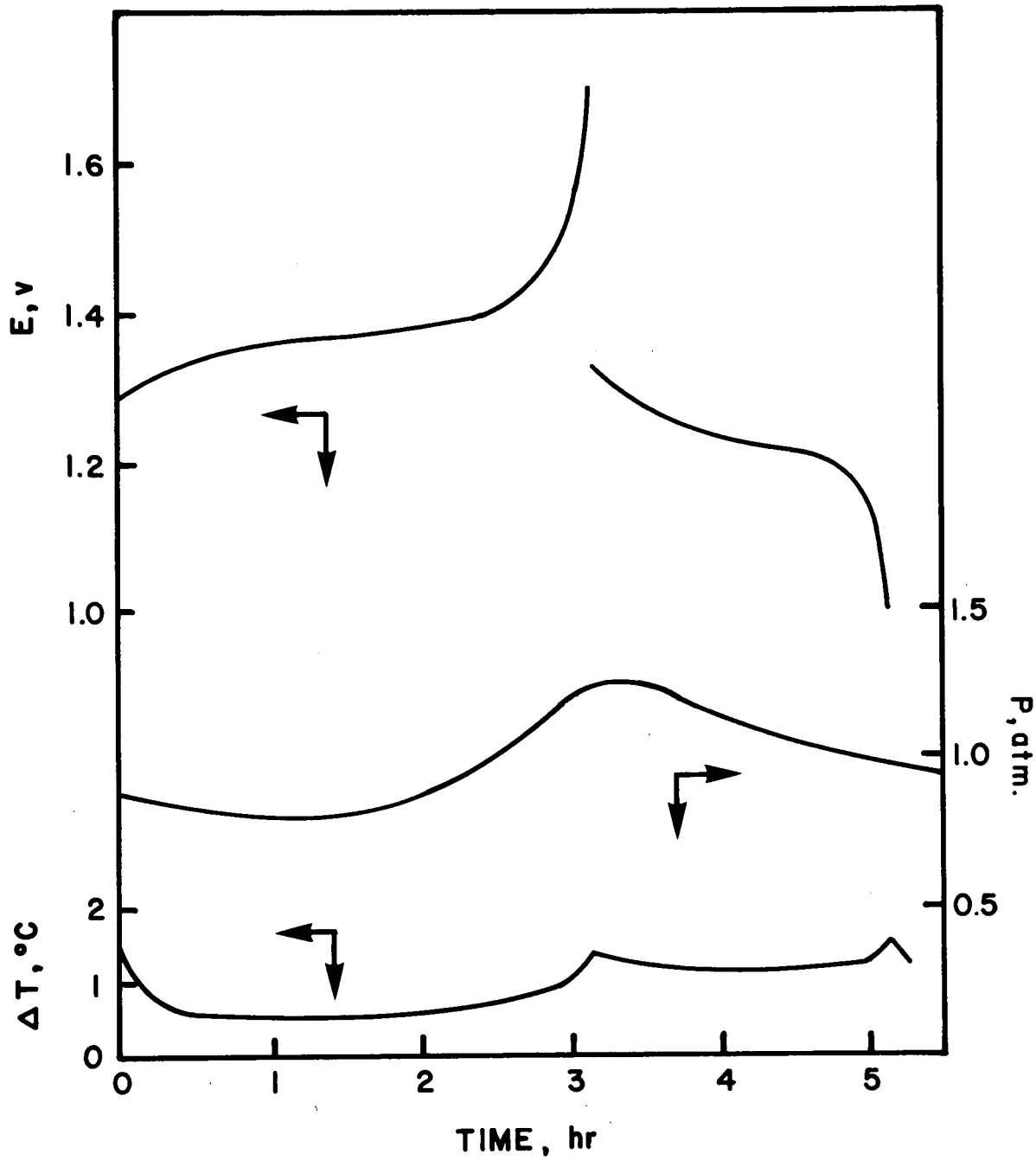

Fig. 73. Changes in cell potential, pressure, and temperature during a charge/discharge cycle (cell No. 3, 25°C, charge current 1.0A, discharge current 1.5A)

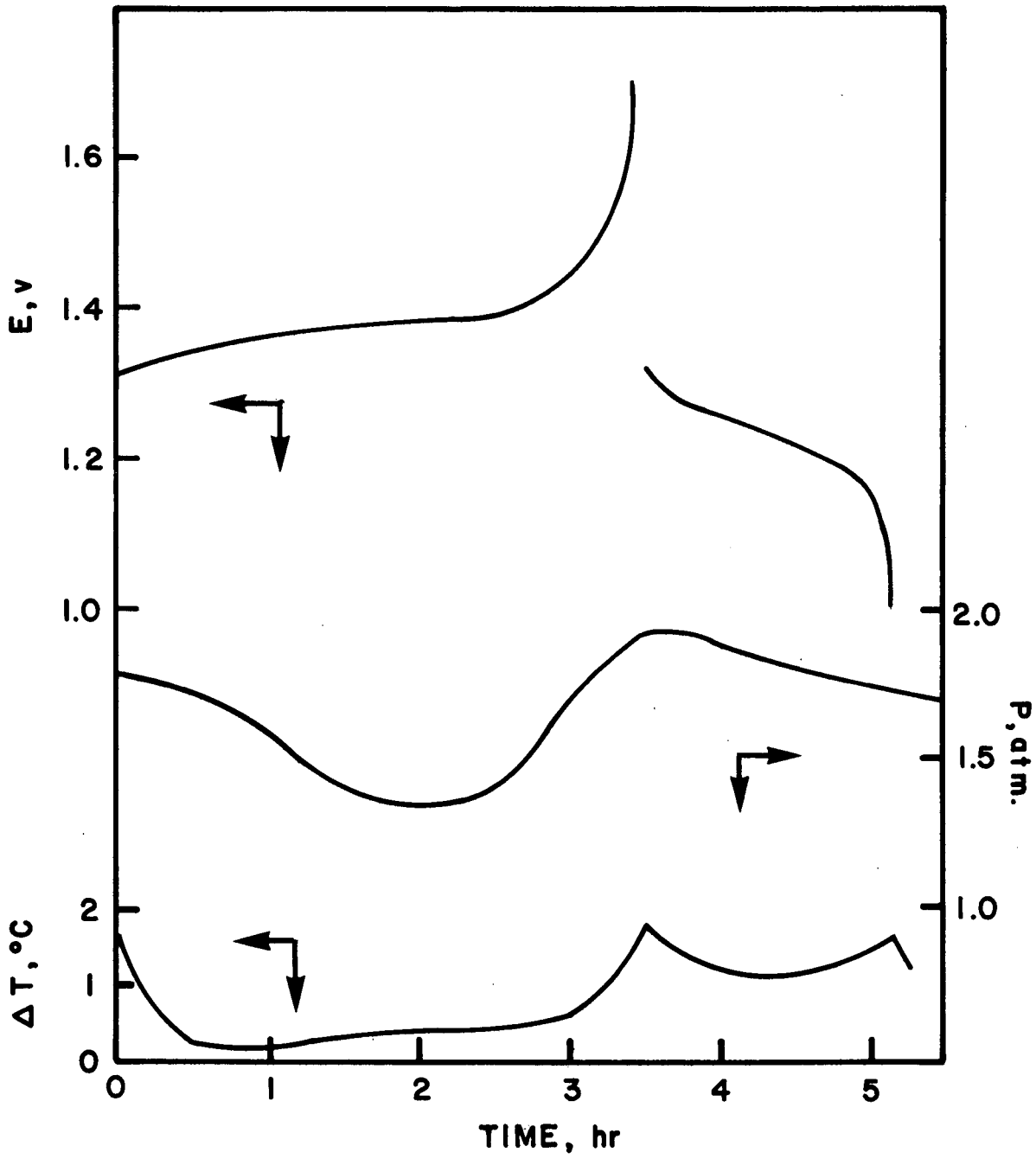

Fig. 74. Changes in cell potential, pressure, and temperature during a charge/discharge cycle (cell No. 5, 25°C, charge current 1.0A, discharge current 1.5A)

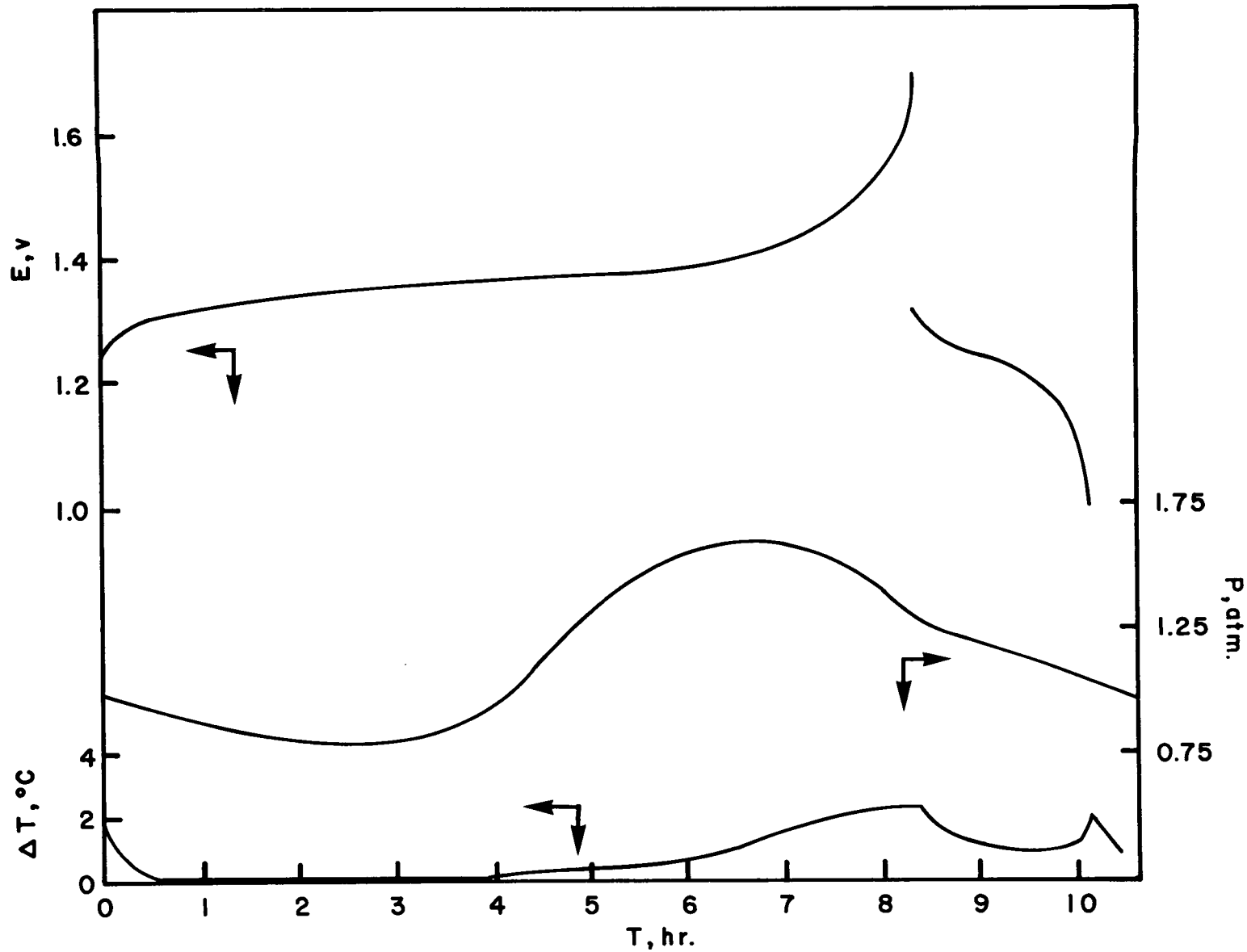

Fig. 75. Changes in cell potential, pressure, and temperature during a charge/discharge cycle (cell No. 3, 25°C, charge current 0.5 A, discharge current 1.5 A)

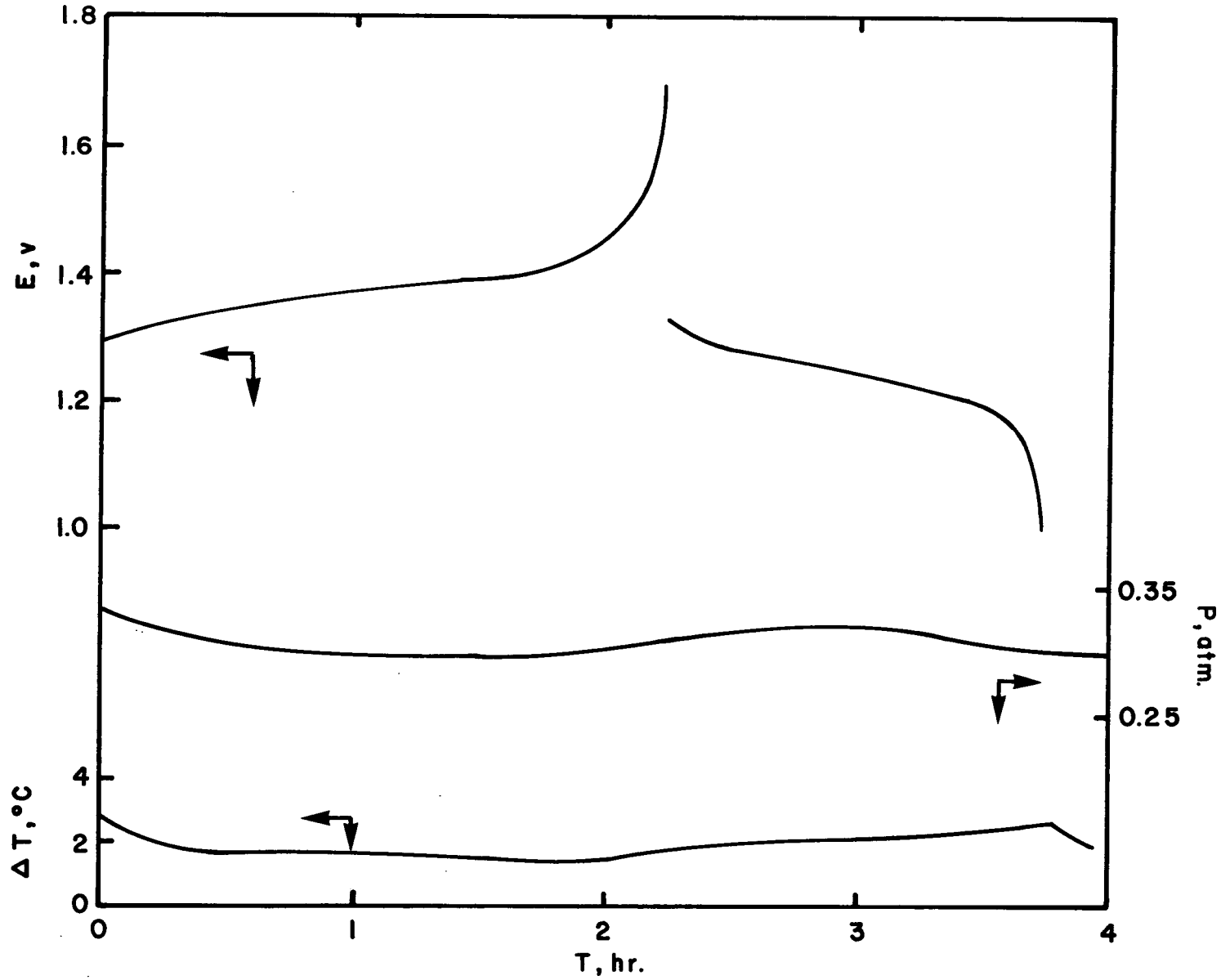

Fig. 76. Changes in cell potential, pressure, and temperature during a charge/discharge cycle (cell No. 3, 0°C, charge current 1.0 A, discharge current 1.5 A)

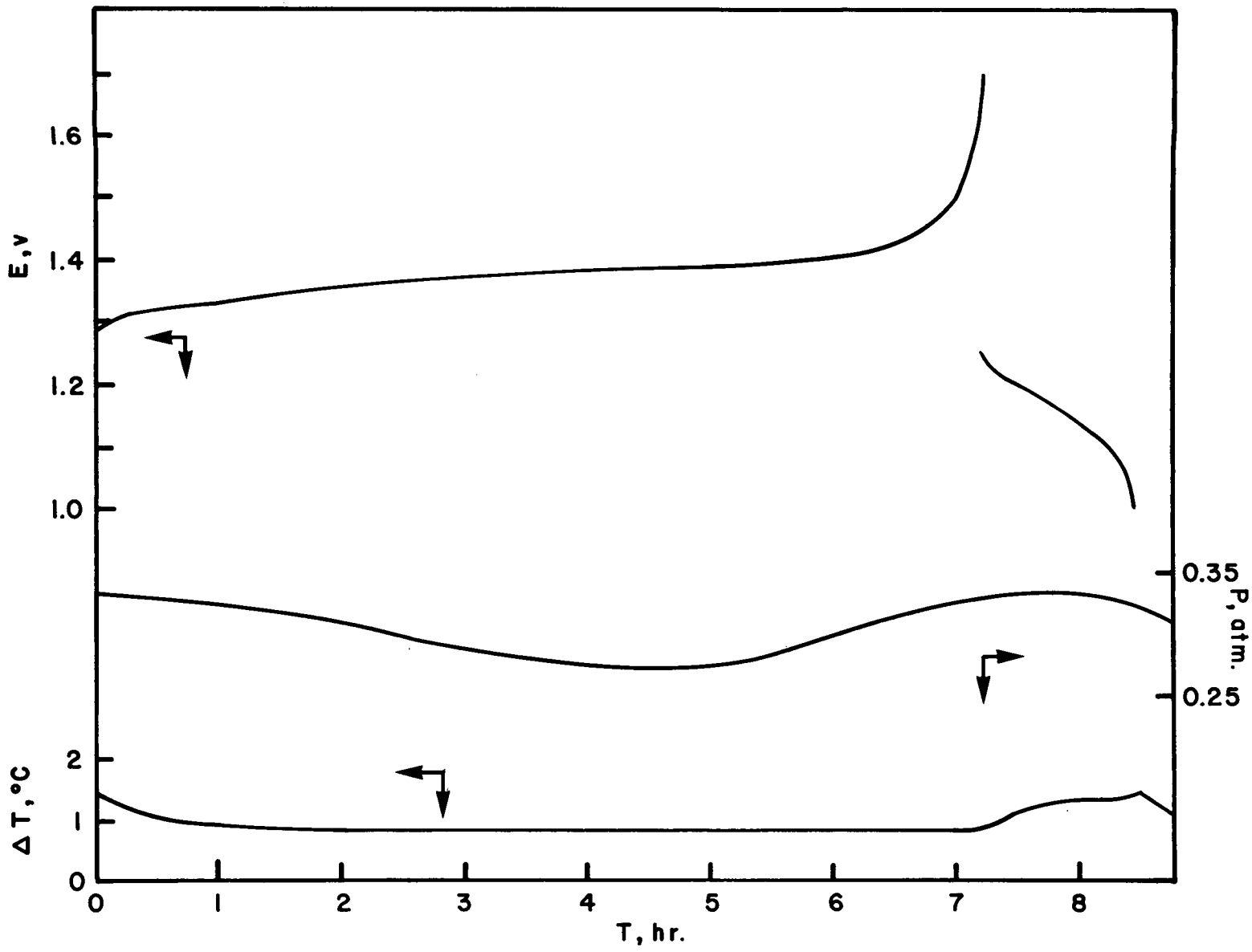

Fig. 77. Changes in cell potential, pressure, and temperature during a charge/discharge cycle (cell No. 3, 0°C, charge current 0.3 A, dishcarge current 1.5 A)

the end of charge. In most cases, the pressure maximum occurred right after the end of charge. During the following discharge the pressure decreased again. The absolute values of the O_2 pressure were dependent on the oxygen recombination rate in the cells. Thus, as one might expect, the wet cells 5 and 6 show the highest pressures. The minimum and maximum values for all cells are listed in Table XVI. During low rate charge at 25°C, the pressure maximum occurred prior to the end of charge, indicating an increased O_2 recombination rate as the cadmium electrode approaches full charge.

At 0°C the absolute pressures were quite low and the pressure fluctuations during the charge/discharge cycles very small.

The temperature difference between the center of the cell and the thermostated bath also followed a typical pattern. It remained at a constant low value throughout most of the charge time and showed a small increase towards the end of charge with distinct maxima at the switching points. The temperature during discharge was generally higher than during charge. At the low rate charge at room temperature, the increased O_2 recombination towards the end of the charging cycle also led to a corresponding temperature increase. (Fig. 75).

The effect of oxygen evolution as a parasitic reaction during charge is reflected in the charge efficiency. This data is summarized in Table XVII. Generally the charge efficiency increases with an increase in charge rate and a decrease in temperature. Again, this is perfectly in line with the gassing behavior of the positive electrodes as a function of temperature and rate. It has been discussed in detail in the previous section. It is interesting to note that the lowest charge efficiencies were observed at the cells containing positive precharge and at cell No. 6, which has the highest capacity. In these cases the positive electrode reaches a higher state of charge and thus shows an increased rate of O_2 evolution at the end of the charge cycle.

It was not possible to test the experimental cells in the negative limited mode of operation at 50°C because of excessive O_2 pressure buildup. As we have seen from the O_2 evolution studies at positive plates, only half the capacity can be realized at 50°C after low rate charging, even after extensive overcharge. At high charge rates the full capacity is obtainable. From these electrode studies we can calculate the O_2 evolution rate for our cells towards the end of charge to be approximately equivalent to a current of 1.0 to 1.5 A. Recombination of oxygen at this rate could not be accommodated by our cells. The cells can, however, be operated at low charge rates in the positive limited mode.

The cells with relatively low electrolyte level (Nos. 1 to 3), could operate at 35°C. The observed O_2 pressures were, however, quite high.

Table XVI. O_2 Pressure in Experimental Cells

O_2 Pressure, Atm

Temperature	25 °C				0 °C				35 °C	25 °C	
Charge Current	1.0 A		0.5 A		1.0 A		0.3 A		1.5 A	1.0 A	
Pressure	max	min	max	min	max	min	max	min	max	max	min
Cell No. 1	1.20	0.73	1.63	1.03	0.33	0.28	0.27	0.25	1.63	1.27	0.96
2	1.37	1.13	1.37	1.07	0.75	0.70	0.87	0.83	1.56	1.42	1.27
3	1.23	0.76	1.60	0.80	0.33	0.30	0.33	0.27	1.60	1.42	0.96
4	1.40	0.87	2.03	1.07	0.68	0.63	0.57	0.50	—	1.80	1.41
5	1.92	1.33	2.17	1.40	0.50	0.43	0.47	0.42	—	2.22	1.87
6	1.38	0.99	2.17	1.20	0.55	0.51	0.48	0.37	—	1.76	1.22

Table XVII. NiCd Cell Charge Efficiencies

Delivered Capacity, % of Charge Input

Temperature	25 °C		0 °C		35 °C	25 °C	
Charge Current	1.0 A	0.5 A	1.0 A	0.3 A	1.5 A	1.0A	0.4 A
Cell No. 1	91	74	97	92	75	85	60
2	91	86	99	95	71	90	76
3	92	69	98	90	56	87	55
4	80	39	97	90	-	71	33
5	82	81	99	94	-	76	45
6	90	61	95	87	-	87	48

VI. CONCLUSIONS

1. Operation of NiCd cells containing high hydrogen overvoltage negatives in the negative limited mode is feasible.

2. The cells show a large voltage increase at the end of charge. A safe cutoff voltage (avoiding H_2 evolution) is 1.7 to 1.75 V (negative plate potential ~ -1.25 V versus Hg/HgO). This voltage can be applied to the entire range of temperature and rate tested without necessity of temperature compensation.

3. High charge rates are possible and safe, also at low temperatures. The effect of charge rate and temperature on capacity is minimal. The capacity at 0 °C was approximately 10 to 15% below the value at 25 °C.

4. Since positive plates start to evolve some oxygen quite early on charge (~ 16% state of charge at 25 °C), limited O_2 gassing occurs and the means for its recombination has to be provided. The amount of O_2 evolved is considerably less than in conventional positive limited cells.

5. The rate of O_2 generation depends on the negative to positive ratio and on operating temperature.

For lower temperature operation (25 °C and below), a negative to positive ratio of 1:1.5 appears to be sufficient from the viewpoint of O_2 evolution. For high temperature operation (50 °C), a negative to positive ratio in excess of 1:2 is necessary (depends on operating condition).

6. No nonconsumable gas (H_2) was generated during cell operation. O_2 pressures varied in a characteristic pattern throughout a charge/discharge cycle. The pressure maximum depends on the relative rates of O_2 generation and recombination. The latter is strongly dependent on electrolyte fill level.

7. The cell temperature remains low. No sizable temperature increase occurs at the end of charge.

Summarizing the results of the tests, we can note that negative limited operation of NiCd cells is feasible. The cells behaved as expected from the test results obtained at individual electrodes. An additional factor of importance for sealed cells is the electrolyte fill level, since it influences the gas recombination rate and thus the extent of pressure buildup in the cells. Both positive to negative ratio and electrolyte level will determine the upper temperature limits at which the cells can be operated successfully. In general, the higher the intended temperature of operation, the larger a positive to negative ratio is necessary and the drier the cell has to be to allow high O_2 recombination rates. The oxygen evolution rate may further be reduced by suitable additions to positive electrodes or changes in electrolyte composition. Alternatively, a third electrode, e.g., a porous silver plaque, connected to the negative terminal could probably accommodate the necessary O_2 recombination while the plate stack is operated wet.

VII. REFERENCES

1. E. J. Rubin and R. Baborian, J. Electrochem. Soc., 118, 428 (1971).
2. D. MacArthur, J. Electrochem. Soc., 117, 422 (1970).
3. O. Glemser and J. Einerhand, Z. Elektrochem., 54, 302 (1950).
4. E. J. McHenry, Electrochem. Tech., 5, 275 (1967).
5. P. U. Popat and E. J. Rubin, Final Report JPL Contract No. 951972.
6. F. G. Will, NASA/GSFC Battery Workshop, November 1970.
7. T. S. Lee, J. Electrochem. Soc., 118, 1278 (1971).
8. First Quarterly Report, this contract.
9. S. Levier and S. Charlip, Final Report NASA contract.
10. Second Quarterly Report, this contract.
11. L H. S. Henderson and S. G. Ladan, Canadian Journal of Chemical Engineering, 46, 355, (1968).
12. R. Beauchamp, NASA GFC Battery Workshop 1970, E. J. McHenry, NASA GFC Battery Workshop 1971, Semiannual Report by Tyco Laboratories, Inc. under contract NAS-5-11561 (1971).
13. Y. Okinaka, J. Electrochem. Soc. 117, 289 (1970).
14. Y. Okinaka and C. M. Whitehurst, J. Electrochem. Soc. 117, 583 (1970).